Conceptual Design Report For the Texas Petawatt Laser

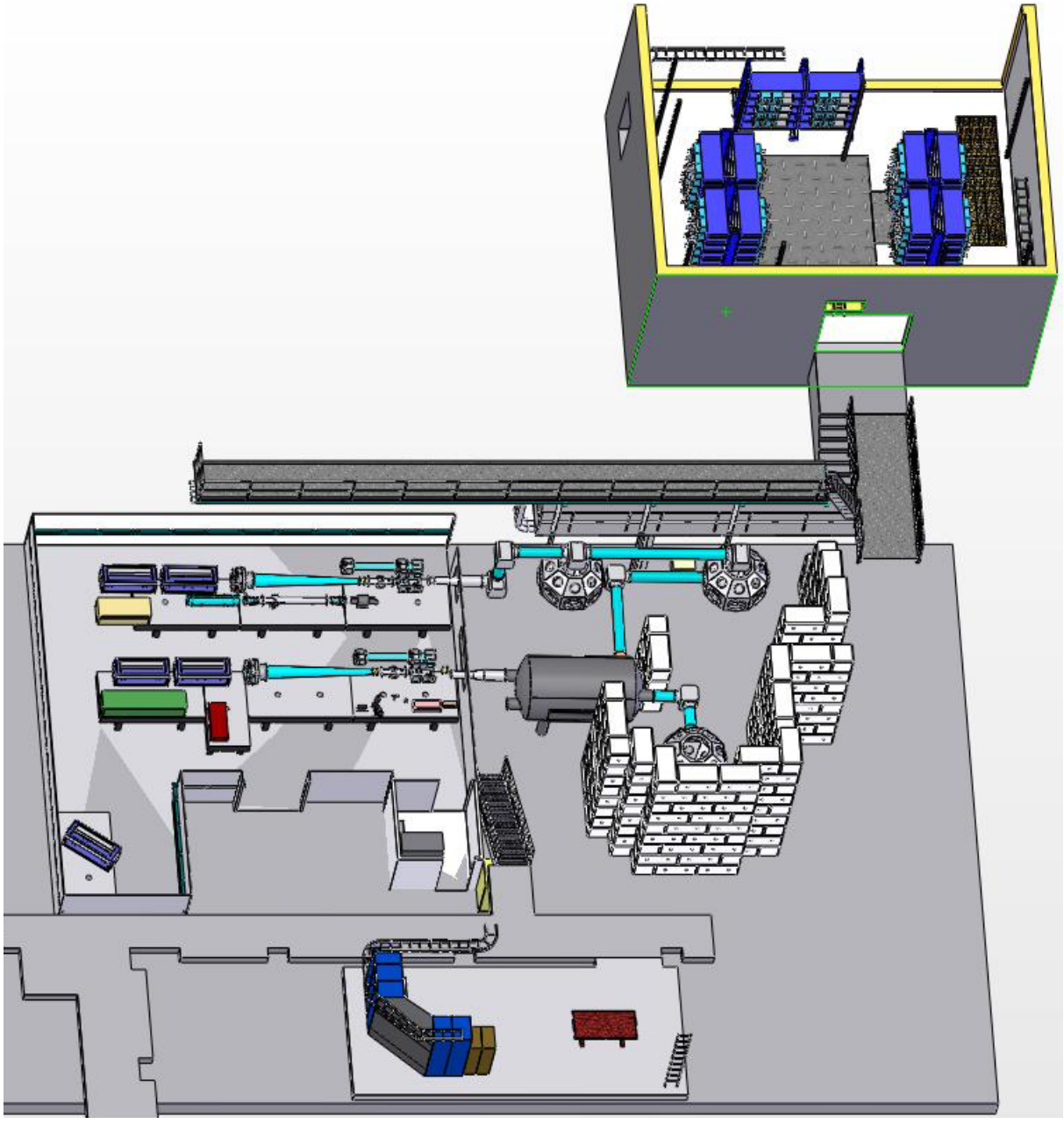

Texas Center for High Intensity Laser Science

Conceptual Design Report
For the
Texas Petawatt Laser
At the
Texas Center for High Intensity Laser Science

Prepared by:

Todd Ditmire—TCHILS Director

Erhard W. Gaul

Mikael D. Martinez

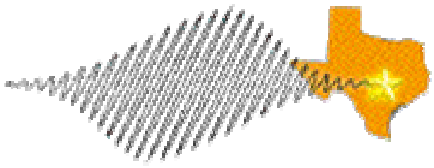

Conceptual Design Report
For the
Texas Petawatt Laser
At the
Texas Center for High Intensity Laser Science

Acknowledgements

The Texas Center for High Intensity Laser Science and the Texas Petawatt Laser Operations team wishes to thank the following collaborators from Lawrence Livermore National Laboratory, John Caird, Chris Ebbers, Al Erlandson, Brent Stuart, Igor Jovanovic, Bill Molander, and Norm Nielson. Their guidance, enthusiasm and technical expertise significantly contributed to this conceptual design report.

The Petawatt team gratefully acknowledges the support of Scott Samuelson and his staff at DOE operations as well as Bob Ehrlich and Tim Weiland at LLNL relative to the allocation of decommissioned NOVA components. Without this equipment, the scale of this laser could not be realized.

Finally, we would like to thank to Scott Pennington and Tracy Tipping from UT ES&H for their support and expertise with the radiation safety design.

Contributors

Below is a roster list of the Texas Petawatt Laser team, which is composed of faculty, staff consultants and students.

Todd Ditmire
Erhard W. Gaul
Mikael D. Martinez
Watson Henderson
Dan Gorski
Skyler Douglas
Joe Narduzzi
Jay Campbell
Keith Carter
Greg R. Hays
Maria Aguirre
Sharee Aery

Table of Contents

List of Figures

List of Tables

1 Executive Summary of the Project

This document describes the conceptual design of the Texas Petawatt Laser. This laser, when complete will deliver two laser beams to three different target chambers. Both beam lines will use NOVA surplus disk amplifier parts which have been allocated to the University of Texas by NNSA. The first beam will be based on chirped pulse amplification [Str 85] and will deliver 200 J pulses at a wavelength of 1060 nm with pulse duration near 150 fs. The second beam will deliver 500 J pulses at a wavelength of 527 nm (frequency double fundamental light) with pulse duration variable between 2 ns and 20 ns. The schematic layout of the facility is illustrated in Figure 1 and the key laser parameters are summarized in Table 1.

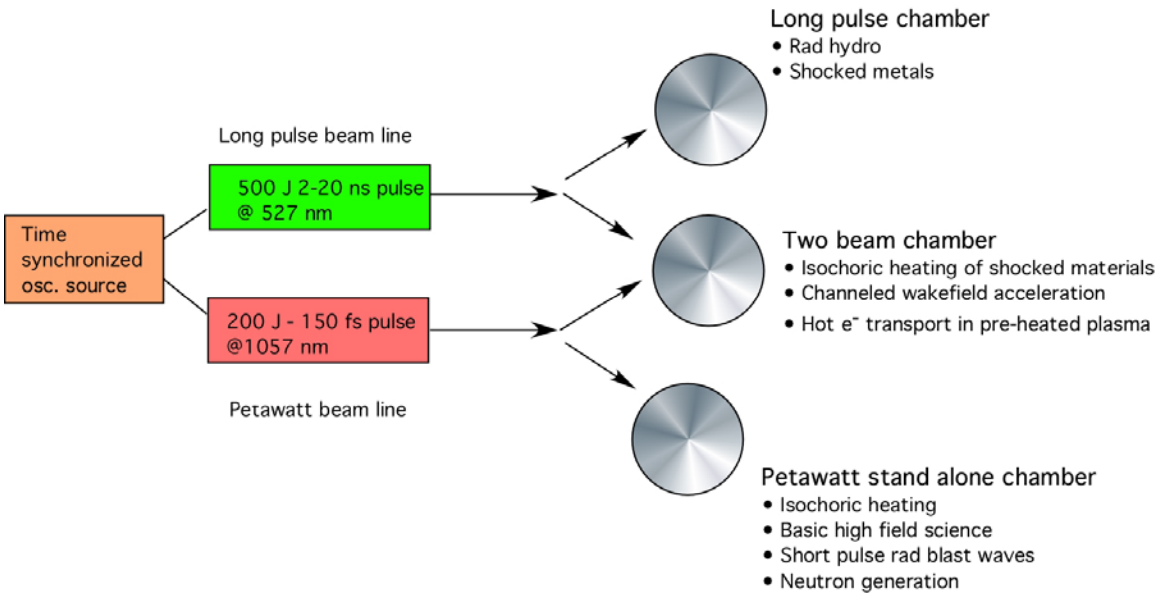

Figure 1 The Texas Petawatt facility.

The design parameters of the Texas Petawatt Laser as described in this document are motivated by a number of novel scientific applications. The Texas Petawatt will be unique from other high energy petawatt lasers presently under development in that it will deliver substantially shorter pulses, a feature which enables many of these unique applications. This will be accomplished by constructing a hybrid CPA system using the recently developed techniques of optical parametric chirped pulse amplification (OPCPA) and mixed Nd:glass laser amplifiers. This design is internationally unique and is described in detail in this report. Some of the scientific applications and how they motivate the design goals of the laser are also described briefly in this design report.

This laser will represent the core scientific research machine of the newly established Texas Center for High Intensity Laser Science (TCHILS). TCHILS was established in July 2003 as an NNSA Center of Excellence under a cooperative agreement (DE-FC52-03NA00156) with the University of Texas at Austin. . The laser system is to be housed in the high bay facility in the Robert Lee Moore Hall on campus at UT Austin. This bay has recently undergone a $1.5M renovation funded by the University and now houses clean room facilities needed for housing both laser beam lines. The estimated per year costs of the system are summarized in Figure 2. The structure of this center is illustrated in Figure 3. This document details the design of both

laser chains, the schedule under which they will be constructed, the plan for the deployment of the experimental area and the plan that will be implemented to operate the entire facility safely. A Solidworks rendition is shown in Figure 4.

	Petawatt laser	Long pulse laser
Pulse energy	**200 J**	**500 J**
Pulse duration	**150 fs**	**2-20 ns**
Laser wavelength	**1057 nm**	**527 nm**
Repetition rate	**1 shot/ hour**	**1 shot/ hour**
Focused intensity	**$>10^{21}$ W/cm^2**	**10^{17} W/cm^2**

Table 1 Key laser parameters

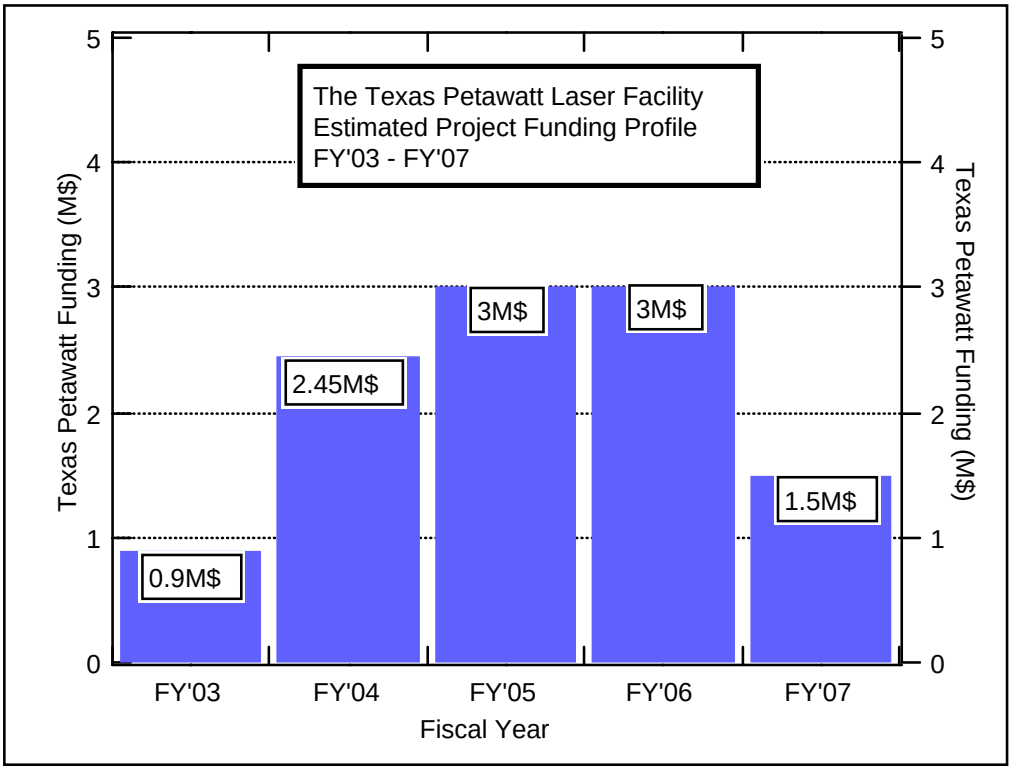

Figure 2 Estimated funding profile.

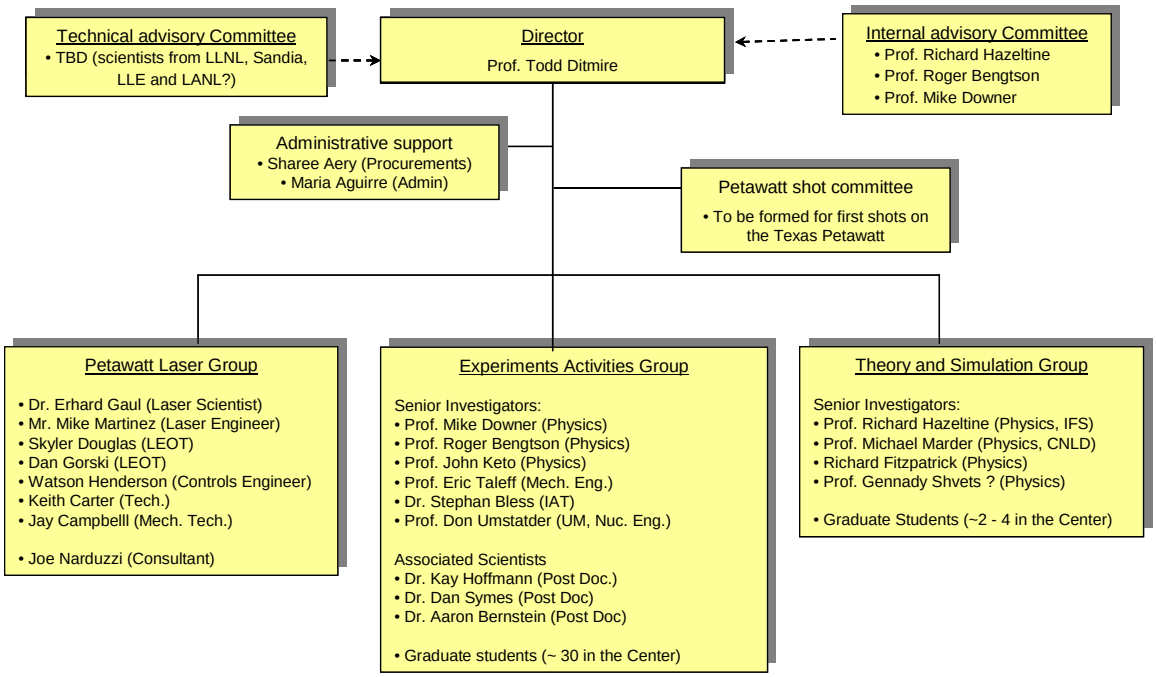

Figure 3 Organization chart of TCHILS.

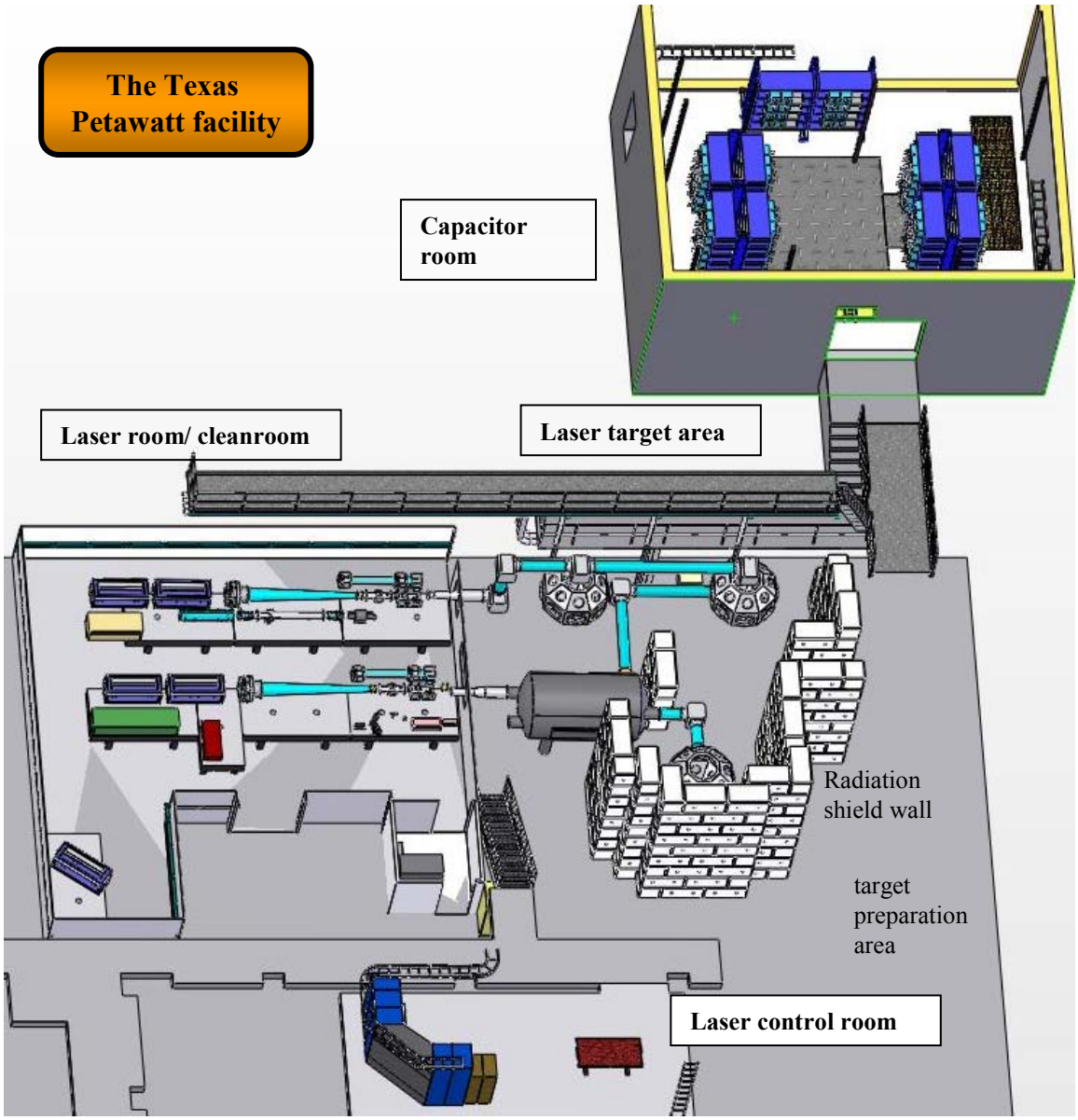

Figure 4 Functional schematic of the laser systems.

2 Scientific motivations and laser requirements

2.1 Introduction

The extreme states of matter that can be accessed with a Petawatt laser are exotic and unprecedented. Study of this matter and the applications that arise from such intense laser matter interactions represents one of the most exiting fields of study in modern physics. This excitement has led to the development of petawatt –class, short pulse lasers around the world. There are a number of unique applications which demand high energy (>100 J) pulses with durations shorter than that found on most high energy petawatt lasers presently under development. These applications represent the motivation for the Texas Petawatt laser. In addition, the scientific capabilities of a novel, near 100 fs high energy petawatt laser can be greatly enhanced if it is accompanied by a temporally synchronized nanosecond kJ class laser. It is these scientific possibilities which have driven the design of the laser described in this report. To motivate the system described here, we briefly address some of the applications envisioned for the Texas Petawatt, and the laser parameters needed to realize these experiments. As a whole, they drive the capabilities designed into the Texas Petawatt facility. Though not a comprehensive set of applications, the experiments described in this section give a flavor of the science program which can develop with the construction of the Texas Petawatt.

2.2 Production of high fluxes of neutrons with lasers

The extreme states of heated matter that can be accessed by a petawatt laser lead to a wide variety of applications. The bright radiation emitted from hot laser plasmas may itself be of interest for many interesting applications, particularly if the short time duration of these radiation bursts is exploited. While x-rays from laser plasmas are an obvious example of such radiation sources and will be an important application of the Texas Petawatt, petawatt laser interactions may lead to more exotic radiation sources, such as bright fusion neutron sources. Such sources may have many uses though perhaps one of the greatest fundamental applications of a bright fusion neutron source will be in the study of how fusion neutrons affect materials (and how these materials are damaged). With this motivation, fusion neutron source development is one of the principal science areas to be explored with the Texas Petawatt.

This research area is driven by some recent, spectacular results on smaller scale lasers. Recent experiments conducted on the interaction of intense, femtosecond laser pulses with atomic or molecular clusters of a few thousand atoms each have revealed that these interactions can be extremely energetic and that high energy ions are produced from the explosion of these clusters [Dit 97, Lez 98]. This phenomenon be exploited to produce DD fusion neutrons in a gas of exploding deuterium clusters (illustrated in Figure 5) [Dit 99]. From this experiment it appears that reasonable fusion efficiencies are possible even with lasers of modest energy per pulse. In particular, we believe that, with the Petawatt laser, and a reasonable extrapolation of current results, we may be able to produce as many as 10^{11} DD fusion neutrons per shot. This suggests an intriguing possibility in which a laser-driven neutron source could be used to realize a high-flux neutron facility for a variety of unique materials science experiments of direct relevance to neutron radiation damage studies or neutron radiography. This approach takes advantage of the small scale associated with a laser-plasma source (<0.1 mm^3 source volume) to achieve high flux over small areas with modest total neutron production. Exploiting the potential advantages of such a laser driven source (which include short pulse duration in addition to small emitting

volume), unique radiation damage materials experiments may be possible, including time resolved pump-probe experiments to explore the fast (nanosecond to picosecond) dynamics of neutron damage or even fusion reactor end-of-life damage testing on small micro-samples [Per 00].

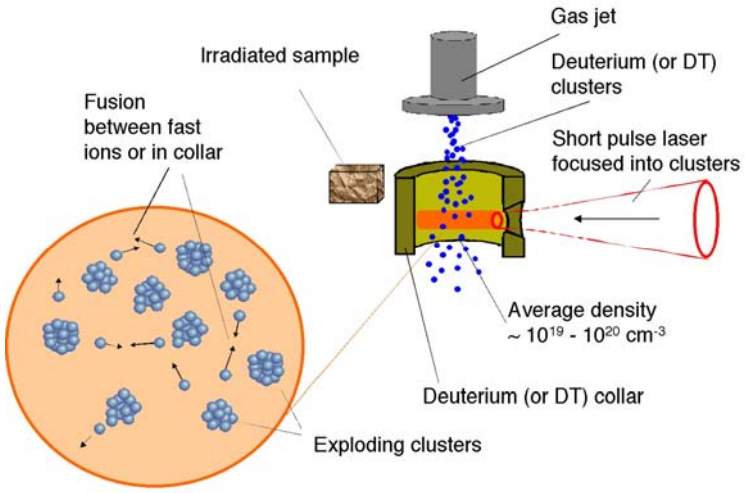

Figure 5 Schematic of the exploding cluster fusion neutron source.

Using intense femtosecond lasers to produce high fluxes of fusion neutrons may now be possible exploiting techniques developed at LLNL and at UT with laser driven deuterium cluster explosions [Dit 99]. Here, ions released from energetic explosions of deuterium clusters irradiated with femtosecond laser pulses drive DD fusion, as illustrated in Figure 5. In this experiment, a high intensity, ultrafast laser pulse is focused into a gas of deuterium clusters and rapidly heats them. These clusters subsequently explode, ejecting deuterium ions with energies of many keV. This process creates a plasma filament with a diameter roughly that of the laser focus and a length comparable to the extent of the gas jet plume (~ 1 mm). The fast deuterium ions ejected from the exploding clusters can then collide with ions ejected from other clusters in the plasma or with ions in a high average density deuterated (or DT) collar. Fast ions in the few keV range will undergo fusion reactions within the heated filament itself. However, if ions with energy greater then 100 keV are produced, the fusion efficiency can be increased by beam-target fusion within a higher density, cold collar surrounding the heated filament. It has also been shown that the neutron burst from this interaction is well under 1 ns in duration and may be as short as 50 ps [Zwe 00].

This kind of neutron source raises the interesting possibility that this source could be used as a fast pump to initiate damage in a material which could then be interrogated with a second, laser derived probe (such as an optical or x-ray pulse). Such a pump-probe experiment could yield unique, fundamental information on the dynamics of radiation damage in materials, shedding light on damage mechanisms such as the thermal spike predicted in neutron damage of metals from molecular dynamics simulations [Ave 98]. This science has been well studied by molecular dynamics simulations but never probed in experiments because suitable high flux, short pulse radiation sources do not yet exist. The ability to probe such dynamics either with part of the ultrafast laser pulse, or with ultrafast x-ray pulses, produced by the same intense laser, offer a wide array of options for studying unexplored dynamics of materials damage by fusion neutrons. In these pump-probe studies the neutron pulse could initiate damage in the material and then the

formation and decay of disordered regions in the material can be studied via optical or x-ray scattering, ultimately validating (or disproving) the thermal spike behavior predicted by simulations. In simulations, such dynamics exhibit time scales ranging from a few ns (amorphization in Si [Cat 96]) to a few ps (thermal spike in mid-Z metals). Thus, an ultrafast neutron source like that proposed here would be completely unique, enabling a class of fundamental experiments that are not possible with any other neutron source. However, we estimate that up to 10^9 n/cm^2/shot will be needed to perform this class of experiment.

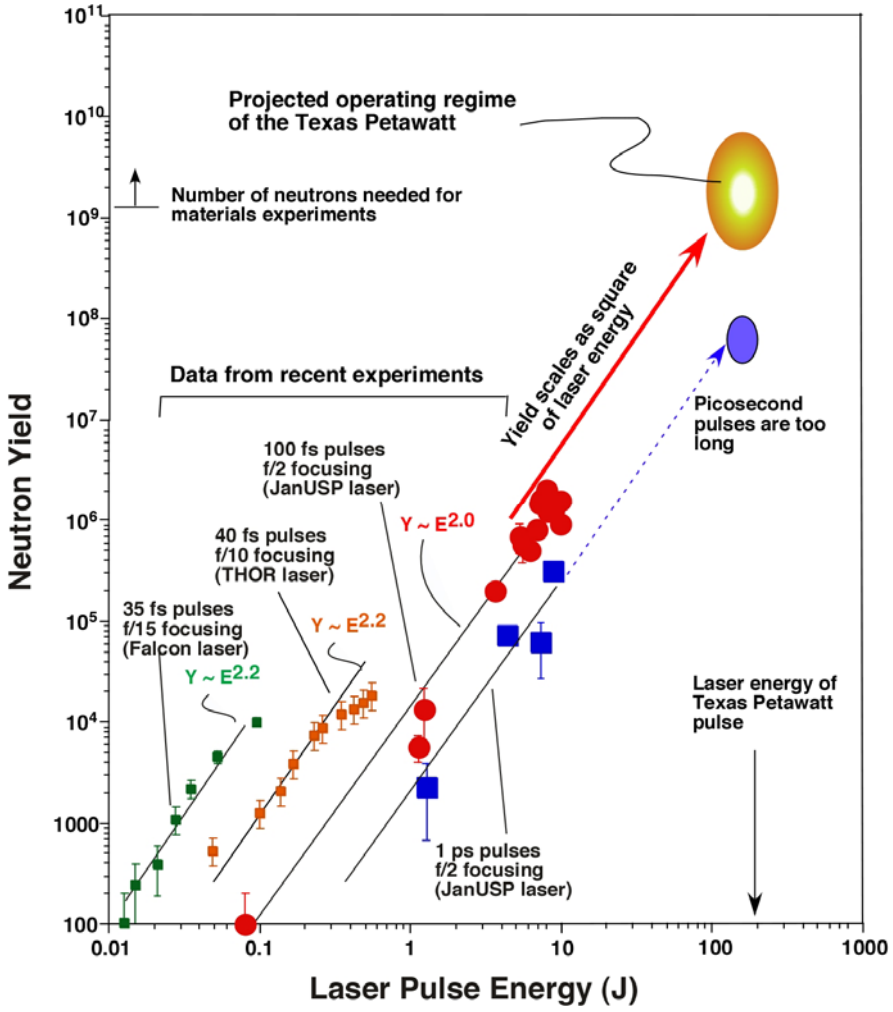

Figure 6 Scaling of neutron yield strongly suggests that a 200 J, 150 fs laser will enable neutron damage experiments with neutron yield approaching 10^{10} n/shot.

Recent experiments suggest strongly that a petawatt laser, with the correct parameters can achieve this yield of neutrons. This is illustrated in Figure 6. We have conducted experiments on neutron yield with laser energy ranging from 10 mJ to 10 J. Over a this wide range of energy, and on various laser systems we find that the yield scales as the square of the energy, a scaling which is easily understandable (see [Mad 04]). Scaling data taken from the LLNL JanUSP laser and the UT THOR laser suggest that neutron yields of up to 10^{10} n/shot will be possible with the Texas Petawatt. An important finding, however, has been that the neutron yield is much higher if 100 fs pulses are used instead of 1 ps pulses (see Figure 6). This large advantage with shorter pulses

motivates the development of a 200 J laser with pulse duration as near 100 fs as possible. The design of the Texas Petawatt should allow us to access the neutron yield regime needed for this new class of time resolved materials damage experiments.

2.3 Study of Laser Heated Matter

Another major motivation for the construction of the Texas Petawatt laser is the study of extreme states of solid or higher density matter. In particular femtosecond petawatt lasers are unique in their ability to concentrate energy in a small volume. A dramatic consequence of this concentration of energy is the ability to create matter in high temperature and pressure conditions. Matter with temperature and density near the center of dense stars can be created in the laboratory with an appropriately designed petawatt laser. For example, solid density matter, or matter shock compressed with another laser, can be heated to temperature of over 10,000,000 ºC (>1 keV). Under these conditions, the particle pressure inside the sample is over 1 billion atmospheres, far higher than any other pressure found naturally on or in the earth and approaches pressures created in nuclear weapons and inertial confinement fusion implosions.

Study of the properties of matter at these extreme conditions, namely solid density (ie $\sim 10^{22}$ cm^{-3}) or higher in the temperature range of 1 eV to 1000 eV, is crucial to understanding many diverse phenomenon, such as the structure of planetary and stellar interiors or how controlled nuclear fusion implosions (inertial confinement fusion or ICF) evolve. Yet, despite the wide technological and astrophysical applications, a true, complete understanding of matter in this regime is not in hand.

Over the last fifteen years, since the development of high energy short pulse lasers, there have been a number of experimental studies aimed at isochorically heating solid density targets with a femtosecond laser pulse [Aud 02, Wid 01]. This class of experiments uses a femtosecond pulse to heat, at solid density, an inertially confined target on a time scale much faster than the hot material can expand by hydrodynamic pressure. Figure 7 illustrates the parameter regime accessible with short pulse laser heating. Here, the phase space of aluminum is illustrated. When the material is heated from its initially cold, solid state, the plasma will be in the "strongly coupled" regime, denoted by the state in which $\Gamma>1$, even at temperature approaching 1 keV. Here Γ is the ratio of particle potential energy to its kinetic energy.

To date, these kinds of studies have centered on an approach in which a laser directly heats a sample, and the energy deposits within an optical skin depth. Direct laser heating has drawbacks. Because of the small depth of the heated region (~10 nm), the expansion time of the sample is often only 100 - 200 fs. The few hundred fs release time of the heated material is comparable to the electron-ion equilibration time [Spi 67] and hampers interpretation of this kind of experiment. Microsopically rough surface finish of the very thin target often leads to a large uncertainty in the initial density, complicating analysis of the data. Consequently, it is desirable to explore mechanisms of heating larger volumes (ie thicker layers) of material. One promising approach is to use fast bursts of penetrating radiation, such as protons or x-rays, to heat thicker layers of material than are possible with direct optical heating. Use of x-rays to perform isochoric heating was first proposed by Lee et al in the context of X-ray free electron lasers sources [Lee 02, Lee 03]. A multi keV x-ray pulse can, for example, penetrate many microns of material (depending on the wavelength and target Z). One way to produce an intense, ultrafast burst of hard x-rays for such an x-ray heating experiment is to use a high peak power short pulse laser to produce K_α

radiation on a solid target, an idea shown in Figure 8. Such x-ray radiation is produced during the illumination of a solid target. Fast electrons are produced in the interaction which travel into the cold target and excite inner shells in the target atoms. These x-rays have been shown to exhibit pulse duration under 1 ps if ultrafast laser illumination is employed.

We believe that this approach has a lot of promise. We have recently conducted experiments using the 10 J JanUSP laser at LLNL to heat with Si K-alpha x-rays an Al target to a temperature of about 0.5 eV. To access higher temperatures will demand a higher energy laser. The Texas Petawatt laser will extend these initial experiments to temperatures of 10 to 100 eV by greatly increasing the x-ray yields available. Again, shorter pulses are optimum for this application, though the pulse duration requirements are not as stringent as those needed for the neutron generation experiments.

In addition, even more exotic regimes can be accessed if the heated material can be first compressed with, say a strong shock wave. This pre-compression can be achieved with a second, high energy shock compression laser pulse. With a pulse of 500 J, initial shock pressures of 1 Mbar can be achieved in ~1 mm size samples. With this motivation, the Texas Petawatt laser is designed with a second, long pulse shock compression beam. A shock compression beam needs to be at shorter wavelengths to prevent hot electron generation that leads to unwanted preheating of the sample. Hence, the Texas Petawatt second long pulse beam will be frequency double to 527 nm.

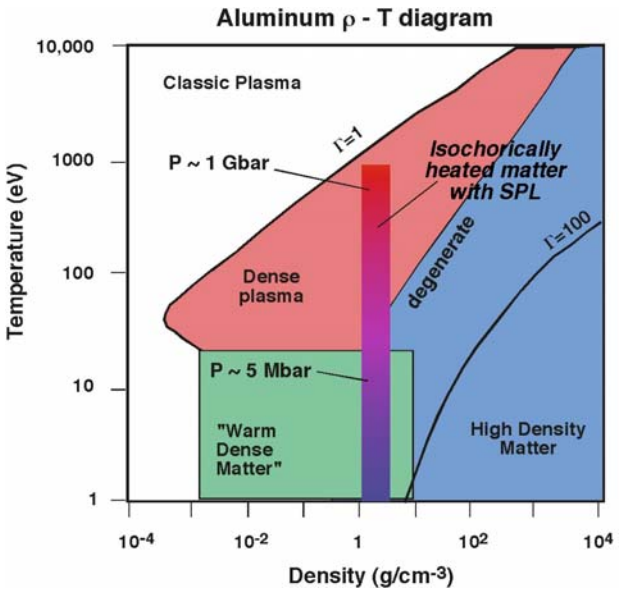

Figure 7 Temperature-density space for an Al target showing the regime accessible with short pulse laser isochoric heating.

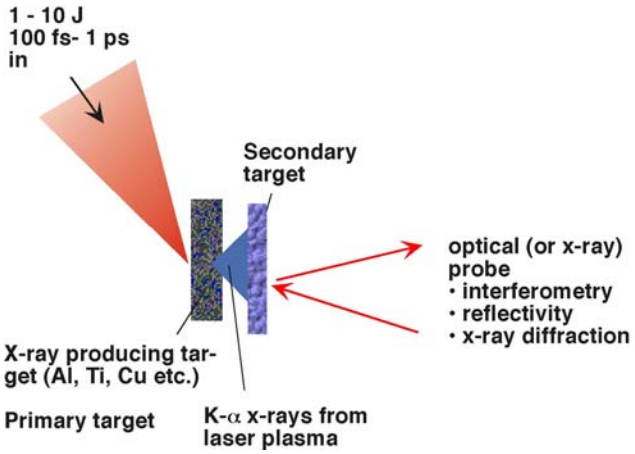

Figure 8 Target heating with laser produced x-rays.

2.4 Dynamics of Shocked Materials

Another class of high energy density experiments which will be possible on the Texas Petawatt laser facility involves the study of materials under shock compression. Equilibrium studies of shock compressed materials are often conducted with gas guns or explosives. However, the development of high power pulsed lasers opened the potential to study shock compression at much higher pressure and higher strain rate [Mos 00]. The laser pulse ablates the surface of a target and the material blow-off acts as a rocket engine which drives a shock into the underlying cold material. Because of the fast rise of such a laser shock drive, quite high strain rates, $>10^7$ s^{-1} can be driven in a material.

High power lasers can access much higher pressures, up to 1 to 10 Mbar, than are obtainable with gas guns or easily derived with small to mid-scale explosive experiments [Tra 79]. More important, however, is the fact that an intense laser can produce a probing pulse, synchronized to the shock driving pulse, to examine the dynamics of the material. This probe can be optical, and can probe the surface properties (like conductivity through reflectivity) with high time resolution. In addition, an intense laser can produce a bright burst of x-rays (via mechanisms discussed in the last section) that can probe the dynamics of the materials on the lattice level. This approach can, in principle, begin to examine atomic motion behind the shock (and around defects) [War 89], a possibility which could yield unprecedented information on deformation mechanisms and defect generation.

The Texas Petawatt will be ideal for this class of experiment. The 500 J long pulse beam can drive shocks into materials with pressure of above 1 Mbar. These shocks can then be probed with the petawatt beam line. Ultrafast optical probes can shed light on the dynamics driven by the long laser pulse. The principle behind these experiments is illustrated in Figure 9. It is possible to use the fact that the linear and nonlinear optical properties of a material differ when the solid becomes a liquid. This means that the material reflectivity will change as it undergoes a phase transition to a liquid and its nonlinear optical properties can change. The latter fact can be exploited if second or third harmonic is generated off the back of a target that is shocked and the harmonic intensity is monitored via pump-probe techniques. This approach has been used in the study of femtosecond laser induced melting in semiconductors such as silicon (Shank et al., 1983). More importantly, the Petawatt pulse can act as a synchronized driver of high brightness

x-rays for diffraction experiments. While long pulse lasers have been used as x-ray backlighters for many years, the higher energy x-rays accessible with a petawatt offer more interesting possibilities. This area of research will be coupled with the advanced x-ray source development envisioned on the Texas Petawatt (discussed below).

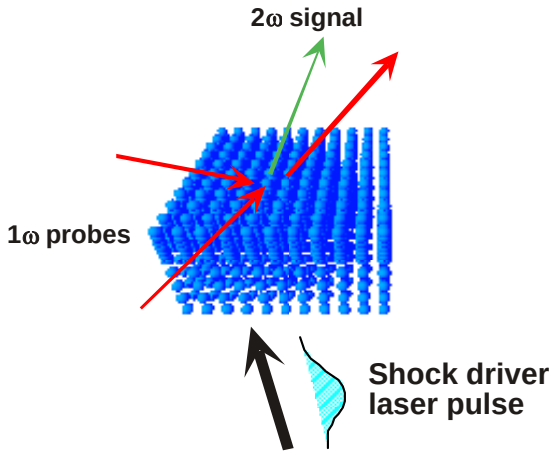

Figure 9 Schematic idea of probing a long pulse driven shock with a synchronized short pulse laser.

2.5 Strong Field Physics

In addition to the high energy density experiments that motivate the Texas Petawatt, there are a number of fundamental high field physics experiments that will be performed on the laser. One example of a fundamental problem that can be addressed with the Texas Petawatt is that of ionization of highly charged ions at highly relativistic intensity (>10^{21} W/cm^2).

The physics of strong field ionization is well studied at intensities below 10^{18} W/cm^2. When an intense laser field of sufficiently long wavelength illuminates an atom, the ionization can be described by tunnel ionization. This tunnel ionization rate has a very strongly nonlinear increase with increasing laser intensity and therefore exhibits a threshold like behavior. The thresholds for various ions are shown in Figure 10. This figure illustrates that at the intensities likely achievable with the Texas Petawatt, high Z ions can be fully stripped by this tunnel ionization.

Strong field tunnel ionization also has an interesting consequence in that it effectively ejects a free electron into the laser field at a well defined phase of the field, with ionization occurring predominantly at the peak of the field where the ionization rate is highest. The electron then acquires some drift energy from the field. This kinetic energy is often termed above threshold ionization energy (or the ATI energy) [Ago 87]. ATI at sub-relativistic intensities is well understood; the tunnel ionized electron picks up a drift velocity that is related to the phase in the laser oscillation at which it is ionized [Bur 89]. In a strongly relativistic field, these dynamics will be different. Ionization of a very highly charged ion effectively "injects" a free electron into the field at phase near the field peak. When the laser field $a_0 >> 1$, the $\mathbf{v} \times \mathbf{B}$ force curves the trajectory of the electron along the laser propagation direction in a small fraction of the field cycle. The electron with $v_z \sim c$ can then "surf" along with the field, acquiring energy from the electric field. This phenomenon was described in detail by Hu *et al* [Hu 02]. Hu and Starace found that electrons ionized from V^{22+} by 8 x 10^{21} W/cm^2 pulses would be ejected with energy up to 2 GeV.

To illustrate the dramatic acceleration of electrons that may occur in the focus of the Texas Petawatt we calculated ionization of Ar^{17+} ions by a laser focused to an intensity of 5 x 10^{21} W/cm^2. These results appear in Figure 11. These electrons emerge from the focus in a narrow cone along the laser propagation axis and exhibit energies up to 0.7 GeV. This is a dramatic departure from the usual, sub relativistic ATI behavior which is well known from strong field ionization experiments. The longitudinal ponderomotive force is responsible for the forward directed electrons seen in this simulation. These kinds of strongly relativistic dynamics will be observable with the Texas Petawatt laser.

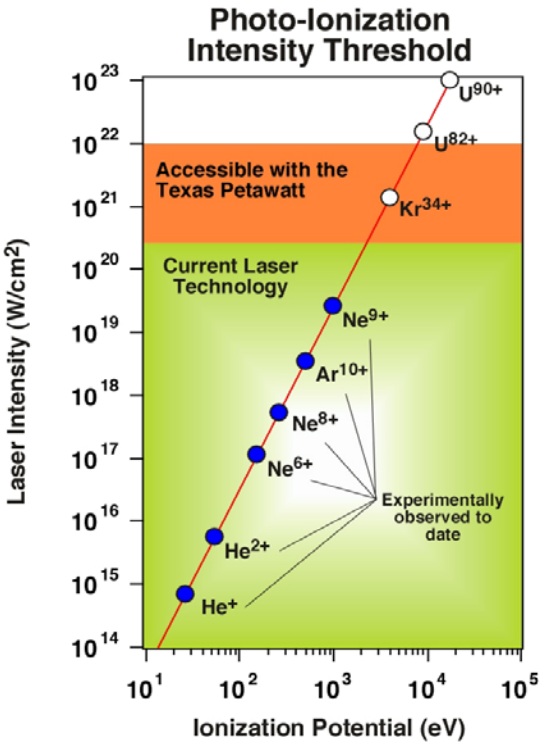

Figure 10 Ionization thresholds of various ions as a function of ionization potential.

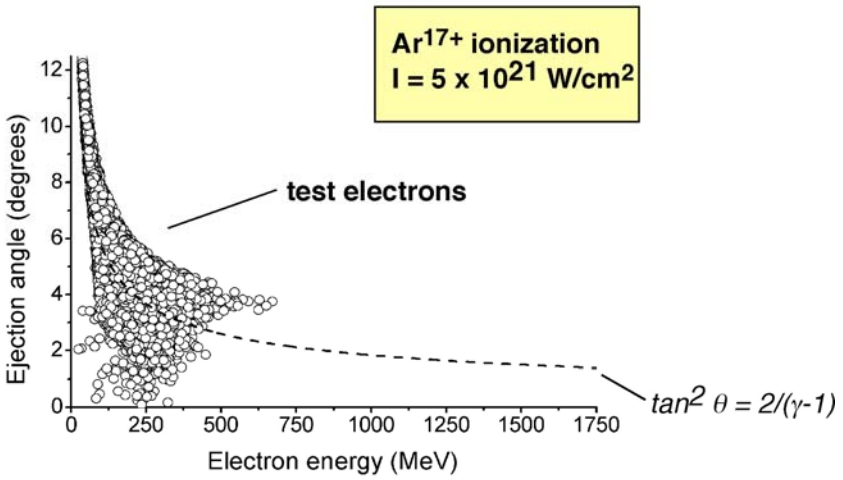

Figure 11 Calculation of electron energies ejected from ionization of Ar ions by a petawatt laser.

2.6 Radiative hydrodynamics

Another area of shock physics which will have many new opportunities with the Texas Petawatt is that of strong shocks in gases. Such shock studies have some relevance to astrophysical phenomena. Astrophysical shocks play an important role in the evolution of the inter-stellar medium providing an energy source, and triggering a variety of phenomena including star formation [McK 91]. On galactic time-scales, supernovae are a frequent source of such shock waves, which expand into the surrounding medium sweeping up material into a thin, dense shell. If the circumstellar medium is sufficiently dense, radiation can play an important role in the energy transport dynamics of the supernova remnant blast wave [Bar, 00]. It is also believed that various shock instabilities associated with these radiative shocks, including the well known Vishniac overstability, have an important effect on the structure of interstellar matter [Vis 83].

To create a laser driven radiative blast wave, it is necessary to produce a localized, high temperature plasma in a modest density gas without perturbing the surrounding medium with the incoming laser. The Texas Petawatt laser will have two ways of accessing these high Mach number blast waves. The first will be possible with a high energy long pulse laser. With a kJ class beam, a pin target immersed in gas can be irradiated to drive a blast wave in the surrounding gas. This has been successfully achieved using the Z-Beamlet laser at Sandia and a picture of such a blast wave is illustrated in Figure 12. The long pulse beam at the Texas Petawatt will allow similar experiments, at a much improved shot rate.

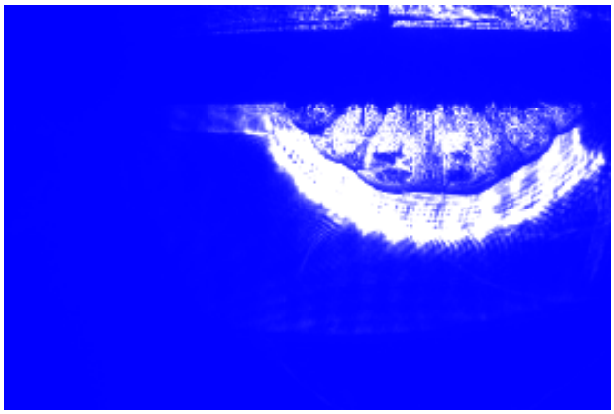

Shot 37: 300ns

Figure 12 Schlieren picture of a cm radius blast wave driven by the Z-Beamlet laser in nitrogen gas.

The second way in which such shocks could be accessed in the Texas Petawatt is to utilize the now well characterized high absorption efficiency of high intensity femtosecond lasers in gases containing large clusters [Dit, 00, Shi 00]. An intense laser focused into a strongly absorbing cluster gas will produce a hot, elongated filament which will subsequently develop into a cylindrical shock [Edw 02]. This approach has the advantage that the laser does not propagate through and disturb the gas in which the blast wave subsequently propagates [Ede 04]. As with the neutron experiments the efficient coupling of the laser to the clusters requires that the pulse is short, again motivating the construction of a near 100 fs Petawatt beam.

2.7 Advanced laser driven x-ray sources

A high energy petawatt laser can, with the right kind of targets, drive very high brightness x-ray sources. The number of approaches possible here is large and this avenue of research is being well cultivated by a number of labs around the world. We envision that the Texas Petawatt will be used in a number of applications where a bright x-ray source is needed (many discussed above).

With this motivation, the Texas Petawatt will be utilized in an experiment program examining K-alpha generation from novel targets. In particular, the use of sharp conical targets holds the promise of much increased x-ray brightness. Sentoku et al [Sen 04] have shown that micro-focusing of laser pulses in a sharp cone leads to focusing of the hot electrons generated by the laser pulse. Such a target is illustrated inFigure 13, where a sharp pyramidal cone has been etched in a silicon wafer. The Texas Petawatt will be coupled to targets like this and x-ray yields will be investigated.

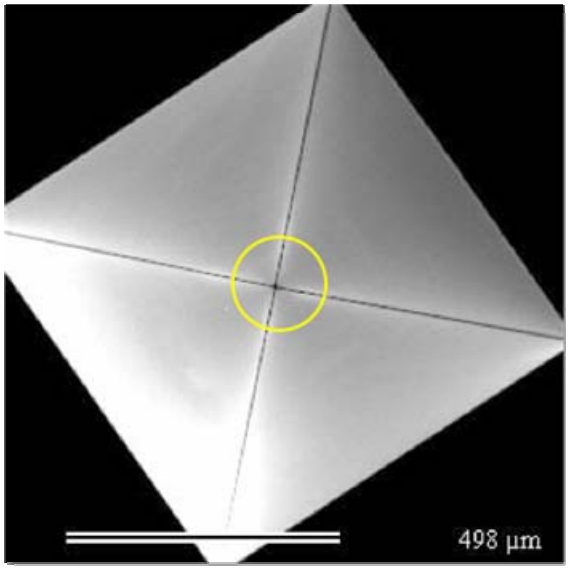

Figure 13 SEM picture of a pyramidal target in a Si substrate.

2.8 Particle acceleration

In addition to driving shock waves and heating materials, intense lasers can also accelerate charged particles. An electron oscillating in an intense laser field will acquire quiver energy, the so-called ponderomotive energy, which can be quite substantial. A near IR laser focused to an intensity of 10^{20} W/cm^2, an intensity easily achieved with a petawatt laser, will drive electrons to ponderomotive energy in excess of 1MeV. The strong forces that the laser can exert on charged particles, then lead to potential applications in high energy density and plasma science in which relativistic electrons are important.

A major milestone in the studies of laser particle acceleration would be to achieve a controlled acceleration of a particle bunch up to ~1 GeV in a single accelerator stage. In controlled laser wake field acceleration (LWFA) the electron density perturbation is at a moderate range ($0.1 < \delta n_e/n_e < 1$). This requires intensities of the order 10^{18} W/cm^2 ($a=eE/m_ec^2 \leq 1$). Furthermore, a large spot size ($w_0 >> \lambda_p$, where λ_p is the plasma wavelength), is desirable to minimize radial

effects and increase the Rayleigh range, which is equivalent to the acceleration length for unguided pulses.

Focusing an ultra-short (≤ 100 fs) petawatt laser pulse in a wide focal spot (w_0~100 μm) in rarefied plasma (n_0~10^{17}cm^{-3}) gives an opportunity to accelerate electrons over a distance of twice the Rayleigh length (~8 cm). These electrons can gain energy up to 1 GeV by LWFA without pulse channeling (Figure 14). Simulations suggest that acceleration of a rather long (τ_b~ 0.3×10^{-2} s) non-resonant electron bunch with initial particle energy of about 1 MeV forms a low-emittance electron bunch with energy in the range 900 ± 50 MeV.

The drive laser for such experiments require short (<100-150 fs) pulses to increase the resonance electron density and acceleration gradient. It also requires high energy (>100J) to increase the spot size at intensities of 10^{18} W/cm^2 and acceleration length >> 1 cm.

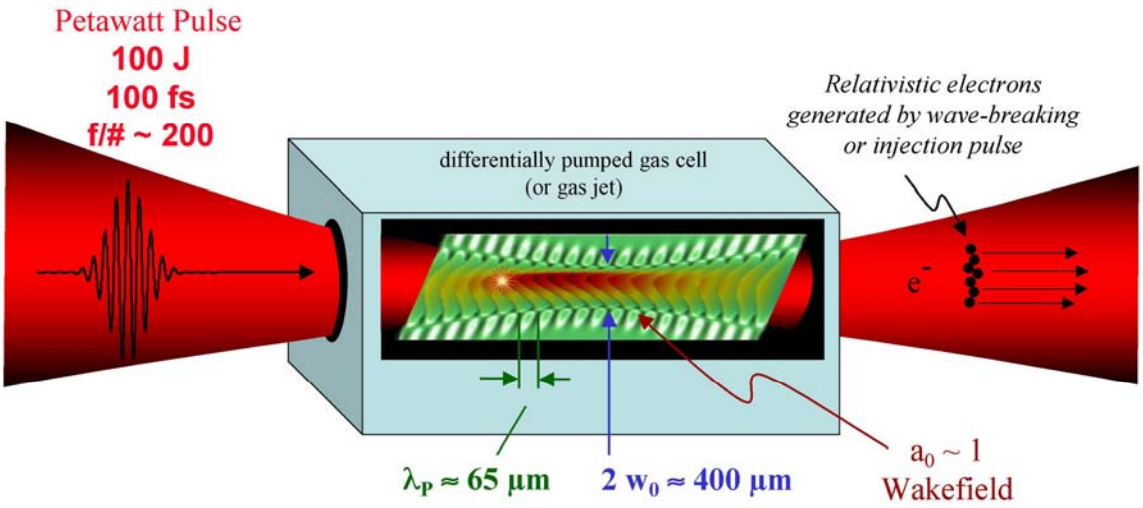

Figure 14 Schematic picture of flat-field, resonant, multi-GeV Petawatt driven LWFA.

The long pulse laser focused onto a line in a rarefied gas would ionize and heat the gas. The resulting cylindrical shockwave can form an electron density channel that is suitable to optically guide a laser pulse. Combining the Petawatt pulse as the wakefield driver with the long pulse laser for channel formation could further increase the energy of the accelerated particle bunch.

3 Conceptual design for the Texas Petawatt

3.1 Introduction

In recent years a number of approaches to high energy lasers using chirped pulse amplification (CPA) techniques have been explored. In particular, Nd:glass systems have been extremely successful in pushing CPA to the multi-joule level, as illustrated by the extreme scaling of CPA in glass by the LLNL Petawatt. While Nd:glass is attractive because of the high optical quality and large apertures that are possible with glass, Nd:glass exhibits a rather limited gain bandwidth of ~ 10 nm. This limited gain bandwidth in glass and the effect of gain narrowing prohibits amplification of laser pulses with recompressed pulse widths much below one picosecond. Due to the nature of many of the experiments proposed under this Center, a pulse width near 100 fs is desirable. Thus, a typical Nd:glass architecture is not appropriate for the laser envisioned.

The current material of choice in the ultrafast laser community for amplification of pulses with width below 100 fs is Ti:sapphire, which exhibits a bandwidth of nearly 300 nm. CPA at a wavelength of 800 nm with pulsewidths as low as 20 fs have been demonstrated in a number of labs [Bar 96]. A number of groups worldwide are currently pushing Ti:sapphire lasers to the multi-hundred TW level by amplifying ~ 30 fs pulses to multi-joule levels. Despite this broad bandwidth, Ti:sapphire's largest disadvantage for high energy systems is that the short excited state lifetime of Ti:sapphire (3.2 μs) demands that it must be pumped by a second laser operating in the green (such as the second harmonic of a ns Nd:YAG or Nd:glass laser).

To push the pulse width attainable in glass laser systems, hybrid systems of Ti:sapphire and Nd:glass have been successfully deployed. In this approach, fs, broadband pulses are initially amplified in Ti:sapphire, at a wavelength of 1057 nm, to the few mJ level, and the remainder of amplification is achieved in the Nd:glass. By limiting the gain in the Nd:glass to <10,000, the gain narrowing of the seed pulse is not so severe. In fact, the LLNL petawatt laser utilized this approach and has demonstrated compressed pulses of ~ 400 fs [Per 99]. Yet this technique has some downsides: the gain in Ti:sapphire at 1 μm is quite low making the preamplification difficult. The short excited state lifetime of the Ti:sapphire also leads to rather extensive amplified spontaneous emission (ASE), an artifact that gives rise to ns scale prepulse on the main laser pulse.

Nonetheless, this hybrid approach has many attractive features. In particular, it should be possible, to push this approach to extreme limits. If a broadband laser front end (such as the Ti:sapphire front end of the Petawatt) can be fielded to the ~1 J level, and gain in the Nd:glass is limited, quite short laser pulses can be achieved. The proposed Texas Petawatt utilizes this proven approach, but, though the use of the latest advances in CPA. will scale the approach to pulse widths as short as 150 fs and energy of 200 J. This will represent an internationally unique laser, with specifications that are different than the longer pulse, higher energy petawatt lasers under development around the world, and with energy much higher than is likely possible in pure Ti:sapphire lasers for some time.

3.2 Scientific design study of the Texas Petawatt

The general approach of this design is to amplify stretched, nJ level pulses to near the 1 J level in a broad band amplifier medium and then further amplify these pulses in mixed silicate and phosphate Nd:glass amplifiers. By reducing the gain in the glass, gain narrowing can be minimized and compressed pulses near 100 fs will be possible. This requires maintenance of 14 to 16 nm of bandwidth through the laser chain at a wavelength of 1057 nm. This can be achieved in principle by minimizing the gain in the Nd:glass to of the order of 100. Furthermore, mixed glass will allow these bandwidths to be maintained up to full energy. This approach builds upon previous work conducted by a number of groups using mixed glass amplifiers for broad band amplification. The general idea is to push the limits of this technique, using glass only as the final stage of amplification.

This approach to developing a petawatt has a couple of distinct advantages. Phase control of chirped pulses at the 100 fs pulse duration is well developed and quite straight forward. This means that the solitary challenge in recompressing the amplified pulses is in defeating the gain narrowing (as opposed to the development of sub 30 fs Ti:sapphire petawatt class lasers which require careful higher order phase compensation because of the large bandwidths involved.) Furthermore, direct amplification in glass allows amplification at 1 μm (instead of 800 nm) where very high quality, high efficiency diffraction gratings can be obtained.

Amplification in glass is straightforward and permits the maintenance of good beam quality at large aperture. The approach taken in this design is to utilize two standard Nova 315 mm disk amplifiers in the final amplification stage.

In practice there are two potential approaches to developing the broad band front end. The first uses the proven technique of Ti:sapphire amplification at 1 μm. This approach has substantial drawbacks because of the very low gain of Ti:sapphire at 1 μm. Many amplification passes are required to boost energies from nJ to mJ. Furthermore, as mentioned, the short fluorescence time of Ti:sapphire tends to cause substantial ASE problems, which are particularly troublesome in CPA because ASE contributes to prepulse in the < 1 ns range before the pulse (where it is difficult to suppress with Pockels cells).

The approach chosen here is to utilize the recently developed technique of optical parametric chirped pulse amplification (OPCPA). This is a nonlinear optical technique relying on difference frequency generation in a nonlinear crystal. Simply, a short wavelength pump light is mixed with chirped, low energy seed light. The difference frequency generation transfers energy from the pump into both the seed and an idler beam. OPCPA has the broad gain bandwidths needed for the front end amplification. The very high gains possible with OPCPA allow simple, few pass amplification, and OPCPA in standard crystals are well suited to amplification at 1 μm because it can be resonantly pumped with frequency doubled YAG/YLF/glass at 0.53 μm.

This technique has been successfully demonstrated by the group led by Ian Ross at the Rutherford Appleton Laboratory in the UK [Col 99, Ros 00] which demonstrated OPCPA amplification of 1 μm seed pulses pumped by the frequency doubled light of 600 ps from the Vulcan laser [Ros 00]. They demonstrated amplification to the 100 mJ level. We propose to extend these successful studies and utilize this technique in the front end of the Texas Petawatt.

3.3 Architecture of the Petawatt laser

The schematic of the laser is illustrated in Figure 15. The system begins with a 100 fs, tunable oscillator. The oscillator pulses are stretched to nearly 2 ns after appropriate isolation. Also the spectrum and spectral phase can be pre-shaped by a Dazzler to optimize the final pulse. After a 10 Hz slicer Pockels cell the pulses are amplified by parametric amplification in three stages. A Ti:sapphire amplifier was added to use efficiently the pump photons residual from the OPCPA and boost the amplified pulses to about 1 J. A silicate glass rod amplifier and a phosphate glass NOVA disk amplifier increase the energy to about 300 J in four passes while keeping the bandwidth broad enough for 150 fs pulses. A grating pair recompresses the pulses to about 150 fs. The total energy will be limited by the damage fluence of the compressor gratings. The design parameters of the laser are summarized in Table 2.

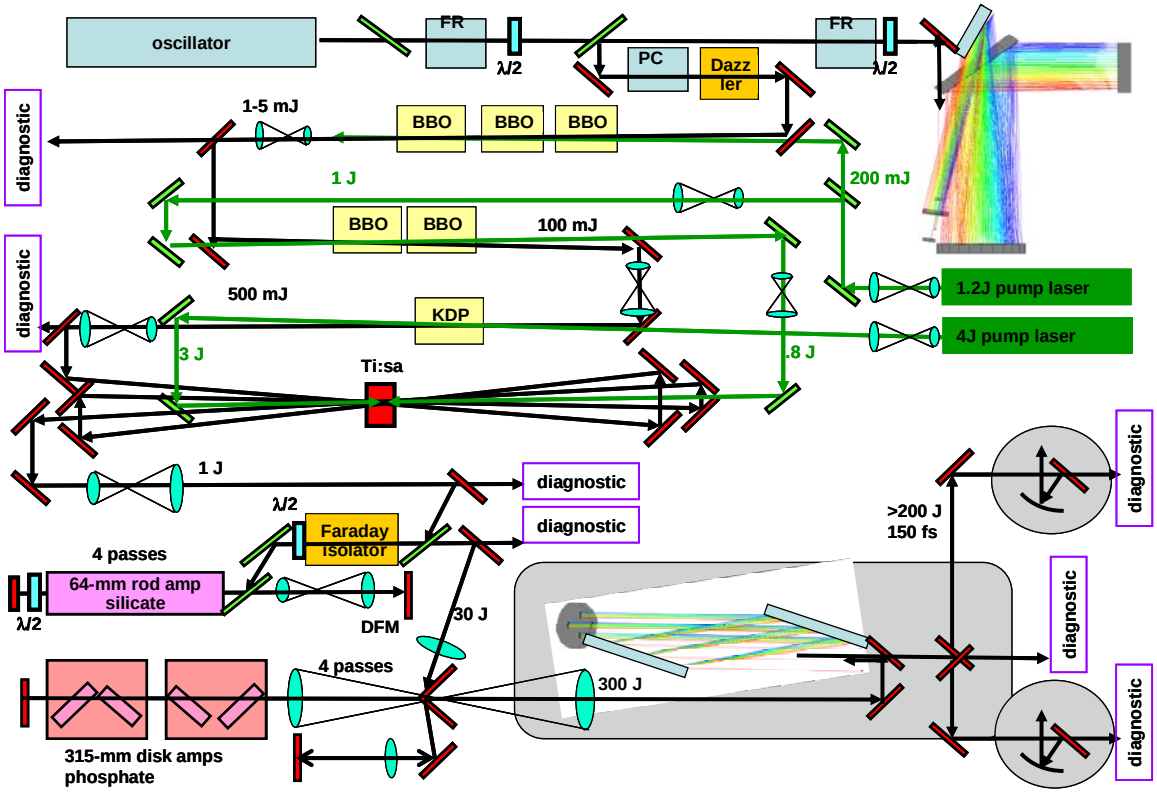

Figure 15 Schematic overview of the Petawatt laser chain.

3.3.1 Critical design issues of the laser

We have identified a number of critical design issues in this laser chain. The most critical is the design of the compressor because the damage fluence on gratings is low compared to mirrors, lenses and amplifiers. It turns out that it is useful to design the compressor first, design a matching stretcher, and work the chain backwards, addressing all critical parameters starting from the large amplifier back to the oscillator.

The timeframe and budget of the project do not allow for significant development of grating technology and the compressor design will therefore be limited by availability, size, damage fluence, bandwidth and cost of the gratings. The final beam size as a result of the compressor design will significantly affect the size and cost of the beam transport, focusing optics and target chambers.

Laser chain element	Pulse energy out (J)	Beam diam (cm)	Beam fluence (J/cm^2)	Pulse spec. width (nm)	Comp. pulse width (fs)	ΣB rad	Pump beam parameters Size (cm) | En (J) | Int. (MW/cm^2) | Fluence (J/cm^2)
Ti:sapphire oscillator	3×10^{-9}	0.1	4×10^{-7}	16.4	100		
Stretcher (to 1 ns)	1×10^{-9}	0.2	3×10^{-8}	16.4	100		
Image telescope 1 (x 5)	1×10^{-9}	1.0	1×10^{-9}	16.4			
BBO group	1×10^{-3}	1.0	1×10^{-3}	14.8			.26 | 0.2 | 300 | 2.4
BBO pair	0.050	1.0	0.08	35	80		.60 | 1.0 | 300 | 2.4
Spatial filter 1 (x 1.2)	0.075	1.2	0.066	35			
KDP amp.	0.550	1.2	0.45	35	80		1.2 | 4.0 | 280 | 1.2
Spatial filter 2 (x 1.25)	0.5	1.4	0.13	35			
Ti:Sapphire amplifier	1.2	1.4	0.36	32	130	.012	1.5 | 0.8 | 200 | 0.8 1.5 | 3.0 | 350 | 1.4
Spatial filter 3 (x 2.5)	1.1	5.2	0.05	32		.015	
64 mm silicate Nd:glass rod amp	25	5.2	2.0	11.9	130	.27	
Faraday isolator	21	3.8	1.9	11.9		.51	
315 mm phosph. glass disk amp	260	8.4	3.8	10.6	160	.91	
Image teles. 2 (x 1.2)	258	13	0.5	10.6		.97	
Compressor	200	13	0.45	10.6	160		

Table 2 Design parameters of the Petawatt laser.

The bandwidth of the pulse after the glass amplifiers is limited to less than 11 nm or equivalent to a 150 fs Gaussian pulse. To reach a Petawatt, the energy out of the final amplifier and injected into the compressor has to be > 200 J. The available amplifiers from the NOVA laser have an aperture of either 94 mm or 315 mm. The 94 mm amplifiers contain six laser disks which has the advantages that a double pass in one amplifier plus a singles pass in a booster amplifier results in enough gain in phosphate glass. Furthermore, some phosphate disk could be exchanged for silicate disks to balance the overall spectrum. However, the average fluence at the final amplifier

is 3-4 J/cm^2 with a fill factor of more than 70 %. This requires use of platinum free laser glass and puts tight tolerances on the beam quality, especially for peak fluence issues. The amplifiers are currently not equipped with Pt-free glass and have to be refurbished resulting in significant project cost. The accumulated nonlinear phase (B-Integral, ΣB) has to be less than 1.5 to achieve reasonable compressibility and focusability of the beam. However, ΣB < 1 is desired and it is therefore necessary to stretch the pulse long enough to achieve low B-integral, higher damage threshold and better spatial overlap between the pump and seed beams in the OPCPA stages.

The 315 mm NOVA amplifiers have only two disks and should be used in pairs to balance the spatial non-uniformity of the gain. The disadvantage of these amplifiers is the lower gain per pass, such that a 4-pass through a pair of amplifiers (4 disks) is required to achieve enough net gain. These amplifiers require also more table space, more pulsed power equipment and a longer cooling time between shots. The advantages are the larger clear aperture, which significantly reduces the risk of damage due to high fluence, and lower ΣB to less than one at energies up to 400 J. Further advantages are that they contain Pt-free glass and can prepared and serviced at UT.

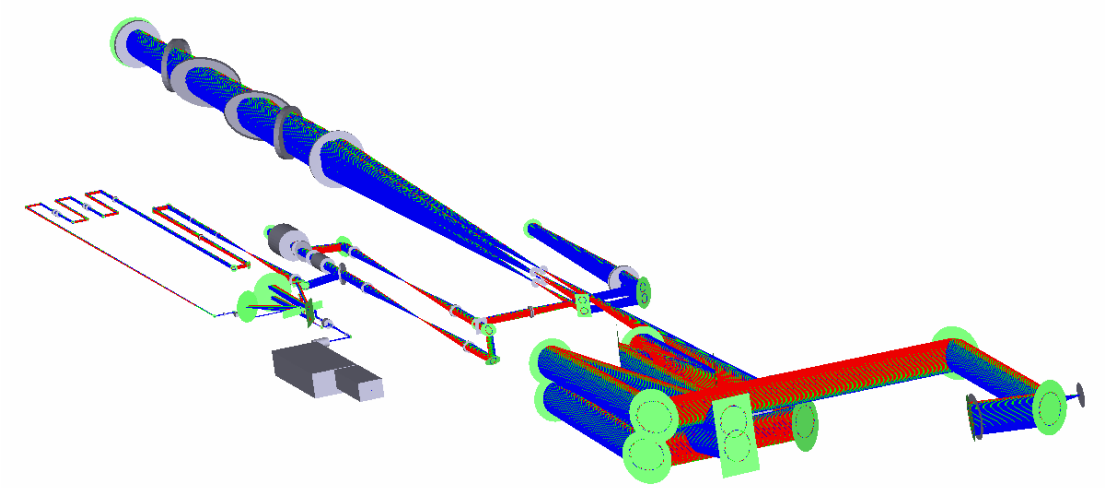

Figure 16 Raytracing plot of the Texas Petawatt Laser.

3.3.2 Compressor and stretcher design

Numerous parameters need to be considered for the design of the compressor. These include given energy, wavelength and a certain bandwidth of the laser. The groove density g and separation angle Δθ (incident angle θin- exit angle θout) define the general geometry along with the grating separation D. The latter depends on the beam size which is itself dependent on energy and damage fluence. For D smaller than D_{min}, the incident beam is clipped on the second grating. An illustration of most parameters is given in Figure 17 and the constraints are summarized in Table 3.

We have studied the compressor geometry and found that for a given energy of 200J at an operating fluence of 0.35 J/cm^2 in a top hat beam and for a given bandwidth of 16 nm, the best choice of groove density is between 1600 - 1700 lines/mm with a separation angle of 8-15 degrees. However, there are currently only two choices of gratings available. The first are gold coated gratings which have been used in the Livermore Petawatt laser and can be routinely fabricated at 1 meter diameter. They have a groove density of 1480 l/mm, operating fluence of 130 mJ/ cm^2 and diffraction efficiency of 90-92 %.

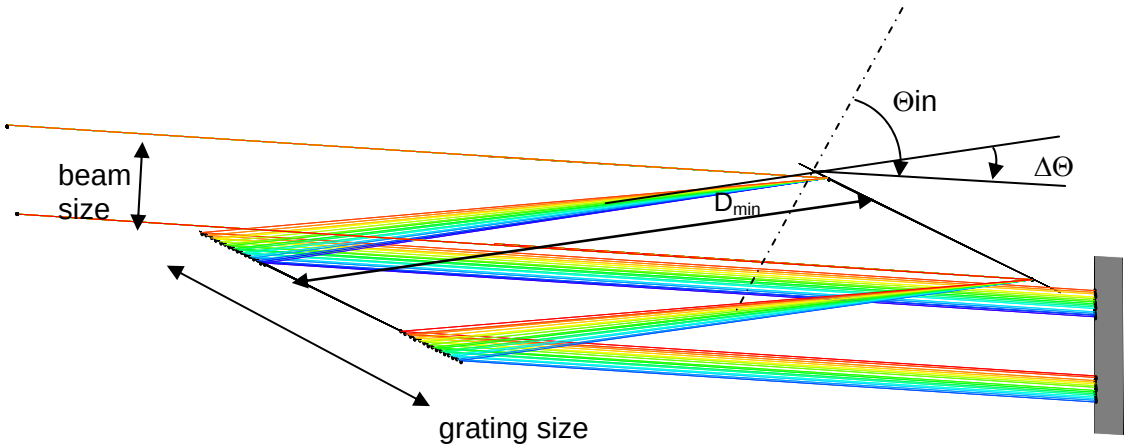

Figure 17 Illustration of compressor parameters.

	upper limit	**lower limit**
groove density	<1800 l/mm, nonlinear chirp, grating size, bandwidth clipping	>1480 l/mm, compressor size
GDD	grating size, compressor size	Dmin, OPCPA pump pulse length
ΔΘ	Grating size, stretcher size, MLD grating reflectivity	Dmin
Foperation ≈ 0.5 * Fdamage (t, ΔΘ,?)	~.3 J/cm^2@ 1740 l/mm f(Θin), ~.13 J/cm^2@ 1480 l/mm	
energy	Fdamage , grating size, Reflectivity (gold, MLD (Δλ))	
Grating size	Gold: 100 cm, MLD 80x40cm ¶¶¶	

Table 3 Constraints of the compressor design.

The second choice is multi layer dielectric (MLD) gratings which can be produced with reasonable manufacturing tolerances at groove densities of 1740 -20+60 l/mm. Present commercial availability limits the size of the 1740 l/mm gratings to 44x50 cm. However, LLNL is currently manufacturing 40x80 cm MLD gratings for use on NIF, JanUSP and other efforts. LLNL manufactured gratings can be made available to us through a statement of work and NNSA funds transfer. This size grating is much more favorable for the compressor design as will be discussed below.

Initial tests suggest that the MLD grating damage threshold is 3.8 J/cm^2 (normal to the beam) for 10 ps and 1 J/cm^2 for 0.5 ps lasers pulses. The fluence scales approximately with $\tau^{0.3}$, where τ is the pulse duration. The expected average efficiency is better than 95% for a large part of the grating.

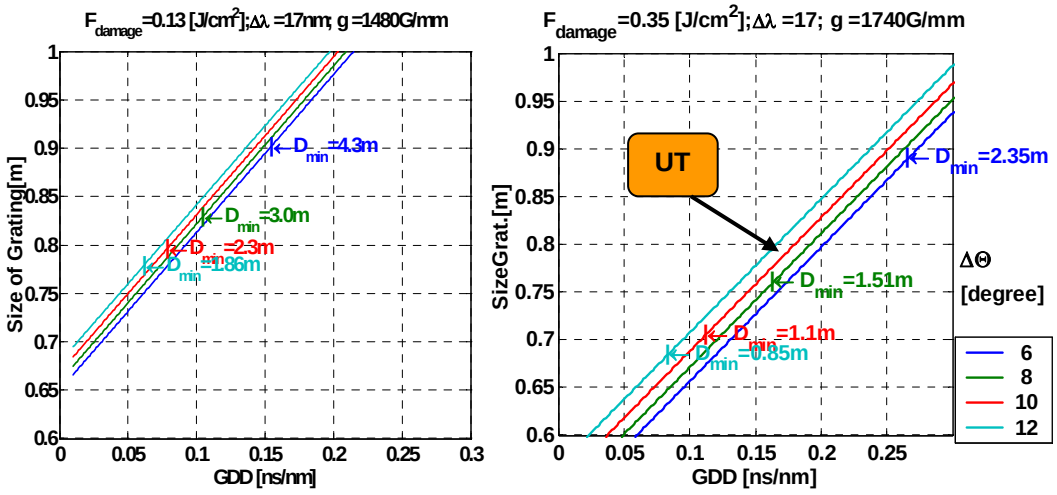

Figure 18 Size of second compressor grating versus group delay and separation angle.

Figure 18 shows the grating size versus group delay dispersion for several separation angles. The left panel shows the parameters for a gold grating with a lower damage threshold. The group delay dispersion should be above 0.08 ns/nm to have a pulse length no less than 1 ns in the final amplifier stage. The beam size on the second compressor grating is therefore 73 cm. A round optic should have a minimum of 78 cm diameter to fit two beams vertically above each other. For each separation angle the point with D=Dmin is shown. The dispersion must be higher than that point to avoid beam clipping. The beam diameter is 33 cm and the grating separation of ~3 m is acceptable. Note that the figure shows the beam size on the first grating at the zero dispersion point, which is ~ 60 cm or 1.8 times the beam size.

The right panel shows the required grating size for MLD gratings. A compressor solution can be found for 1740 l/mm gratings with a separation angle of 10 degrees. To fit the beam on the grating, the bandwidth had to be slightly reduced. The same bandwidth reduction would decrease the size of the gold gratings by ~2 cm. The grating separation of 110 cm allows for a very compact compressor. With a separation angle of 10 degrees or less, the gratings efficiency is above 90% for wavelengths from 1030-1080 nm and typically above 95% from 1045-1068 nm. Note that the horizontal size of the beam on the grating is about 3.3 times the incident beam size.

The bandwidth transmitted by the stretcher and compressor is critical since it can severely affect prepulses of the final pulse. It turns out that the bandwidth transmitted by the stretcher must me several times the full width half maximum (FWHM) bandwidth of the amplified pulse to minimized prepulses. Figure 19 shows an input of 16.4 nm FWHM spectrum of a 100 fs Gaussian pulse at 1057 nm. The spectral transmission of the stretcher and compressor are shown as comparison. There is no apparent spectral clipping on a linear scale (left panel), but there is clearly clipping on a logarithmic scale. The stretcher limits the bandwidth more than the compressor which is a result of the larger beam size in the compressor or sharper spectral clipping

in the stretcher. We intend to optimize the contrast ratio after the amplified spectrum out of the OPCPA stages is measured and can be included in the model.

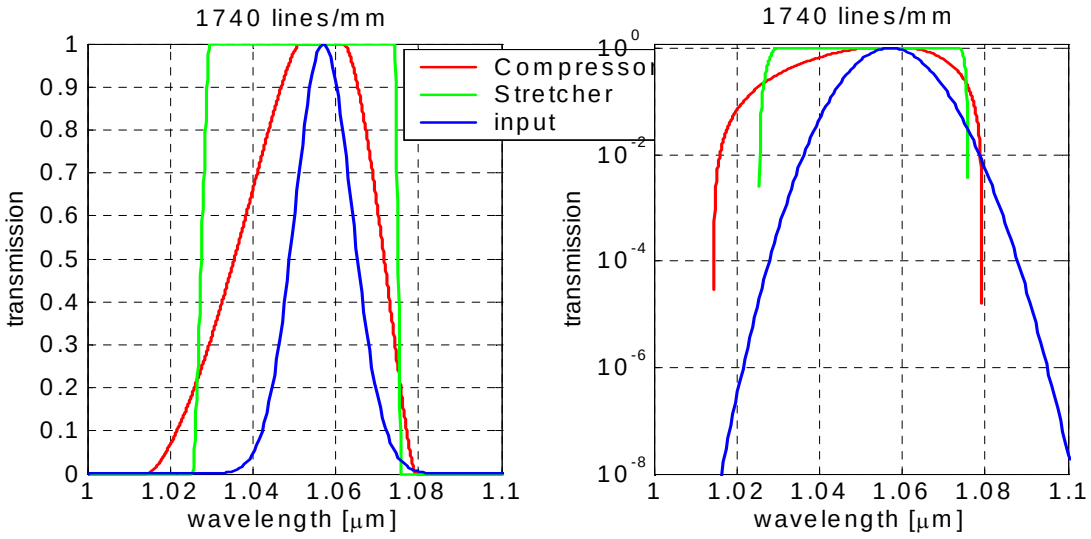

Figure 19 Bandwidth transmission of stretcher and compressor.

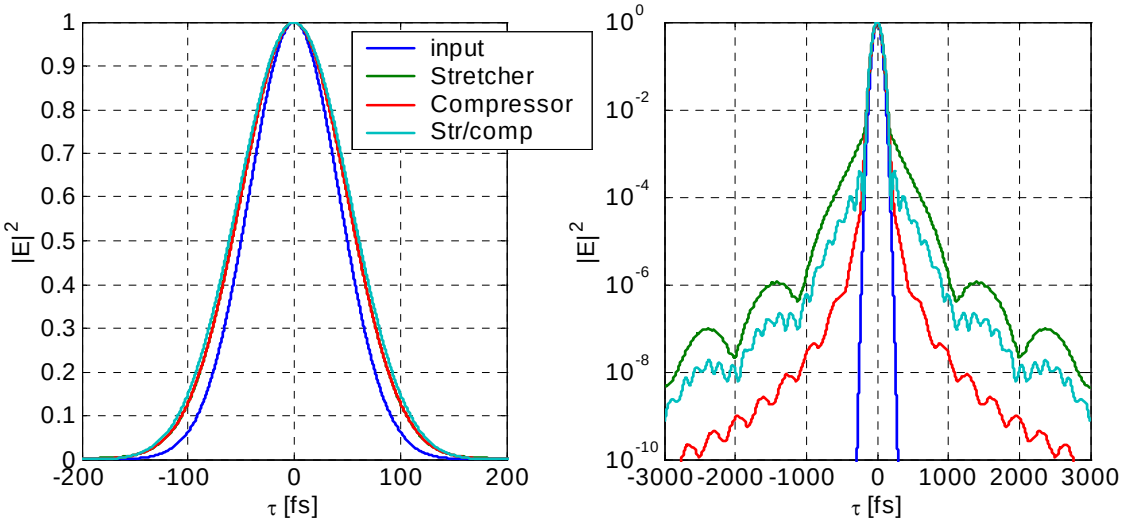

Figure 20 Prepulses level due to spectral clipping.

Figure 20 shows the compressibility of the spectrum from the 100 fs Gaussian pulse after it has been clipped by the stretcher, the compressor and by both. For this stretcher/ compressor configuration prepulses 4 orders of magnitude lower than peak power are expected. This could be further reduced by increasing the size of the stretcher optics.

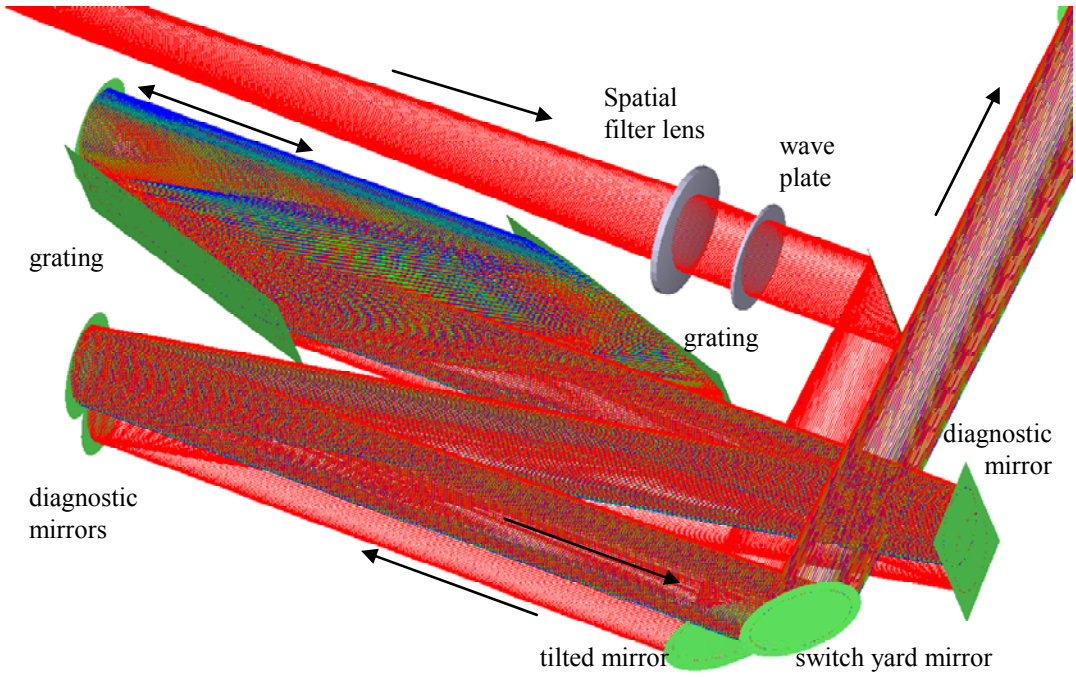

Figure 21 Raytracing plot of the compressor.

The Texas Petawatt compressor will use MLD gratings for several reasons. First, they have higher efficiency and a higher damage threshold as compared to gold gratings. Second, the higher groove density leads to a more compact compressor, which reduces vacuum hardware cost and fits much better within the limited space. The compressor design uses two 40x80 cm MLD gratings at 1740 lines/mm with a gratings separation of 128 cm. The compressor has the standard configuration two pass (four gratings hits) and a retro reflecting mirror after the second grating as illustrated in Figure 21. The separation of the input and output beam is achieved by a small vertical tilt of 0.58 degree at one input mirror. This type of separation allows the beams to overlap partially on the grating and therefore increase the beam footprint (Figure 22) on the gratings by about 50% compared to a compressor with a rooftop mirror. A tilt in the beam path through the compressor results in a small vertical chirp of less than 1 mm/nm.

The beam path has been folded before (and after) the first grating for several reasons. First to increase the overlap of the beam on the grating. This allows an increase in beam size and a reduction in the operating fluence. Second, to add leaky mirrors for diagnostic purposes. The group delay dispersion is 116 ps/nm and the pulse duration is 1.8 ns. The stretch factor could be varied by about -10 % to +20 %.

A half waveplate at the input of the compressor after the final telescope lens is needed to rotate the polarization of the beam. The polarization is given by the laser disk mounted at Brewster angle in the last amplifier. The disks are vertical to the table surface and the polarization is therefore horizontal. MLD gratings are designed to work efficiently at s-polarization while gold gratings are better in p-polarization. In the MLD compressor layout the polarization must therefore be rotated.

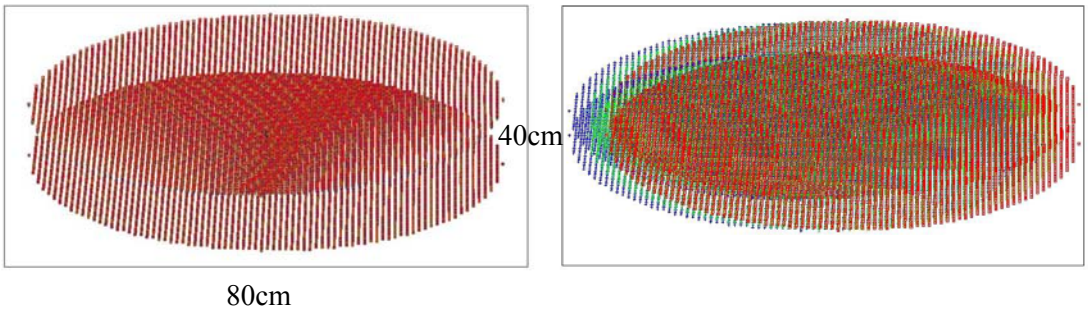

Figure 22 Beam footprint diagrams of the compressor gratings.

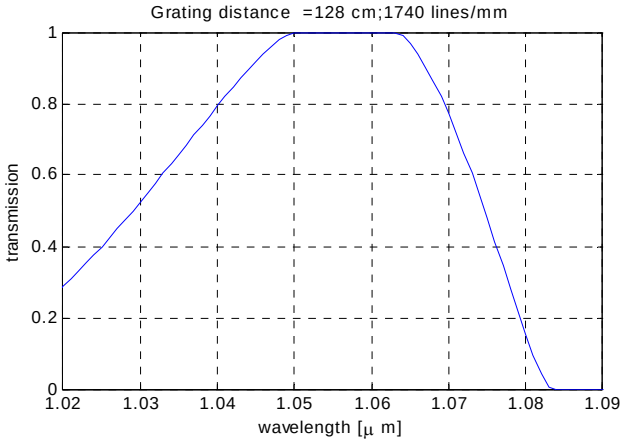

Figure 23 Spectral transmission of the compressor.

The spectral transmission through the compressor of a top hat beam, i.e. with fill factor of 100 %, is show in Figure 23. We assume a fill factor of 70 % such that the spectral clipping will be much less and the contrast (Figure 20) will also improve. The elliptical beam in Figure 22 has an area of 540 cm^2 normal to the beam (1915 cm^2 on the grating). We estimate 200 J maximum output energy with a 70% fill factor. Assuming a grating damage threshold of 0.7 J/cm^2 in the incident beam, the peak fluence of the beam will be at or below 75 % of the damage threshold.

The stretcher is shown in Figure 24. To keep the grating and optic size reasonable, we use a 2 pass configuration, i.e. the beam reflects 8 times off of the grating. The incident and exiting beams are separated by a Faraday isolator. The stretcher is a modified version the Banks stretcher [Ban 97] design which has a mirror stripe coated on the center of the grating. Since the mirror must be typically larger than the grating to avoid spectral clipping, we choose to place a separate mirror stripe in front of the grating at a reduced incident angle. This also allows a dielectric coating on the mirror to improve the overall throughput. There are 21 reflections of dielectric mirrors (0 degree mirror (4x), curved mirror (8x), mirror stripe (8x), and 2^{nd} pass mirrors (1x)) at 99.5 %, 8 grating reflections at 90 %, one Faraday transmission at 90% and 4 reflection of a gold rooftop (98%). The overall transmission is about 30% for the bandwidth of 1032 nm to 1077 nm. The stretch factor can be adjusted to match the compressor.

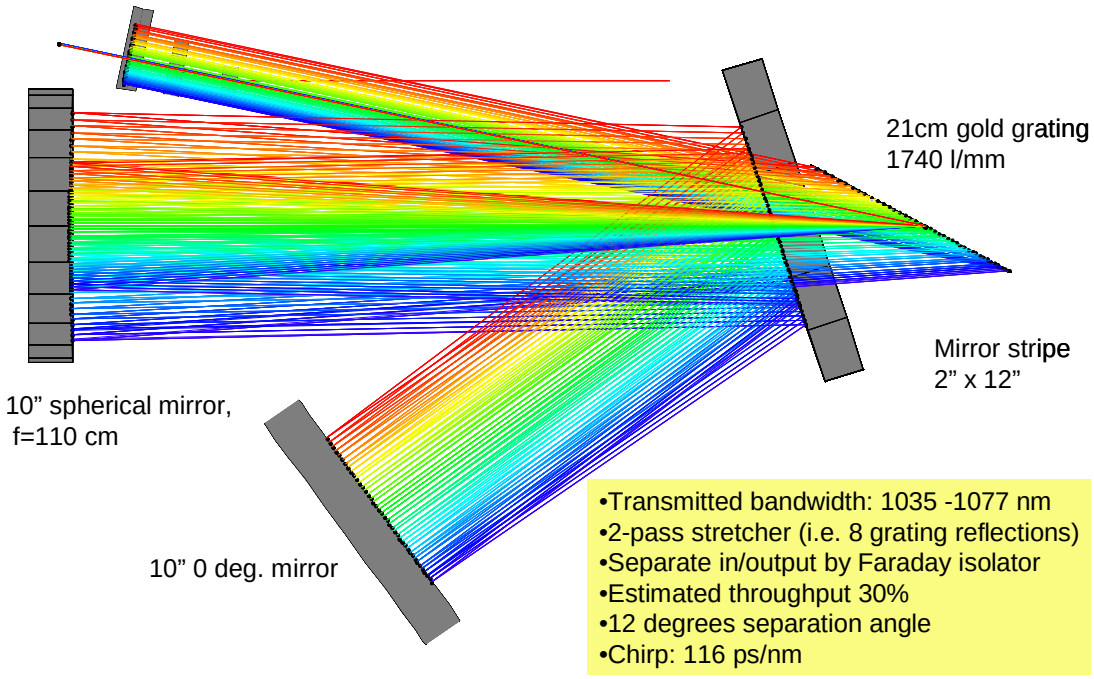

Figure 24 Raytracing plot of the stretcher design.

3.3.3 Dispersion analysis of the system

The technique of chirped pulse amplification enabled the production of high power laser pulses. To extract the energy efficiently out of the amplifier pulses are stretched by a factor of ~ 10000 before amplification and recompressed to their Fourier-transform limit for which the group delay must be nearly constant over the pulse bandwidth. We can expand the spectral phase $\phi(\omega)$ in a Taylor series about the central frequency ω_o

$$\phi(\omega) = \phi(\omega_o) + \phi_1(\omega - \omega_o) + \phi_2(\omega - \omega_o)^2 + \phi_3(\omega - \omega_o)^3 + \phi_4(\omega - \omega_o)^4 + \dots ,$$

where $\phi(\omega_o)$ is the phase, ϕ_1 is the group delay, ϕ_2 is the group delay dispersion (GDD), ϕ_3 and ϕ_4 are the third- and forth order terms, respectively. For pulses shorter than 150 fs, GDD and third order terms have to be considered, while fourth order terms have to be taken into account for pulses shorter than 30 fs.

In an analysis that considers only the central ray the condition for a transform limited pulse is

$$\phi_2^{\text{stretcher}} + \phi_2^{\text{material}} + \phi_2^{\text{compressor}} = 0,$$
$$\phi_3^{\text{stretcher}} + \phi_3^{\text{material}} + \phi_3^{\text{compressor}} = 0.$$

The dispersion terms for the stretcher and compressor are much larger than the material dispersion ($\phi_i^{\text{stretcher}}$, $\phi_i^{\text{compressor}} >> \phi_i^{\text{material}}$) and the compressor balances the phase of the stretcher. The equations above can be fulfilled simultaneously by using the compressor grating separation and the compressor grating angle as variables.
For an extended laser chain, especially one with lenses, the spectral phase across the laser pupil

$$\phi(\omega, x, y) = \phi(\omega_o, x, y) + \phi_1(\omega - \omega_o, x, y) + \phi_2(\omega - \omega_o , x, y)^2 + \dots,$$

must be taken into account. The phase does not have any spatial dependence in standard grating pair compressor and the spatial aberrations in the stretcher are negligible. The wavefront $\phi(\omega_o, x, y)$ can be a made constant by careful lens design or with the aid of a deformable mirror.

Therefore, the next highest term to consider is the group velocity across the pupil as a function of the material which has to be constant.

$$\phi_1^{material}\ (\omega - \omega_o, x, y) = \text{constant}.$$

The pulse front in the center of the beam is typically lagging the pulse front of the marginal ray in a laser with vacuum spatial filters [Bor 88]. This can be corrected with achromatic lenses or by balancing the total material between the center and the edge of the beam. Cemented achromats can not be used in the laser system because of the high fluence. Air spaced achromats can be designed such that $\phi_1^{material}\ (\omega - \omega_o, x, y)$ is constant but extra curved surfaces add numerous ghost foci which makes the placement of the optics impossible within the limited table space. We correct the spatial group delay be adding a negative lens in the disk amplifier chain and correcting the wavefront with a curved mirror. The uncorrected and corrected relative group delays are shown in Figure 25. Note that this effect has been reduced by two orders of magnitude.

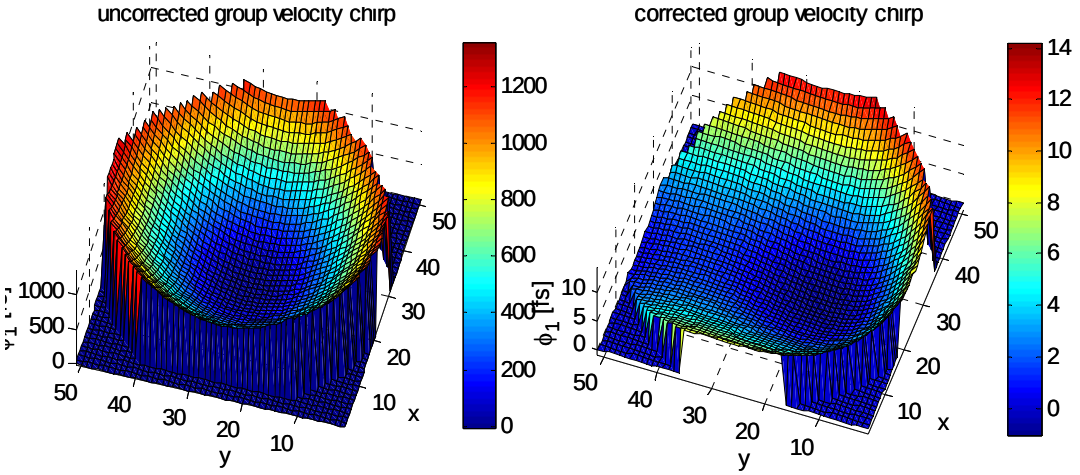

Figure 25 Spatial group velocity chirp due to lenses.

The remaining spatial group delay chirp stretches a Super Gaussian pulse with 70 % fill factor by less than 3 fs. The group velocity dispersion across the pupil $\phi_2^{material}(\omega - \omega_o, x, y)^2$ is about $N \approx 45$ times lower than $\phi_1^{material}$, where N is the number of cycles in the pulse, and can be ignored after $\phi_1^{material}$ has been corrected.

The phase of the compressor (and stretcher) are $\phi_2 = -7.16\ 10^7$ [fs^2], $\phi_3 = 9.83\ 10^8$ [fs^3], and $\phi_4 = -2.25\ 10^{10}$ [fs^4]. The material dispersion for 60 m air, 2.54 m BK7, 10 cm Ti:sapphire, 10 cm KDP, and 10 cm TGG is $\phi_2 = 7.49\ 10^4$ [fs^2], $\phi_3 = 1.43\ 10^5$ [fs^3], and $\phi_4 = -1.53\ 10^5$ [fs^4], where we assume that the laser glass dispersion is similar to BK7. After increasing the incident angle of the compressor by 25 arcsec and increasing its grating separation by 1.5 mm the total dispersion error including higher orders terms broadens the pulse less than 3 fs.

3.3.4 OPCPA stages and Ti:sapphire stage

The majority of the system gain is achieved in a broadband OPCPA stage. OPCPA offers many advantages for our application and are listed below:

- High gain in a short path length
- No thermal management issues
- Flexible peak of the gain spectrum
- Broadband gain
- Spectral gain tuning with the temporal shape of the pump energy delivered to the OPA crystal.

We intend to build the first two stages are similar to a system operating at LLNL [Jov 02]. This system used two sets of BBO crystals and a commercial 1.2 J pump laser.

The first stage uses three 15 mm long BBO crystals with walk-off compensation and an unsaturated gain of ~100 per crystal. It is pumped by 200 mJ in an 8 ns FWHM pulse. The total crystal length is increased and the pump intensity is kept low at 200 MW/ cm to reduce the risk of damage. This reduced risk improves the reliability and enable the use of a commercial pump laser. The output beam will be imaged onto the next stage and the idle beam will be blocked.

The second stage uses a walk-off compensated pair of BBO crystals which is pumped by 1 J at a similar intensity as the first stage. We assume a saturated total gain of ~100 and an output bandwidth > 30 nm. The pulse energy will be 50-100 mJ.

We performed some simulations of the parametric amplification in this stage. For this a 1.8 ns, 1 mJ chirped Gaussian pulse is seeded into a 25 mm long BBO crystal at a collinear phase matching angle (22.78 degree). The crystal is pumped by an 800 mJ, 8 ns Gaussian pulse with a 4^{th} order super-Gaussian spatial profile at a rather low intensity (100 MW/cm^2).

The results (**Error! Reference source not found.**) show broadening of the seed spectrum from 16 nm to about 33 nm (top right panel) due to saturation. The energy is clearly transferred from the overlap region of the beam as can be seen from the fluence graphs (lower panels) and the temporal plot (top left panel). The asymmetry in the output fluence is due to walk-off and can be compensated by using a pair of crystals. The phase matching bandwidth can be increased to over 100 nm in a non-collinear geometry with 1 degree desperation between pump and seed beam.

After the beam is expanded it will be shaped by a serrated aperture to a 6-8^{th} order super-Gaussian profile. The spatial profile is also slightly truncated on the sides give the beam a 4:3 aspect ratio, where the profile is taller than wide. We intend to relay image this beam profile throughout the rest of the laser chain. The aspect ratio is primarily chosen to match the beam to the compressors horizontal clear aperture given by the grating size. This aspect ratio will also reduce the size of some optics further along the laser chain, such as the Ti:sapphire crystal cut at Brewster angle and most of the large 90 degree turning mirrors.

The simulation for the third OPCPA stage use a 4 J, 4.5 ns, 3^{rd} order super-Gaussian temporal shpae and 4^{th} order super-Gaussian pulse spatial profile with some diffraction noise was added. The pump intensity is also kept near 100 MW/cm^{2}and the 3.2 ns chirped seed pulse has 100 mJ with 33 nm bandwidth. A 12 mm BBO crystal was used in collinear geometry. The results for the third stage are shown in Figure 27. This stage with a gain of 8 is also saturated and broadens the spectrum to about 40 nm.

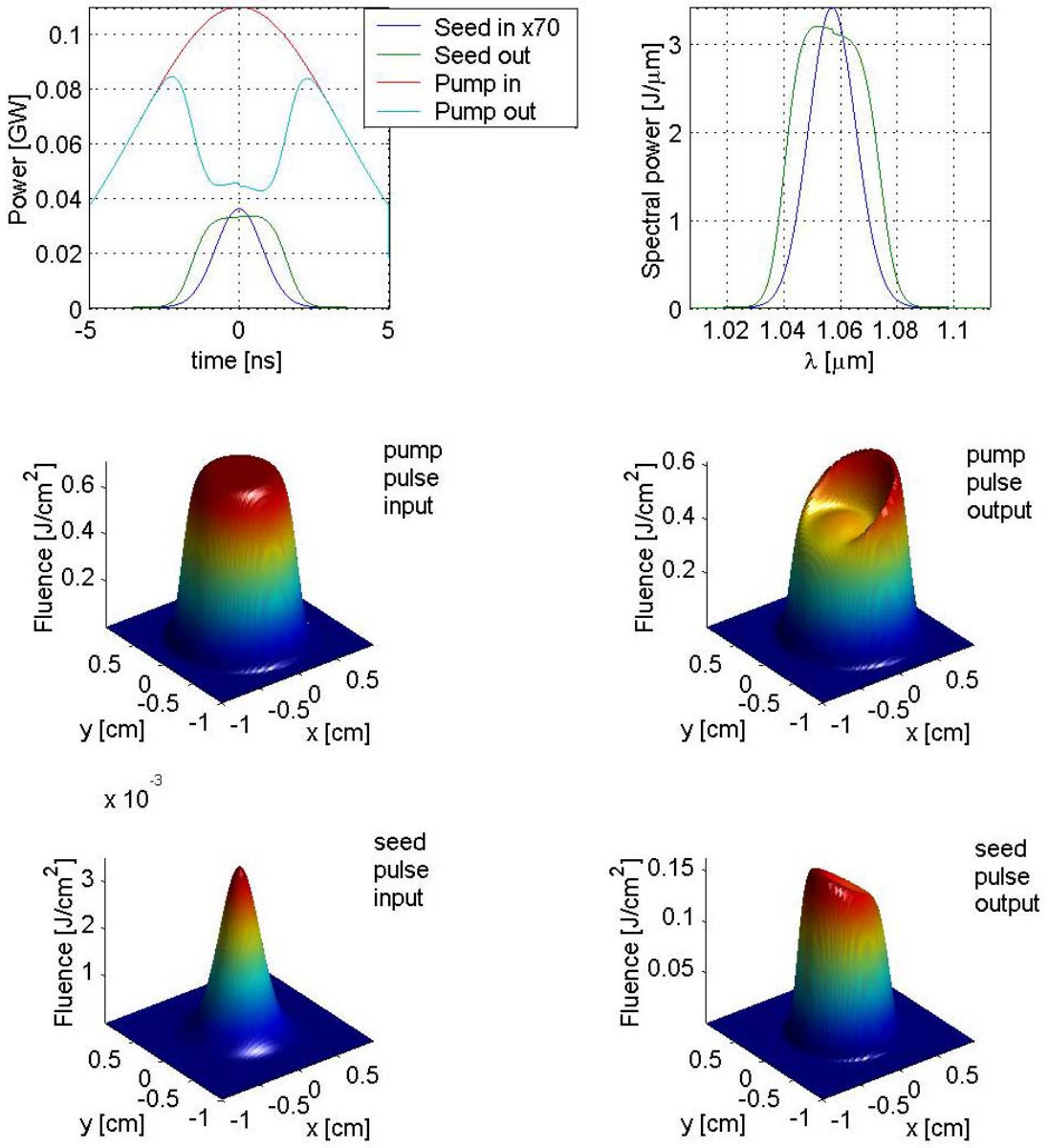

Figure 26 Second OPCPA stage simulations.

For a less perfect amplification in we intend to increase the crystal length and the intensity on crystals. The remainder of the unconverted energy (3-4 J) of the two pump laser can also be used to amplify the pulse further in a Ti:sapphire crystal as indicated in Figure 15. A loss in energy due to spectral and spatial shaping can be compensated in such a stage. We expect a gain of ~1.3 per pass in a multi pass configuration, which is limited to about 4 pass due to the beam size. Alternatively, a ring regenerative amplifier could have many more passes but would have a lower gain (~1.2 per pass) due to additional Fresnel losses at the polarizers and Pockels cell.

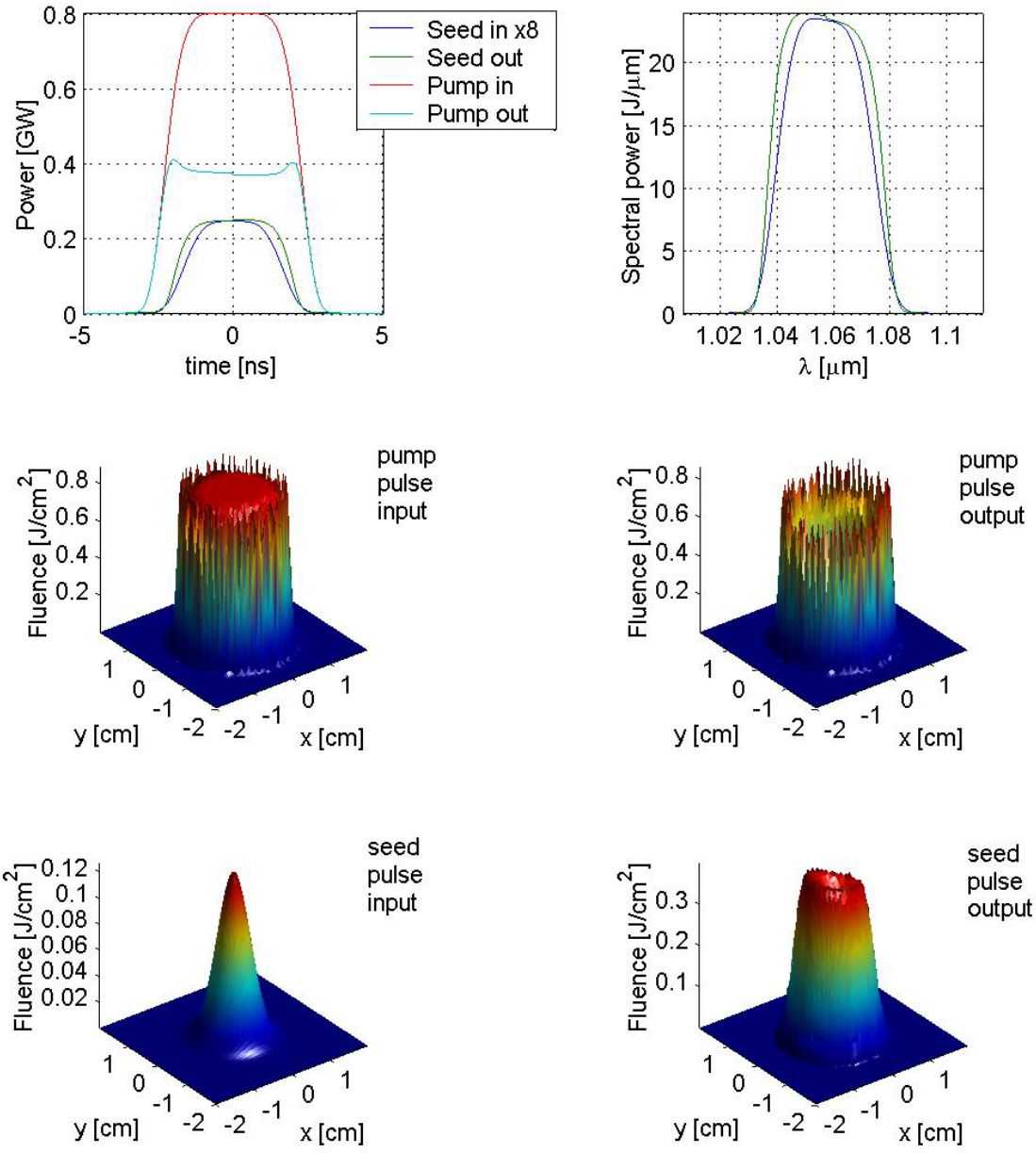

Figure 27 Final OPCPA stage simulations.

3.3.5 Mixed glass amplifiers stages

The 1J Front End pulses are then seeded into two Nd:glass amplifiers. The first (Figure **28**) consists of a 64 mm diameter commercial rod amplifier pumped by flashlamps. This amplifier contains silicate glass and will be four passed with a waveplate, polarizer, and static 70 mm Faraday isolator. The silicate rod is assumed to exhibit a small signal, single pass gain of 4 at the peak fluorescence of 1061 nm (e.g. Schott LG 680), which is centered slightly to the red side of the seed pulse. The beam is relay imaged from the broad band amplifiers to the glass rod, the deformable mirror (DFM) and to the input of the disk amplifier.

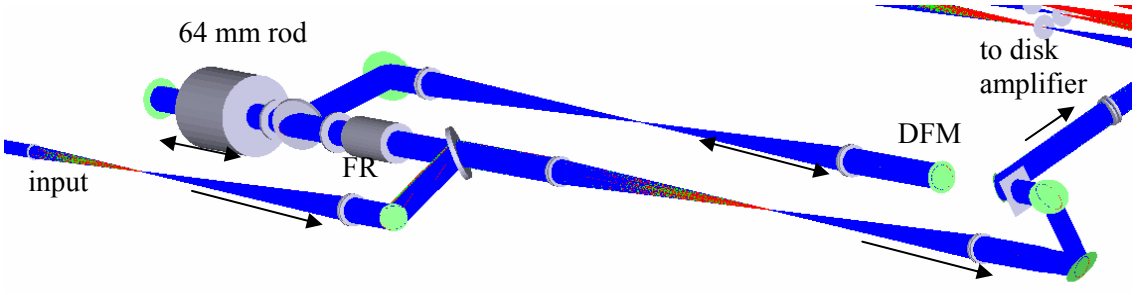

Figure 28 Silicate glass amplifier section.

The seed pulse is again spatially filtered and magnified to a beam diameter of 5.4 cm. It is assumed that the strong gain saturation in the OPA section of the system will yield a spatially flat-top beam profile which will be relay imaged through the remainder of the laser chain. The calculation of four pass gain in this amplifier indicates that it is saturated. The saturated gain is reduced from 256 to 35 for 31 J output energy after losses at the Faraday isolator. Here as expected, the output spectra exhibit large pulling to the red (illustrated in Figure 31) and a bandwidth of 12 nm. The final energy and spectrum depends on the available silicate glass, the seeded spectrum and energy. The B-Integral (ΣB) is typically about 0.6 rad but depends on the spectrum (equivalent to pulse duration) and energy of the pulses. The fluence of the laser beam is up to 1.5 J/cm^2 and the local peaks are around 2 J/cm^2 if we assume up the 30 % ripples in the beam profile. Platinum free glass is required typically for fluences above 2.5 J/cm^2, thus the design does not require a Pt-free glass rod.

The 30 J pulses from this amplifier are then relay imaged and magnified by a factor of 3.9 to a beam diameter of 21.1 cm. These pulses are four passed through a pair of 315 mm using angular multiplexing. We assume a small signal gain per disk up to 1.31 at the peak fluorescence of the phosphate glass. However, the gain per disk will be reduced to about 1.28 in order to limit the output energy below the damage fluence of the gratings and to limit gain narrowing. The ray tracing through the disk amplifier is shown in Figure 29.

As mentioned above, the large aperture (315 mm) amplifiers have several advantages over the smaller (94 mm) alternative. Foremost is the large clear aperture which allows extraction of 400-500 J with a ΣB < 1 rad. The highest fluences in the disk amplifier section are at the final disk and at the pick off mirror after the pinhole between the second and third pass. The fluence values are similar to the rod amplifier for an output energy of 400 J and are equivalently lower for the 250 J targeted output energy. These NOVA amplifiers have already been equipped with Pt-free phosphate glass as an extra benefit. This section will only contribute a ΣB = 0.3-0.4 rad. The energetics simulations are summarized in Figure 30. They were done with a 3D Frantz-Nodvik calculation. By balancing the gain factor between silicate and phosphate glass we can optimize spectrum, ΣB, or pulse energy.

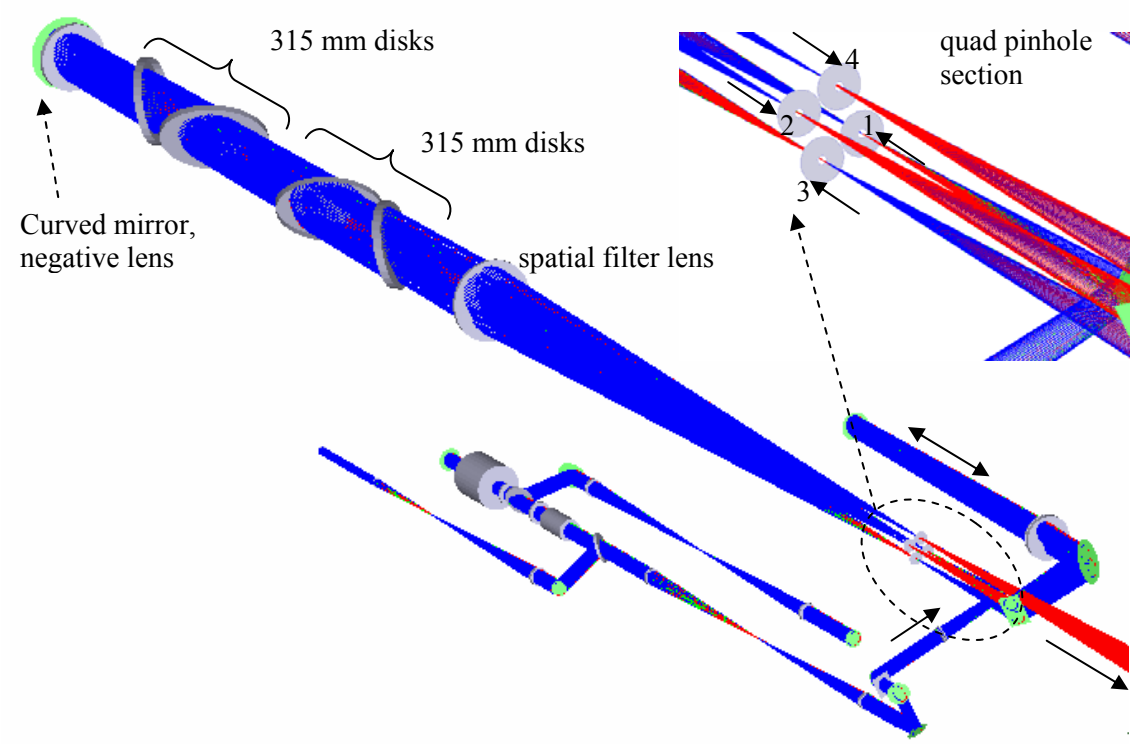

Figure 29 Four pass disk amplifier.

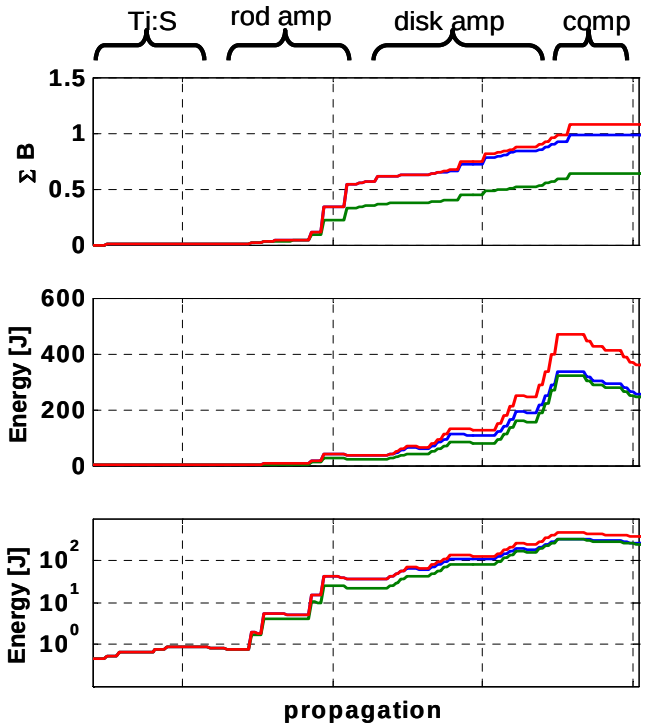

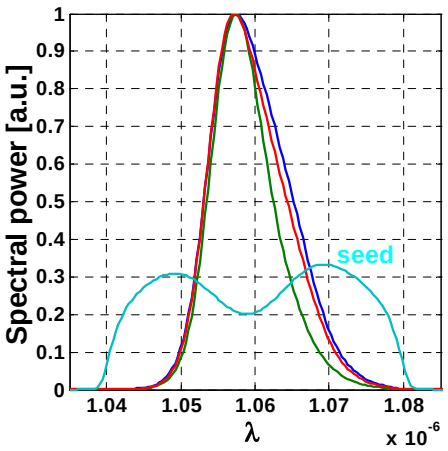

G_0 rod	G_0 disk	FWHM
4.0	1.278	12.1
3.4	1.32	10.6
4.0	1.32	11.2

Figure 30 Laser energetics of the glass amplifies.

The pinholes in the spatial filter are spaced 70 mm apart vertically and 60 mm apart horizontally. The difference is due to the slightly elliptical beam shape. Closer pinhole spacing could improve the wave front distortions from about 3 wave numbers (peak to peak) by 20 %. However, this reduces the tolerance level on the edges of the pick off mirrors. The wavefront needs to be corrected by either a static phase plate, which could be placed at the image plane before the injection into the disk amplifier section, or by the deformable mirror in the rod amplifier section. We intend to use a static phase plate after the system aberrations have been measured.

The amplified spectrum (absolute and relative spectral power) is illustrated in Figure 31. The phosphate amplifier has pulled the spectrum back to the initial center of 1057 nm. The final bandwidth for a modest pre-shaped spectrum is 12 nm which can be compressed to 150 fs. The actual spectrum will depend on the silicate glass and the shaping capabilities of the Dazzler and the OPCPA stages.

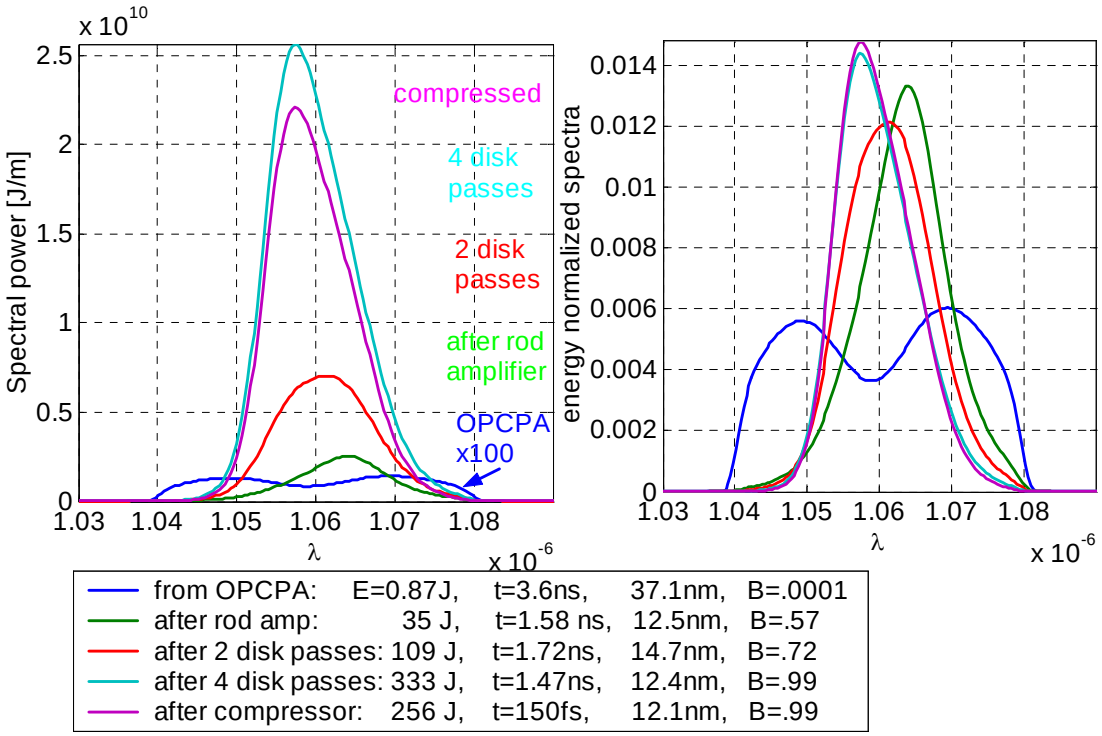

Figure 31 Spectrum after various amplifier stages.

The 250 J pulses will be radially expanded by 1.21 for compression to reduce the fluence on the gratings. The large lens next to the final disk and a second lens inside the compressor chamber build the expanding telescope. The relay plane will be pushed close to the final grating.

The hardware for a major part of this telescope will be from NOVA parts. The first lens will be a NOVA lens drive assembly. The lens is a meniscus lens to avoid damaging ghost foci and the focal length is 4.30 m, which is the maximum focal length within the constraints of the table and cleanroom size. The second lens of this telescope is inside the compressor. The length is also constrained by the laboratory size, but suitable NOVA lenses could be found.

The chamber for the pick off mirrors and for the path between the second and third pass will be fabricated at the UT machine shop. The chamber for the compressor is about 6 feet in diameter and 11 feet long. The design will be done in house and fabrication needs to be determent.

3.3.6 Layout of the Cleanroom and target area

The table space for the laser is very limited due to the overall size of the cleanroom and the total available space. The Petawatt laser will be constructed on a set of four optical tables with a total length of 34 feet. One side of the table is occupied by the glass amplifier sections which is mainly the two NOVA 315 mm amplifiers and the large spatial filter. Note that the second half of the spatial filter extends outside the cleanroom into the compressor vacuum tank via an evacuated beam transport tune. The other half is reserved for the oscillator, stretcher, broadband amplifiers and the pump lasers. A sketch of the component layout of the table is shown in Figure 32.

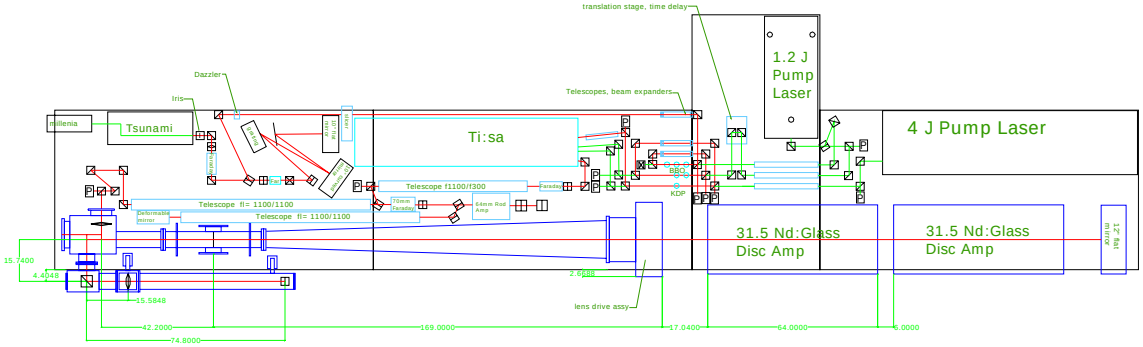

Figure 32 Preliminary layout of on the optical table.

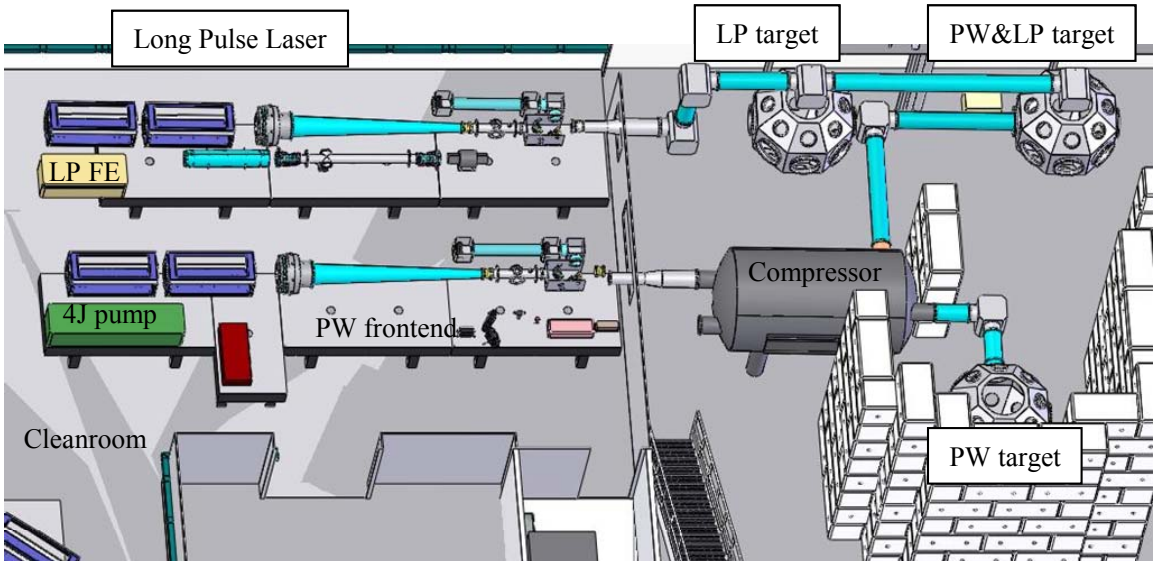

Figure 33 CAD illustration of laser layout.

3.3.7 Diagnostic and alignment

Numerous diagnostics will be necessary to align, operate and trouble shoot the laser chain. A pair of turning mirrors between all major sections (oscillator, stretcher, … compressor, target) will allow an independent alignment of each section. The frontend operates at a modest repetition rate of 10 Hz and 2.5 Hz providing more than 1 W of power for alignment of the glass sections and the compressor. A summary of the permanently installed laser diagnostics is listed in Table 4. Some additional diagnostics will be necessary for laser chain construction and to characterize the final pulse (i.e. pulse contrast measurement).

Laser chain element	**Pulse energy**	**Near field**	**Far field**	**Pulse spectra**	**pulse width/ timing**	**Wave front**	**Pickoff optics**
Ti:sapphire oscillator	Power meter			Spectro meter	Photo diode		Leaky mirror/ pellicle
Stretcher (to 1 ns)		CCD			Photo diode		Leaky mirror/ pellicle
OPCPA I + II pump	Power meter	CCD			Photo diode		Leaky mirror
OPCPA I BBO group	CCD	CCD	CCD		Photo diode		Leaky mirror/ pellicle
OPCPA II BBO pair	Joule meter	CCD		Spectro meter	Photo diode		Leaky mirror/ pellicle
Serrated aperture		CCD					Leaky mirror
OPCPA III pump	Power meter	CCD			Photo diode		Leaky mirror
OPCPA III BBO amp.	Joule meter	CCD	CCD		Photo diode		
Ti:Sapphire amplifier	Joule meter	CCD	CCD	Spectro meter	Photo diode		Leaky mirror
Ti:sapphire pump	CCD	CCD			Photo diode		
64 mm rod amp 2 passes	CCD	CCD				Shack Hartm.	Leaky mirror
64 mm rod amp 4 passes	Joule meter	CCD	CCD	Spectro meter	Photo diode		Leaky mirror
Large spatial filter, pinhole		CCD	CCD				image
315 mm disk amp 2 passes	CCD	CCD	CCD		Photo diode		Ghost foci of negative lens, retro mirror, image
315 mm disk amp 4 passes	Joule meter	CCD (2x)	CCD				Ghost foci of negative lens, image
Compressor	Photo diode	CCD (4x)	CCD	SPIDER	Photo diode, SPIDER, autocorrel	Tilted WFI, Shack Hartm,	NOVA mid chain sensor, leaky mirror, near field images of gratings
Target	Joule meter	CCD	CCD		Photo diode	focus	

Table 4 Summary of permanent diagnostic on the PW laser.

4 Conceptual design of the long pulse laser

4.1 Architecture and design

A complimentary long pulse laser is designed to produce up to 500 J in 2 -20 ns at the second harmonic (527 nm). The fundamental (1054 nm) can contain over 1 kJ. However, the fundamental beam is not envisioned as a target shooter, since the only optical isolation between the final amplifier and the target is the doubling crystal and a spatial filter.

The laser chain starts with a front end that produces 2.5 J, 1.5-20 ns pulses which are temporally pre-shaped to compensate for square pulse distortions in the main amplifiers. A commercial solution to this laser is appropriate. A possible design to this front end is illustrated in the schematic of the long pulse laser (Figure 34). An oscillator produces pre-shaped pulsed via a fast Pockels cell. The timing of the Pockes cells is synchronized to within 0.5 ns to the Petawatt chain. The pulses are amplified to tens of mJ in a regenerative amplifier and boosted to 2.5 J with a pair of Nd:glass or birefringence compensated Nd:YLF rods. The front end repetition rate operates at several Hz so it can be used for system alignment. Spatial beam shaping of the pulses has to be done before the injection in the rod amplifiers. In addition to spatial filters, a Pockels cell is inserted to suppress ASE.

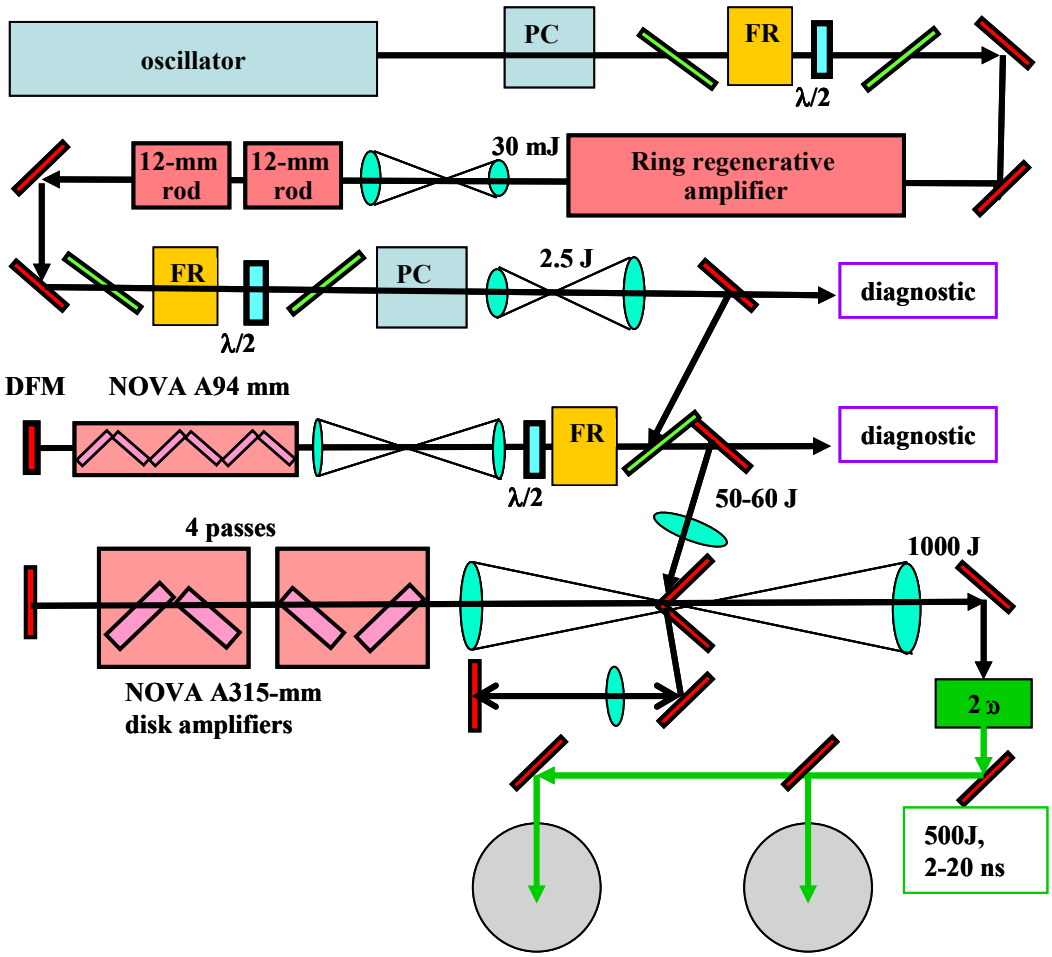

Figure 34 Schematic of the long pulse laser.

The front end pulse will be injected into the 94 mm amplifier off of a mirror near the pinhole plane. The p.4cm amplifier is two-passed by angular multiplexing or, alternatively, with a Faraday isolator. The beam size through this disk amplifier is 5.8 cm FWHM. We assume a single pass small signal gain of 5.9 and a slightly saturated gain of 23 after the double pass. A NOVA 94 mm Faraday isolator will be placed after the spatial filter. The B-integral ΣB of the 94 mm amplifier and Faraday isolator is only 0.015 -0.15 radians and the peak fluence is less than 1.5 J/cm2. It is therefore not necessary to replace the current glass disk in the amplifier with Pt-free glass.

The pulses are further amplified in a pair of NOVA 315 mm amplifiers. This section is similar to the main amplifier of the Petawatt chain. The main difference is that the long pulse laser is better centered on the peak fluorescence of the amplifiers. If we assume a small signal gain of 1.31 per disk the total gain is $(1.31)^{16} = 75$. However, this chain is much more saturated and the total gain is about 24. The beam is relay imaged and magnified by 3 at the input. The clear aperture is 22 cm and the beam size is about 17 cm FWHM. The clear aperture is less than for the Petawatt disk amplifier. This is a result of the space limitations for the long pulse laser, which limits us to shorter focal length lenses in main spatial filter. The higher F/# telescopes increase the off-axis separation of the beam for the individual passes.

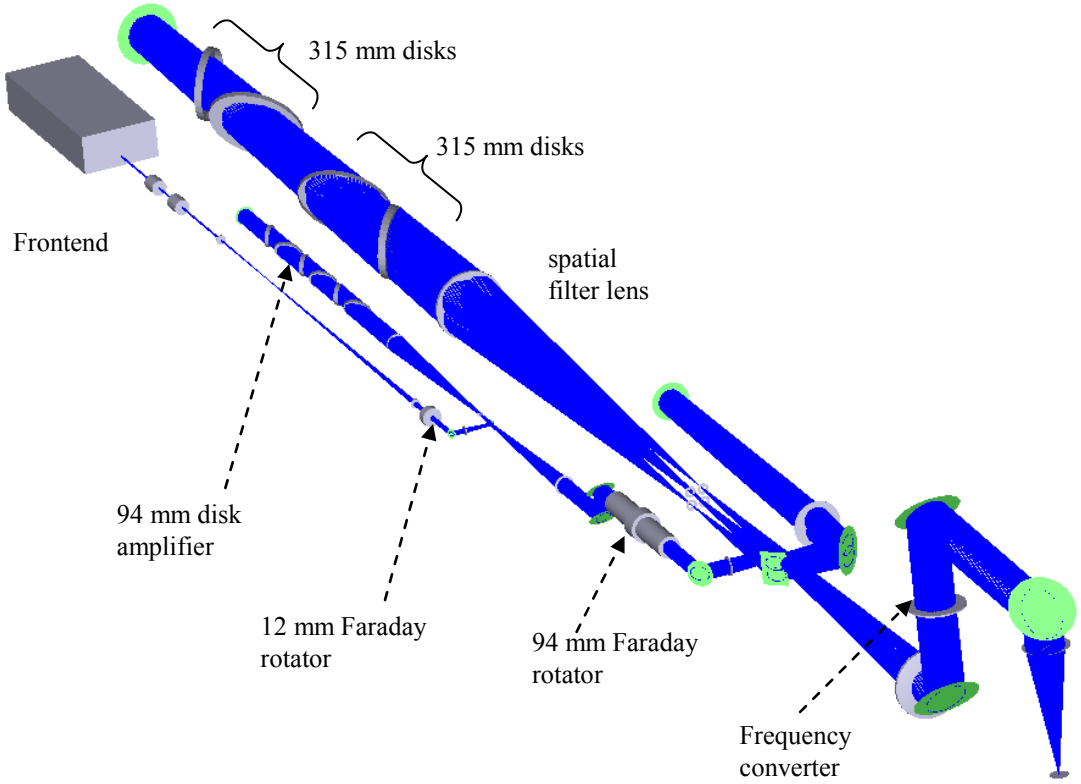

Figure 35 Long pulse laser ray tracing plot.

The limiting factors of this chain are the damage fluence and ΣB. For 2 ns, 1.0 kJ pulses ΣB = 1. More critical is the damage fluence after the final pass and at the optics between the second and third passes. For 1 kJ , the peak fluence for a smooth beam is in each case about 4 J/cm2. Commercial, state of the art optics have a damage fluence of typically 20 J/cm2 for a 10 ns pulse and square root scaling for pulses between 1-10 ns. If we assume 50 % intensity ripples in the beam profiles and a 1.5 ns pulse, the highest beam fluence is close to the damage threshold. The

disks in the 315 mm amplifiers have already been replaced with Pt-free glass during NOVA operation.

4.1.1 Diagnostic and alignment

Laser chain element	Pulse energy	Near field	Far field	pulse width/ timing	Wave front	Pickoff optics
oscillator	Power meter			Photo diode		Leaky mirror/ pellicle
Regenerative amplifier	Power meter	CCD		Photo diode		Leaky mirror/ pellicle
12 mm rods	Power meter	CCD		Photo diode		Leaky mirror
Front end	CCD	CCD	CCD	Photo diode		Leaky mirror
94 mm disk amp 2 passes	CCD	CCD		Photo diode		Leaky mirror
Large spatial filter, pinhole			CCD			image
315 mm disk amp 2 passes	CCD	CCD	CCD	Photo diode		retro mirror, image
315 mm disk amp 4 passes	Joule meter	CCD (2x)	CCD		Inter ferometer	NOVA mid chain sensor, leaky mirror
Doubling crystal	Power meter	CCD	CCD	Photo diode		Ghost of focusing lens
Target	Joule meter	CCD	CCD	Photo diode	Shack H, focus	

Table 5 Summary of permanent diagnostic on the long pulse laser.

4.1.2 Long Pulse Frequency Conversion.

Once the 1 kJ, 1ω pulse is extracted from the final long pulse disk amplifier, we will use a Type I KDP crystal to convert the frequency from the fundamental 1ω (1053 nm) to the second harmonic 2ω (527 nm).

The baseline design for the converter will be a single KDP crystal measuring ~ 24 x 24 x 1.5 cm thick. Due to the wide pulsewidth range (2-20 ns) that the long pulse laser operates, care needs to be given to the irradiance incident on the conversion crystal. Although conversion efficiency increases for a unit decrease in pulsewidth, one suffers from an increase in ΣB.

With this in mind and taking into account the parameter space the laser is required to perform, we intend to operate within an irradiance range of between 0.2 – 2 GW/cm^2 for 1 kJ laser pulses ranging from 2 -20 ns.

These crystals are commercially available. The mounting cell and alignment fixtures will be designed and fabricated in house.

5 Pulsed power conditioning

The two lasers use five amplifiers and one Faraday rotator from the NOVA laser. The equipment needs to be transported from LLNL to UT. Most of the components for the pulsed power have been exposed for several years outdoors and needs total refurbishing and testing, which will be done at UT after transport. It remains to be seen how many parts must be replaced. Current estimations suggest that there are enough spare functional parts of all major components plus spares.

The capacitor bank will be installed in the room next to the target laboratory. Since the laboratory is underground the capacitor room is almost completely surrounded by walls and dirt. It is excellently shielded and suitable for the pulsed power equipment. Figure 36 shows a CAD drawing of the capacitor room with the proposed layout of the racks and shelves, which are part of the equipment transfer from LLNL. The existing cable trays are attached along the side walls and run through and opening above the only access door.

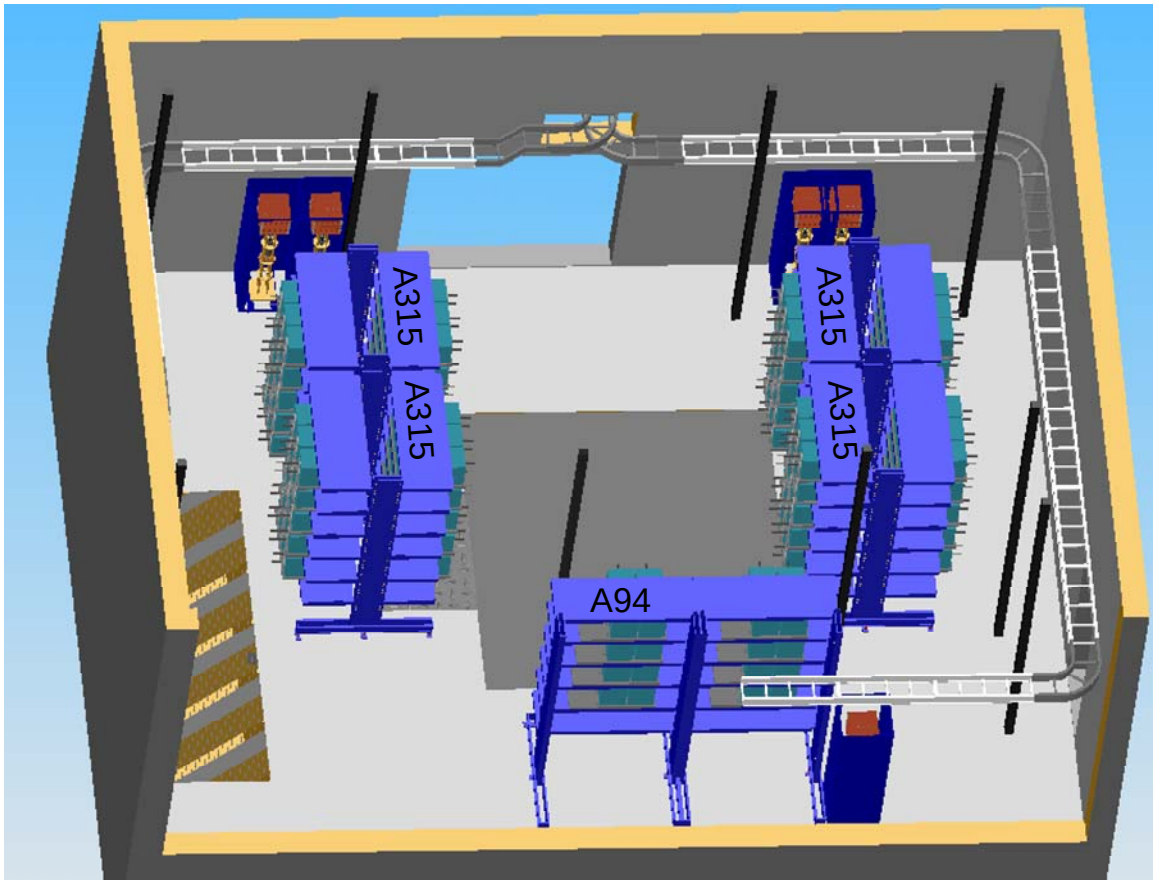

Figure 36 Layout of the capacitor room.

An illustration of the pulsed power circuit for the 315 mm amplifiers is shown in Figure 37. A power supply charges a set of capacitors for each flashlamp circuit. A trigger pulse initiates the discharge of all circuits of an amplifier simultaneously by a NOVA ignitron pair.

We intend to operate the pair of 315 mm amplifiers with one power supply, since they operate at the same voltage. This will help to balance the gain across the aperture. The 94 mm amplifier and the Faraday isolator will have one charging power supply and independent voltage control.

The flashlamp operating voltage will remain at a maximum of 20 kV and a nominal voltage of 18 kV. The maximum stored energy is 31.2 kJ per circuit on the A315 amps or 312 kJ total and 20.8 kJ per circuit or 166 kJ total for the A94 amp. The total stored energy for all components is nearly 1.5 MJ. The chargers will be Maxwell 8000J CCDS power supplies for the 315s and smaller chargers for the other circuits. Pre Ionization Lamp Check (PILC) circuitry will be configured. There are total of 48 circuits for amplifiers, each with a Pulse Forming Network (PFN) consisting of Capacitors, inductor, fuse, charge resistor, and shorting switch.

Power transmission between the capacitor room and the laser room will use RG-217 coaxial cable. The cable will be routed along about 130 ft of existing cable tray, where additional isolation will be added. The cables will then penetrate through the ceiling of the laser cleanroom and terminate in the NOVA junction boxes which will be attached to the ceiling of the clean room above each laser amplifier.

The flash lamp wires are connected to the junction boxes. A high voltage ground wire will be installed between the laser head inner reflectors and the ignitron ground to minimize current through the building ground in case of flash lamp failure. The high voltage ground and building ground will be connected at the Maxwell power supplies.

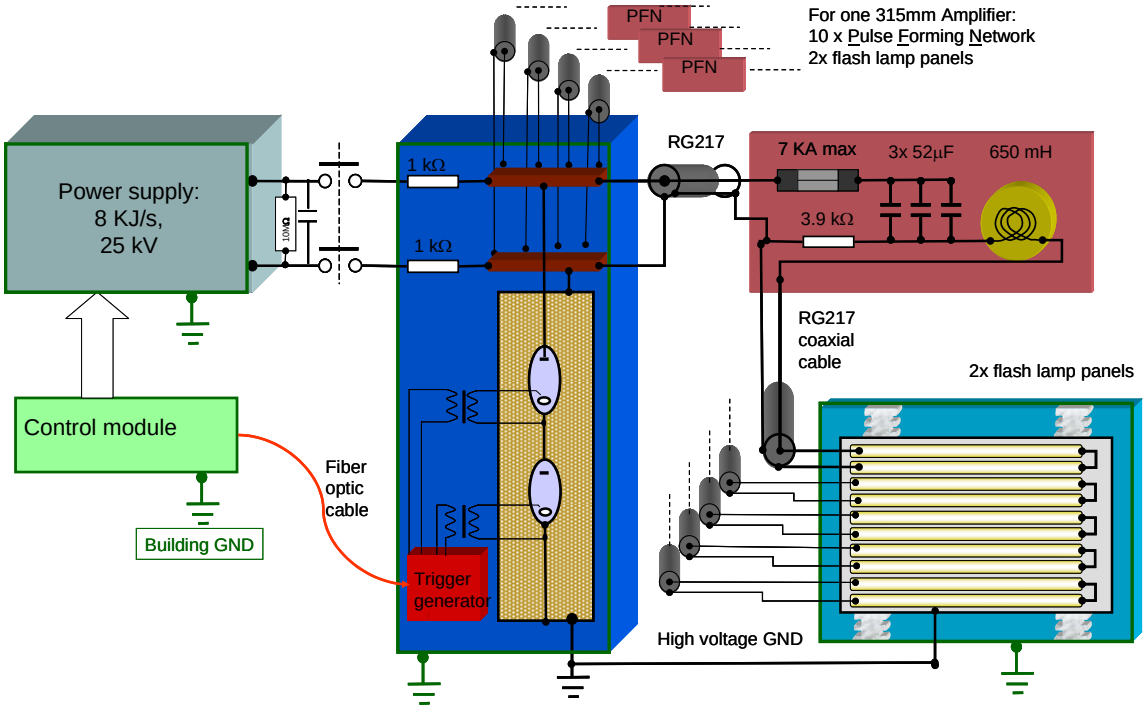

Figure 37 Illustration of the amplifier circuit.

6 Controls system

The diagnostics and controls system for the laser will manage all aspects of laser operations including the pre-shot routine, system shot sequence and post shot data acquisition. (including experiment data). The system checks for human and machine safety, controls and indicates the laser parameters and records all laser data. The human safety will not be controlled by software but will be hard wired as discussed below. The controls system verifies human safety before it can initiate laser operation or a laser shot.

The controls system architecture is illustrated in Figure 38. At the core of the control system is a central processor, which controls the shot sequence of the laser. It interfaces or hosts a data server with the data logging and supervisory control (DSC) engine. All interlocks are linked to the central processor. This processor interfaces with one or most likely several field PCs which run the appropriate software procedures and interface via software drivers to the instruments. An operator can use one or several user PCs to interface (remotely) with the central processor. Only one operator will have control while other can only observe the processes and read data.

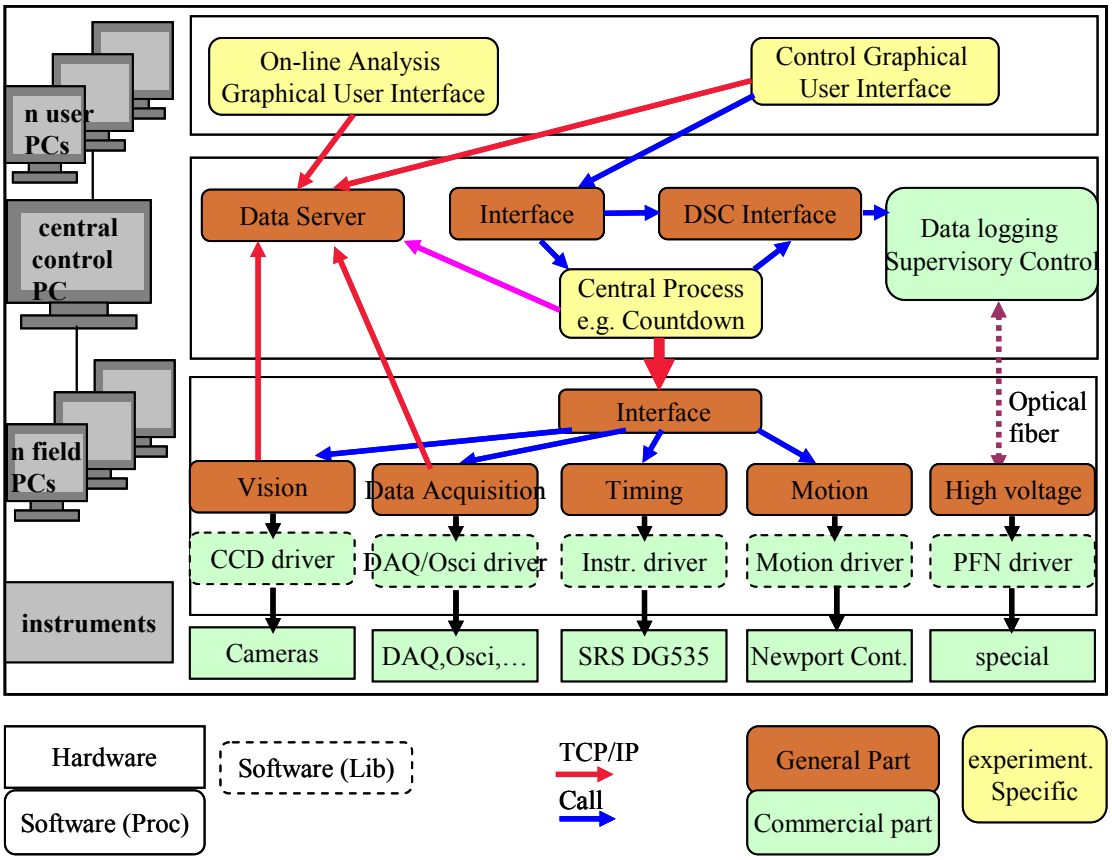

Figure 38 Control system architecture.

The controls system will use Labview as the programming language. Instrument drivers in Labview are available for the majority of the instruments proposed for this laser. Labview has a DSC module, data server capabilities and web capabilities, which is allows remote observation and user control by easy to program Graphical User Interfaces (GUI). The field processors are PCI extension (PXI) chassis which operate headless (without monitor) under Labview Realtime.

Data type	Total count	What is controlled?
Motion (I/O)	62	Stepper or DC motor via controller
Vision (Input)	22	Triggered CCD (shot camera)
Vision (Input)	24	CCD alignment cameras
Data trace (analog I/O)	106	PFN currents, PFN charging voltages, ground current
Data trace (analog I/O)	30	photo diodes (oscilloscopes), power meters, vacuum gauges, spectrum …
Switch (digital I/O)	40	Vacuum pumps, vacuum valves, laser warn lights, countdown lights, door interlocks, search buttons, …
Switch with limits (multi digital I/O)	40	Cross hairs, dump rods, shutters, vacuum valves, water flow, ignitron cool water resistivity, …
Trigger (output)	30	Laser timing, PFN charging,…
Special (I/O)	15	Laser controllers, vacuum controller, PFN chargers, …

Table 6 Summary of controls

A summary of the controlled objects is given in Table 6. The main applications are motion, vision, timing, data acquisition and pulsed power control. Further applications are control of specific instruments such as the commercial lasers, wave front sensors, deformable mirror, etc….

Vision control acquires various images throughout the laser and the vast majority of the data. To capture a beam profile image it is preferred to trigger the cameras and buffer the data without a frame grabber. We envision using triggered IEEE 1394 (Firewire) cameras as shot cameras and lower quality cameras for additional alignment. The controls system adjusts and records the camera settings for various beam intensities, reads out the data and evaluates basic beam parameters such as beam position and size.

The motion control system primarily controls the motors for beam alignment. All optics from the disk amplifier to the target will be motorized in addition to cross hairs, some small wave plates, some lenses and small beam steering mirrors. This operation will be performed manually but remotely by an operator in conjunction with the vision control. A number of cameras are used for alignment and for the full shot and require motorized variable neutral density filters.

The high voltage control operates the charging sequence of the PFNs and initiates the discharge of the capacitor bank. All lamp currents and the ground fault current is monitored during the shot and logged into a database. The operator must be able to control manually the firing for testing purposes and will also be able to perform a pre-ionization lamp check PILC for testing and in between shots. The high voltage controls also control one Faraday isolator for the long pulse laser.

The timing system for the Petawatt laser is illustrated in Figure 39. The shot sequence will be triggered by charging the capacitor bank about two minutes before the pulse arrives on target (T_0). At this time all laser parameters have been set, the laser is aligned and the area and systems are safe. Once the end of charge (EOC) is reached for the rod and disk amplifier, the trigger sequence is phase locked to the clock of the fs oscillator. Appropriate time delays will be added to (T_0-1 μs) to synchronize the trigger of the slicer Pockels cells and pump laser Q-switches with the optical delay of the amplified laser pulse. The timing of the long pulse laser is very similar.

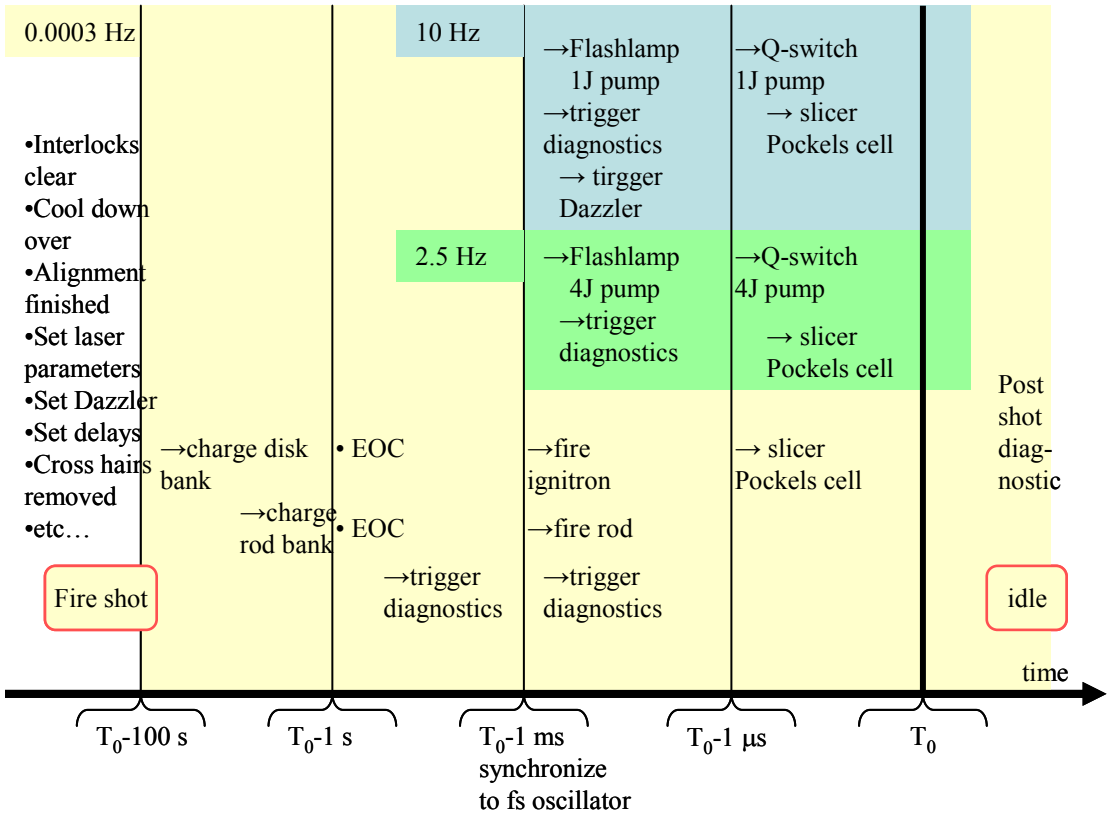

Figure 39 Timing sequence of the Petawatt laser.

7 Laser and radiation safety concepts

There are a number of safety concerns for the operation of this facility. These include laboratory safety, fire safety, hazardous material safety, laser safety, and nuclear radiation safety. Generally, all of these issues will be addressed by the University of Texas Environmental Health Safety office (UT EH&S). UT has established policies to address all safety issues and has personal safety training for its employees. However, this laser is not standard laboratory equipment and its safety needs to be addressed, especially laser, high voltage and nuclear radiation safety. Fire safety is currently being updated as part of the facility renovation.
We have the following definitions for our safety concept:

- *All clear:* The laser and target area have free access.
- *Warmup:* The laser and target area have free access, but warning lights indicate that the laser shutter might be opened any time.
- *Laser alignment*: Any class 3b or higher laser is turned on. This requires laser warning lights and laser safety goggles must be worn by all persons in the appropriate areas.
- *Rod amplifier shot*: A *laser shot* where a rod amplifier is triggered (for now only the 65 mm rod amplifier). Only qualified personal from the laser operations group will be allowed in the laser room.
- *Full shot*: A disk amplifier shot which requires high voltage safety precaution in the appropriate areas, i.e. the laser room and capacitor bank room are evacuated and access is monitored.

A shot director will be appointed to enforce this concept. The shot director is responsible for the controlled access to the laser and target area, i.e. for activating interlocks and evacuating the appropriate areas during the shot countdown. The access status to facility is summarized in Table 7.

	All clear status	**Warm up**	**Alignment**	**Rod shot**	**Full shot**
Door Interlocks	Passive	Passive	Set	Set (Abort if Violated)	Set (Abort if Violated)
Door Locks	OPEN	OPEN	OPEN	CLOSED	CLOSED
Warning Lights	OFF	ON	ON	ON	ON
Safety Glasses	NOT REQUIRED	NOT REQUIRED	REQUIRED	REQUIRED	REQUIRED
Area access	Free access	Access limited to authorized personnel	Access limited to authorized personnel	Unauthorized personnel Cleared from Clean Room and Area Search Required	All personnel Cleared from Clean Room and an Target Area Search Required
Capacitor room	Free access	Free access	Free access	Free access	All Personnel Cleared, no access

Table 7 Summary of area access control.

The laser group safety officer must search the rooms and manually press all search buttons before a disk amplifier shot. The search buttons are placed in the back of the laser room and target areas to ensure that nobody can be overlooked. Additionally, we will install several video cameras. After the search buttons are pushed door interlocks will be activated, such that one can only exit the laser and target area and the capacitor room, but not enter it. The capacitor bank can only charged when all search buttons are pressed and the door interlocks are activated. Emergency/ panic buttons are placed in opposite corners of the laser room, in the control room and in near the capacitor bank. These buttons will activate the dump rods which annihilates all stored energy in the capacitor bank. The layout of the search buttons, laser warning lights, laser switches and interlocks are indicated in Figure 40.

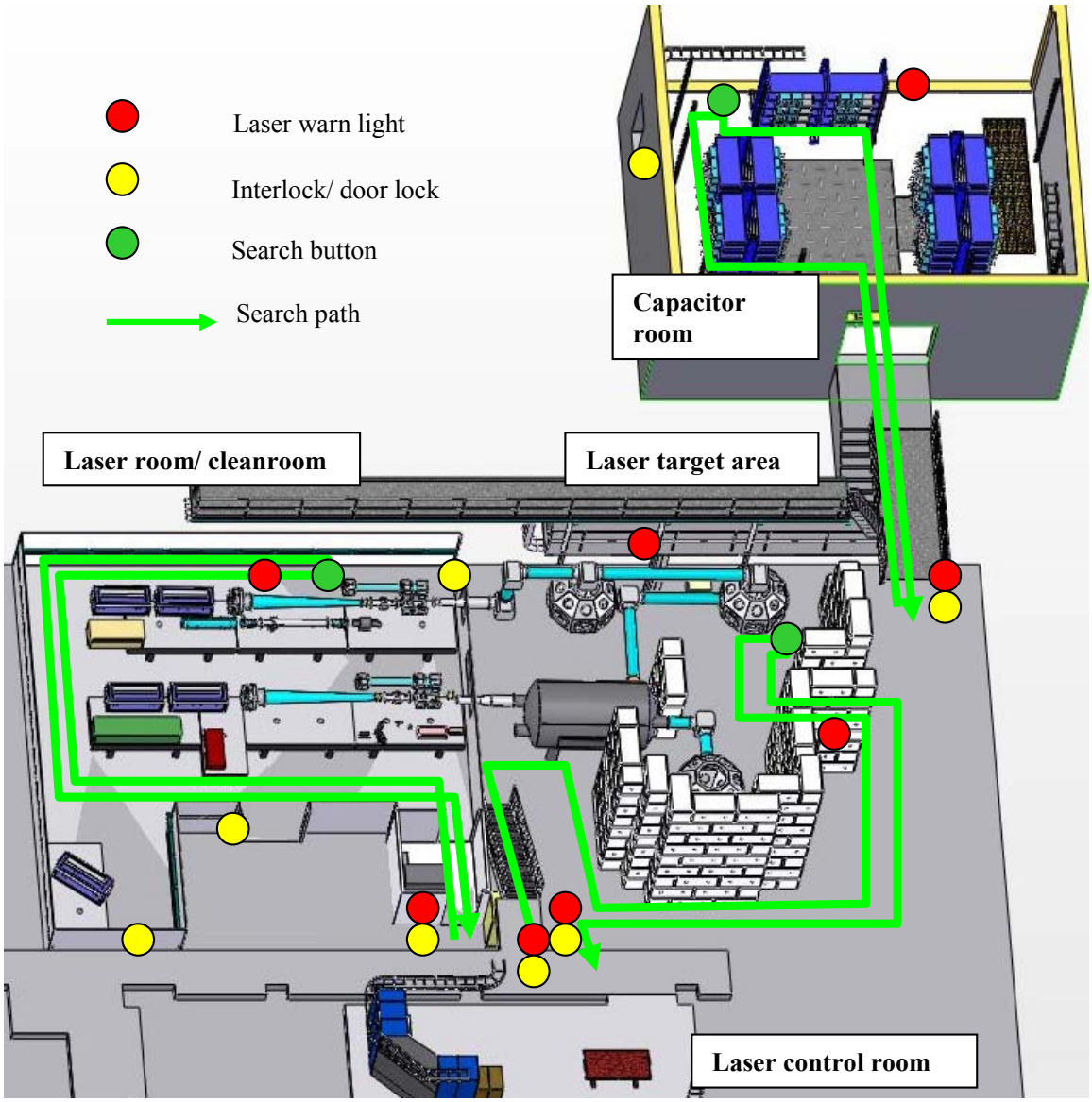

Figure 40 Safety installations overview.

For a Petawatt shot, radiation safety must be considered. To estimate the source of radiation we make the assumption that 150 J are focused to 10^{21} W/cm^2. Half of the energy is converted into fast electrons and the mean kinetic energy of a relativistic Maxwellian plasma is three times the electron temperature. The estimated dose from 10 MeV gamma rays at the chamber wall (0.5 m from the source) is 10 rem. 1-10 % of that dose is isotropic and 90-100 % is in the forward direction of the laser beam. The proposal calls for (isotropic) neutron production of up to 10^{10} neutron at 2.45 MeV which produce 11 mrem dose per shot at the chamber wall.

We over estimate the use of the facility by assuming 2000 full system shots per year, which leads to an annual dose of 22 rem from neutrons and 2000 rem from gamma rays isotropic and 20000 rem from gamma rays in the forward direction at 0.5 m distance from the source. The allowed annual radiation dose of the general public is 100 mrem/year. We split the dose arbitrarily to 10/90 for neutrons and gamma and calculate the required attenuation form the actual dose to safe levels for the general public. Attenuation is achieved by distance and shielding. Table 8 lists the doses at various distances and the required shielding for sufficient attenuation. Point A is closest accessible point to the Petawatt target chamber and point B is the closest point to the two beam chamber. The two target areas are surrounded by a two foot thick concrete wall 8-18 feet tall, which will be built with blocks available at UT. Although the ceiling is further away, the thickness is not quite sufficient for the required attenuation. Note that the laser high bay is a laboratory three stories below ground. However, if one considers the occupancy factor (1/16) of the outside space above the ceiling, the shielding is sufficient. The shielding is not sufficient in forward direction of the gamma rays. We intend to direct the laser in a southerly direction into many meters of dirt. We estimate that air activation and secondary radiation are not critical. Several radiation area monitors will be installed in the laboratory to survey the actual radiation. A more detailed investigation of the shielding in all directions will be performed and actual doses will be measured during commissioning of the laser.

Distance from source	annual dose [rem](~r-2)	N(DD) Shield concrete/ PE	g-ray main concrete/ lead	g-ray isotropic concrete/ lead	3D Concrete thickness [cm]
4 m Point A	22 neutron 20000 $\tilde{\gamma}$ray	45 cm/ 9 cm	168 cm/ 21 cm	75 cm/ 11 cm	120 -140 cm
5 m Point B	.344 neutron 313 $\tilde{\gamma}$ray	40 cm/ 8 cm	156 cm/ 20 cm	70 cm/ 22 cm	90 -100 cm
10 m ceiling **10 m ceiling (1/16)**	.22 neutron 200 $\tilde{\gamma}$ray	23 cm/ 5 cm 6 cm/ 1 cm	132 cm/ 17 cm	84 cm/ 11 cm 24 cm/ 4 cm	51-75 cm

Table 8 Required radiation shielding for Petawatt shots

We intend to build the interaction chambers out of aluminum or line the inside with aluminum to minimize activation of long lived products in steel. A more detailed risk assessment will be conducted incorporating working procedures for chamber and target activation and target handling.
It is not intended do train and classify the laser operations group, graduate students and visiting scientist as radiation workers. The target areas should remain highly flexible to accommodate the variety of proposed experiments.

8 Texas Petawatt Project Plan

8.1 Work Breakdown Structure (WBS)

The work break down structure (WBS) shown below describes how the Texas Petawatt project schedule and construction are organized. The WBS flowchart is composed of four main sections, Facility Construction, Laser Bay, Target Bay and Laser Operations. The sub-categories that follow describe the system in much more detail.

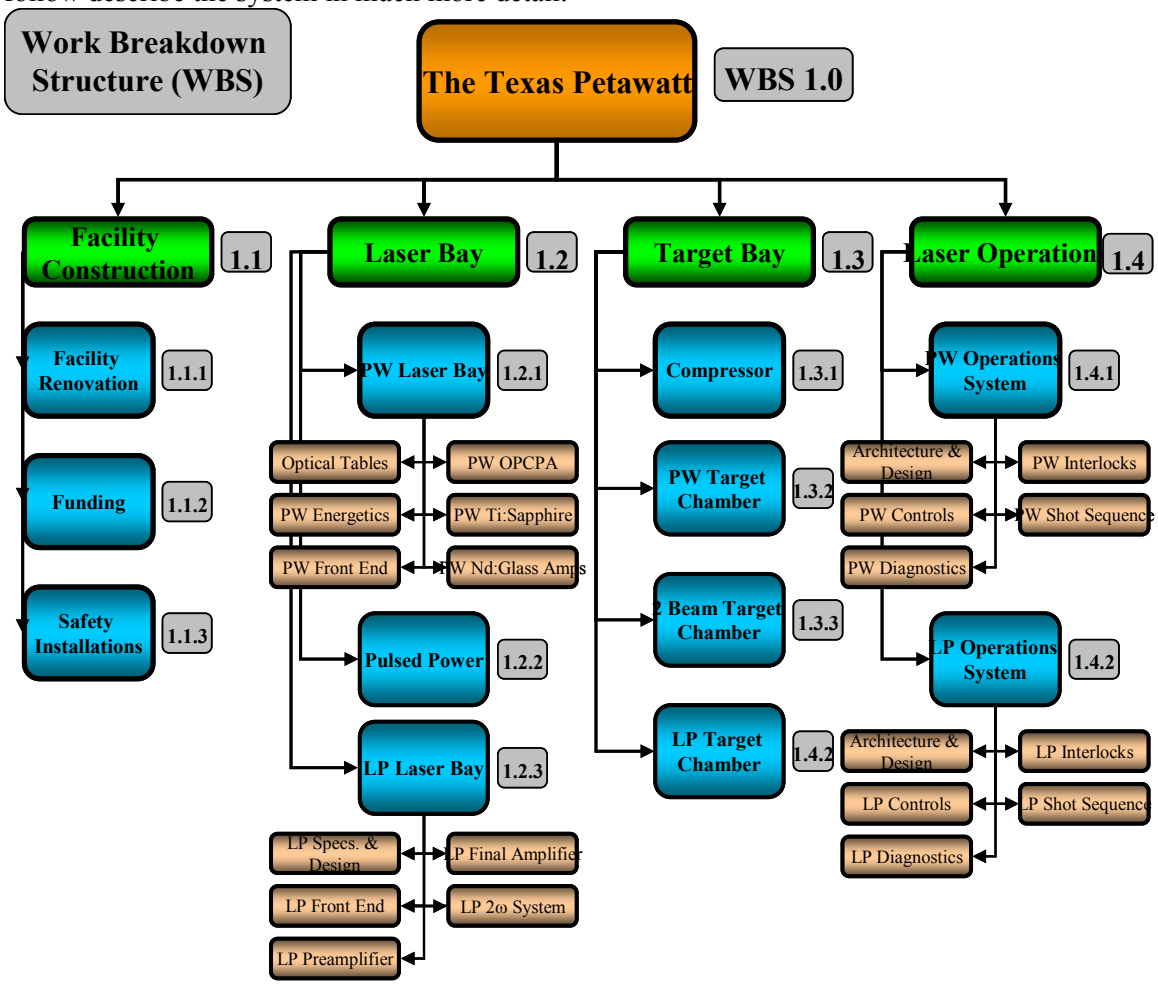

Figure 41 (WBS) describes the project organization for schedule and construction.

8.2 Project Schedule

The Project schedule for the Texas Petawatt is managed with AEC Software's Fastrack Schedule. For the purposes of this document, the following figure describes a top-level view of the entire project with milestones and project highlights called out for easier reading. The complete project schedule with all 700 plus, line items can be found in Appendix A.

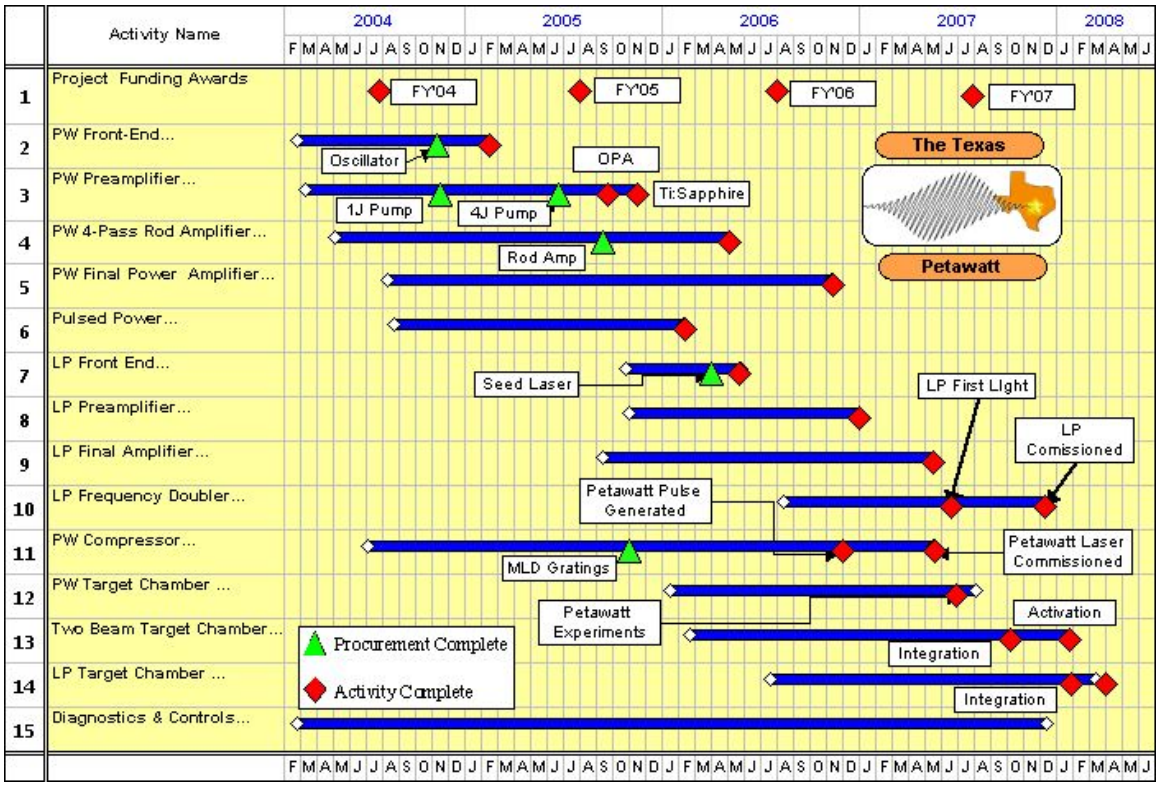

Figure 42 Texas Petawatt project schedule rolled up to major subsystems and shown in a Gantt chart.

8.3 Project Budget

The budget for this project was derived from a combination of the estimated funding profile (Table 2), project schedule activities (Appendix A) and resource loading. The following fiscal years are defined from August 1st to July 31st. Our fiscal year is determined by the arrival date of FY' 04 funds. We assume that funds are available at UT for each year in August.

8.3.1 FY' 03

The Texas Petawatt award for fiscal year 2003 is 0.9M$. These funds will be used to as startup for the Center for High Intensity Science. The largest line items for FY' 03 are:

- Staffing (Project Scientist)
- Scientific design of the laser facility.
- Some equipment purchases are also planned (Laser Tables, general laser lab equipment)

8.3.2 FY' 04

Fiscal Year 2004 marks the beginning of the capital equipment purchases for the Petawatt. With the facility complete, laser construction will begin and long lead time (>6 months) component procurements will begin. Please refer to Table 9 below for the FY' 04 budget as a function of WBS.

8.3.3 FY' 05

In FY' 05, the remainder of the short pulse laser procurements takes place and the long pulse laser procurements begin.

WBS	Item Description	FY'04 Costs (k$)
N/A	**Salary, Fringe, Overhead**	685
N/A	**LLNL Support**	155
N/A	**Travel**	55
N/A	**Operations**	35.3
N/A	**General Lab Equipment**	65
N/A	**Lab Renovation**	12
N/A	**PW Scale Laser**	83
1.1.3	**Safety Equipment**	13
	Radiation Wall	
	Glasses etc.	
1.2.1.3	**Front End**	
	Oscillator	136
	Optics	10
	Opto-Mechanical	8
1.2.1.4	**OPCPA I**	
	1J Pump Laser	125
	Optics	25
	VRT Hardware	2
	Power Meters	15
	Pulse Detectors	1.6
	Beam Profilers	12
1.2.1.4	**OPCPA II**	
	Optics	24
	Optomechanics	8
	4J Custom Laser	345
1.2.1.4	**OPCPA III**	
	Optics	24
	VRT Hardware	2
1.2.1.5	**Ti:Sapphire**	
	Crystal	30
	Optics	10
	Mounts	8
1.2.1.6.1	**64mm Rod Amplifier**	
	Rod Procurement	50
1.2.1.6.2	**31.5 Amplifier**	
	Spatial Filter	2
1.2.2	**Pulsed Power**	70.1
	RG-217	
	Cable Tray	
	Refinish Cap Rack	
	Refinish Iggy Rack	
1.3.1	**Compressor**	411
	Misc. Hardware	
	MLD Gratings	
	Vacuum Chamber	
	Vacuum Equipment	
1.4.1.2	**PW Controls**	26
	PW PXI Chassis	
	PW Motors & Controllers	
	PW Alignment Cameras	
	PW Pulsed Power	
1.4.1.4	**Interlocks**	
	Laser Bay	2
	Total FY'04 Budget	**2450**

Table 9 Texas Petawatt annual budget for fiscal year 2004

WBS	Item Description	FY'05 Costs (k$)	Contingency (%)	Extended Costs (k$)
N/A	**Salary, Fringe, Overhead**	753.5	0%	753.5
N/A	**LLNL Support**	200	0%	200
N/A	**Travel**	60	0%	60
N/A	**Operations**	40	0%	40
N/A	**General Lab Equipment**	30	0%	30
N/A	**PW Scale Laser**	50	0%	50
1.2.1.4	**OPCPA III**			
	4J Pump Laser	145	0%	145
1.2.1.6.1	**64mm Rod Amplifier**			
	Amplifier Procurement	155	0%	155
	Faraday Rotator	60	30%	78
	DFM	80	30%	104
	TFP	4	30%	5.2
	Waveplates	5	30%	6.5
	Lenses	3.6	30%	4.68
	Mirrors	3	30%	3.9
	TRT	4	30%	5.2
	VRT	2	30%	2.6
	Opto-Mechanics	13	30%	16.9
	Vacuum System	10	30%	13
1.2.1.6.2	**31.5cm Amplifier**			
	Repolish Disks	40	30%	52
	Refurbish Amplifiers	15	30%	19.5
	Main Retro Mirror	5	30%	6.5
	Fold Mirrors	2.5	30%	3.25
	Fold Lenses	2	30%	2.6
	Mounts	7	30%	9.1
	Beam Tubes	10	30%	13
	Pulsed Power	20	30%	26
1.2.3.2	**LP Front End**			
	Seed Laser	225	30%	292.5
	Mirrors	0.4	30%	0.52
	Waveplates	1	30%	1.3
	Lenses	0.5	30%	0.65
	Mounts	10	30%	13
1.2.3.3	**LP Pre-Amplifier**			
	Mirrors	5	30%	6.5
	Lenses	4.2	30%	5.46
	Waveplates	3	30%	3.9
	Mounts	10	30%	13
	VRT	6	30%	7.8
	Vacuum Pump System	10	30%	13
	9.4 Fixture/Cleanrrom	30	30%	39
	9.4 Refurbish	20	30%	26
	9.4 Disk Repolish	15	30%	19.5
	9.4 Rotator Glass	20	30%	26
	9.4 Rotator Pulsed Power	10	30%	13
1.3.1	**Compressor**			
	MLD Disffraction Gratings	398	0%	398
	Rooftop Mirror	5	30%	6.5
	Waveplate	5	30%	6.5
	Mirrors	30	30%	39
	Optics Mounts	50	30%	65
	Grating Mount	15	30%	19.5
	Breadboard	5	30%	6.5
1.4.1.2	**PW Controls**			
	PW Motors & Controllers	60	25%	75
	PW Alignment Cameras	12	30%	15.6
1.4.2.4	**PW Diagnostics**			
	PW Power & Energy	15	30%	19.5
	PW Shot Cameras	22	30%	28.6
	PW Current & Voltage	2	30%	2.6
	PW Vacuum Gauge	2	30%	2.6
	PW Diagnostics Hardware	5	30%	6.5
	PW Autocorrelator	15	30%	19.5
1.4.1.4	**Interlocks**			
	CapRoom	2	30%	2.6
	FY' 05 Totals	**2732.7**		**3000**

Table 10 Texas Petawatt annual budget for fiscal year 2005

8.3.4 FY' 06

The final long pulse laser procurements occur in FY' 06. Also, all three target chambers and spares are planned. Operations costs increase as the facility is activated.

WBS	Item Description	FY'06 Costs (k$)	Contingency (%)	Extended Costs (k$)
N/A	**Salary, Fringe, Overhead**	828.85	0%	828.85
N/A	**LLNL Support**	200	0%	200
N/A	**Travel**	75	15%	86.25
N/A	**Operations**	70	20%	84
N/A	**General Lab Equipment**	50	20%	60
1.2.3.4	**LP Main AMP**			
	31.5 Disk Repolish	40	30%	52
	Refurb amplifier	15	30%	19.5
	Lenses	10	30%	13
	Mirrors	30	30%	39
	Mounts	20	30%	26
	Beam Tubes	15	30%	19.5
	Spatial Filter	30	30%	39
	Vacuum System	10	30%	13
1.2.3.5	**LP Frequency Doubler**			
	Conversion Crystal	50	30%	65
	System Optics	20	30%	26
	Beam Tubes	20	30%	26
	Crystal Cell	20	30%	26
1.3.2	**PW Target Chamber**			
	Material	15	30%	19.5
	Chamber	20	30%	26
	Switchyard	5	30%	6.5
	Beam Transport	10	30%	13
	Vacuum System	35	30%	45.5
	Switchyqard Optics	10	30%	13
	Switchyard Optics Mounts	15	30%	19.5
	Focusing Optics	10	30%	13
1.3.3	**Two Beam Chamber**			
	Material	15	30%	19.5
	Chamber	20	30%	26
	Switchyard	5	30%	6.5
	Switchyard Optics	20	30%	26
	Focusing Optics	15	30%	19.5
	Vacuum Windows	5	30%	6.5
	Switchyard Optics Mounts	30	30%	39
	Vacuum System	35	30%	45.5
	Beam Transport	20	30%	26
1.3.4	**LP Chamber**			
	Material	15	30%	19.5
	Switchyard	5	30%	6.5
	Chamber	20	30%	26
	Switchyard Optics	10	30%	13
	Focusing Optics	10	30%	13
	Vacuum Pump	20	30%	26
	Mounts	30	30%	39
	Beam Transport	15	30%	19.5
	LP PXI Chassis	7	30%	9.1
1.4.2.2	**LP Controls**			
	LP Motors & Controllers	78	30%	101.4
	LP Alignment Cameras	12	30%	15.6
	LP Pulsed Power	15	30%	19.5
	LP Pulsed Power Controls	4	30%	5.2
1.4.2.3	**Diagnositcs**			
	Scientific Camera	40	30%	52
	LP Power/Energy	15	30%	19.5
	LP Shot Cameras	25	30%	32.5
	LP Current/Voltage	2	30%	2.6
	LP Vacuumm	2	30%	2.6
	LP Diagnostics Hardware	5	30%	6.5
1.4.1.4	**Interlocks**			
	Target Bay	4	30%	5.2
	Experiement Diagnostics			
	50mJ Ti:Sapphire	90	30%	117
	Spares			
	Repolish 9.4cm Disks	30	30%	39
	Repolish 31.5cm Disks	40	30%	52
	OPCPA/Ti:Sapphire Crystals	75	30%	97.5
	31.5cm& 9.4cm Flashlamps	150	30%	195
	General Optics	25	30%	32.5

Table 11 Texas Petawatt annual budget for fiscal year 2006

8.3.5 FY' 07

Final Texas Petawatt procurements are scheduled for fiscal year 2007. Long pulse diagnostics are planned as well a deformable mirror. The operations budget continues to increase as the laser facility becomes operational.

WBS	Item Description	FY'07 Costs (k$)	Contingency (%)	Extended Costs (k$)
	Salary, Fringe, Overhead	911.68	0%	911.68
	LLNL Support	200	0%	200
	Travel	60	5%	63
	Operations	80	5%	84
	General Lab Equipment	30	10%	33
1.2.3.5	**LP Frequency Doubler**			
	DFM w/ Wavefront Sensor	80	30%	104
1.3.4	**LP Target Chamber**			
	LP Diagnostics Package	80	30%	104
	FY '07 Totals	**1441.68**		**1500**

Table 12 Texas Petawatt annual budget for fiscal year 2007

References

[Ago 87] P. Agostini, P., Kupersztych, J., Lompre, L. A., Petite, G. and Yergeau, F. Direct Evidence of Ponderomotive Effects Via Laser-Pulse Duration in above-Threshold Ionization, *Phys. Rev. A,* **36**, 4111-4114 (1987).

[Aud 02] P. Audebert, Shepherd, R., Fournier, K. B., Peyrusse, O., Price, D., Lee, R., Springer, P., Gauthier, J. C. and Klein, L. Heating of thin foils with a relativistic-intensity short-pulse laser, *Phys. Rev. Lett.,* **89**, art. no.-265001 (2002)

[Ave 98] R. S. Averback, and T. Diaz de la Rubia "Displacement Damage in Irradiated Metals and Semiconductors," *Solid State Phys.* **51**, 281 (1998).

[Ban 97] P. Banks et al ,"Novel all reflective stretcher for chirped pulse amplification of ultrashort pulses" " *IEEE Jour. of QE.* **36**, 268 (1997).

[Bar 00] N. Bartel, Bietenholz, M. F., Rupen, M. P., Beasley, A. J., Graham, D. A., Altunin, V. I., Venturi, T., Umana, G., Cannon, W. H. and Conway, J. E. The Changing Morphology and Increasing Deceleration of Supernova 1993J in M81, *Science,* **287**, 112 (2000).

[Bor 88] Z. Bor, "Distortion in femtosecond laser pulses inlenses and lens systems," *Jou of Mod Opt.* **35**, 1907 (1988).

[Bur 89] N. H. Burnett, N. H. and Corkum, P. B. Cold-Plasma Production for Recombination Extreme-Ultraviolet Lasers by Optical-Field-Induced Ionization, *J. Opt. Soc. Am. B,* **6**, 1195-1199 (1989).

[Cat 96] M.-J. Caturla et al. "Ion Beam Processing of Silicon at KeV Energies: a Molecular Dynamics Study," *Phys. Rev. B* **54**, 16683 (1996).

[Dit 97] T. Ditmire, J. W. G. Tisch, E. Springate, M. B. Mason, N. Hay, R. A. Smith, J. P. Marangos and M. H. R. Hutchinson, "High Energy Ions Produced in Explosions of Super-Heated Atomic Clusters," *Nature,* **386**, 54 (1997).

[Dit 99] T. Ditmire, et al., "Nuclear Fusion from Explosions of Femtosecond-Laser Heated Deuterium Cluster," *Nature.* **398**, 492 (1999).

[Dit 00] T. Ditmire, T., Shigemori, K., Remington, B. A., Estabrook, K. and Smith, R. A. The production of strong blast waves through intense laser irradiation of atomic clusters, *Astrophys. J. Suppl. Ser.,* **127**, 299-304 (2000).

[Ede 04] A. D. Edens, T. Ditmire, J. F. Hansen, M. J. Edwards, R.G. Adams, P. Rambo, L. Ruggles, I.C. Smith, and J. L. Porter, "Study of high Mach number laser driven blast waves" *Phys. Plas.* 11, 4968 (2004).

[Edw 01] M. J. Edwards, A. J. MacKinnon, J. Zweiback, K. Shigemori, D. Ryutov, A. M. Rubenchik, K. A. Keilty, E. Liang, B. A. Remington and T. Ditmire, "Investigation of Ultrafast Laser Driven Radiative Blast Waves," Phys. Rev. Lett. 87, 085004 (2001).

[Hu 02] Hu, S. X. and Starace, A. F. GeV electrons from ultraintense laser interaction with highly charged ions, *Phys. Rev. Lett.,* **88**, art. no.-245003 (2002).

[Lee 02] R. W. Lee, Baldis, H. A., Cauble, R. C., Landen, O. L., Wark, J. S., Ng, A., Rose, S. J., Lewis, C., Riley, D., Gauthier, J. C. and Audebert, P. Plasma-based studies with intense X-ray and particle beam sources, *Laser Part. Beams,* **20**, 527-536 (2002).

[Lee 03] R. W. Lee, Moon, S. J., Chung, H. K., Rozmus, W., Baldis, H. A., Gregori, G., Cauble, R. C., Landen, O. L., Wark, J. S., Ng, A., Rose, S. J., Lewis, C. L., Riley, D., Gauthier, J. C. and Audebert, P. Finite temperature dense matter studies on next-generation light sources, *J. Opt. Soc. Am. B-Opt. Phys.,* **20**, 770-778 (2003).

[Lez 98] M. Lezius, S. Dobosz, D. Normand, and M. Schmidt, "Explosion Dynamics of Rare Gas Clusters in Strong Laser Fields," *Phys. Rev. Lett.* **80**, 261 (1998).

[Mad 04] K. W. Madison, R. Fitzpatrick, P. K. Patel, D. Price, T. Ditmire, "The role of laser pulse duration in Coulomb explosions of deuterium cluster targets" *Phys. Rev. A* **70**, 053201 (2004).

[McK 91] McKee, C. F. and Draine, B. T. 1991. Interstellar Shock Waves, *Science,* **252**, 397.

[Mos 00] E. Moshe, Eliezer, S., Henis, Z., et al. Experimental Measurements of the Strength of Metals Approaching the Theoretical Limit Predicted by the Equation of State, *App. Phys. Lett.,* **76**, 15555. (2000).

[Per 99] M. Perry et al., "Petawatt laser pulses," *Opt. Lett.* **24**, 160 (1999).

[Per 00] L. J. Perkins, et al., "The Investigation of High-Intensity-Laser-Driven Micro Neutron Sources for Fusion Materials Research at High Fluence," *Nuc. Fusion* **40**, 1 (2000).

[Ros 00] I. Ross, et al., "Generation of terawatt pulses by use of optical parametric chirped pulse amplification," *App. Opt.* **39**, 2422 (2000).

[Sen 04] Y. Sentoku, Mima K, Ruhl H, et al. "Laser light and hot electron micro focusing using a conical target" *Phys. Plas*. 3083 (2004).

[Sha 83] C. V. Shank, Yen, R. and Hirlimann, C. Femtosecond-Time-Resolved Surface Structural Dynamics of Optically Excited Silicon, *Phys. Rev. Lett.,* **51**, 9001 (1983).

[Tra 79] R. J. Trainor, Shaner, J. W., Auerbach, J. M. and Holmes, N. C. Ultrahigh-Pressure Laser-Driven Shock Wave Experiments in Aluminum, *Phys. Rev. Lett.,* **42**, 1154 (1979).

[Vis 83] E. T. Vishniac, The Dynamic and Gravitational Instabilities of Spherical Shocks, *Ap. J.,* **274**, 152 (1983).

[War 89] Wark, J. S., Whitlock, R. R., Hauer, A. A., Swain, J. E. and Solone, P. J. Subnanosecond X-Ray-Diffraction From Laser-Shocked Crystals, *Phys. Rev. B-Condens Matter,* **40**, 5705 (1989).

[Wid 01] K. Widmann, Guethlein, G., Foord, M. E., Cauble, R. C., Patterson, F. G., Price, D. F., Rogers, F. J., Springer, P. T., Stewart, R. E., Ng, A., Ao, T. and Forsman, A. Interferometric investigation of femtosecond laser-heated expanded states, *Phys. Plasmas,* **8**, 3869-3872 (2001).

[Zwe 00] J. Zweiback, T.E. Cowan, J. Hartley, G. Hays, R. Howell R.A. Smith, C. Steinke, and T. Ditmire, "Characterization of Fusion Burn Time in Exploding Deuterium Cluster Plasmas ," *Phys. Rev. Lett.,***85,** 3640 (2000).

Appendix A: Project schedule for The Texas Petawatt.

The following appendix contains the project schedule in much more detail than the main body of this report. For space considerations, we have collapsed the 8 level project to the 5th level and included it below.

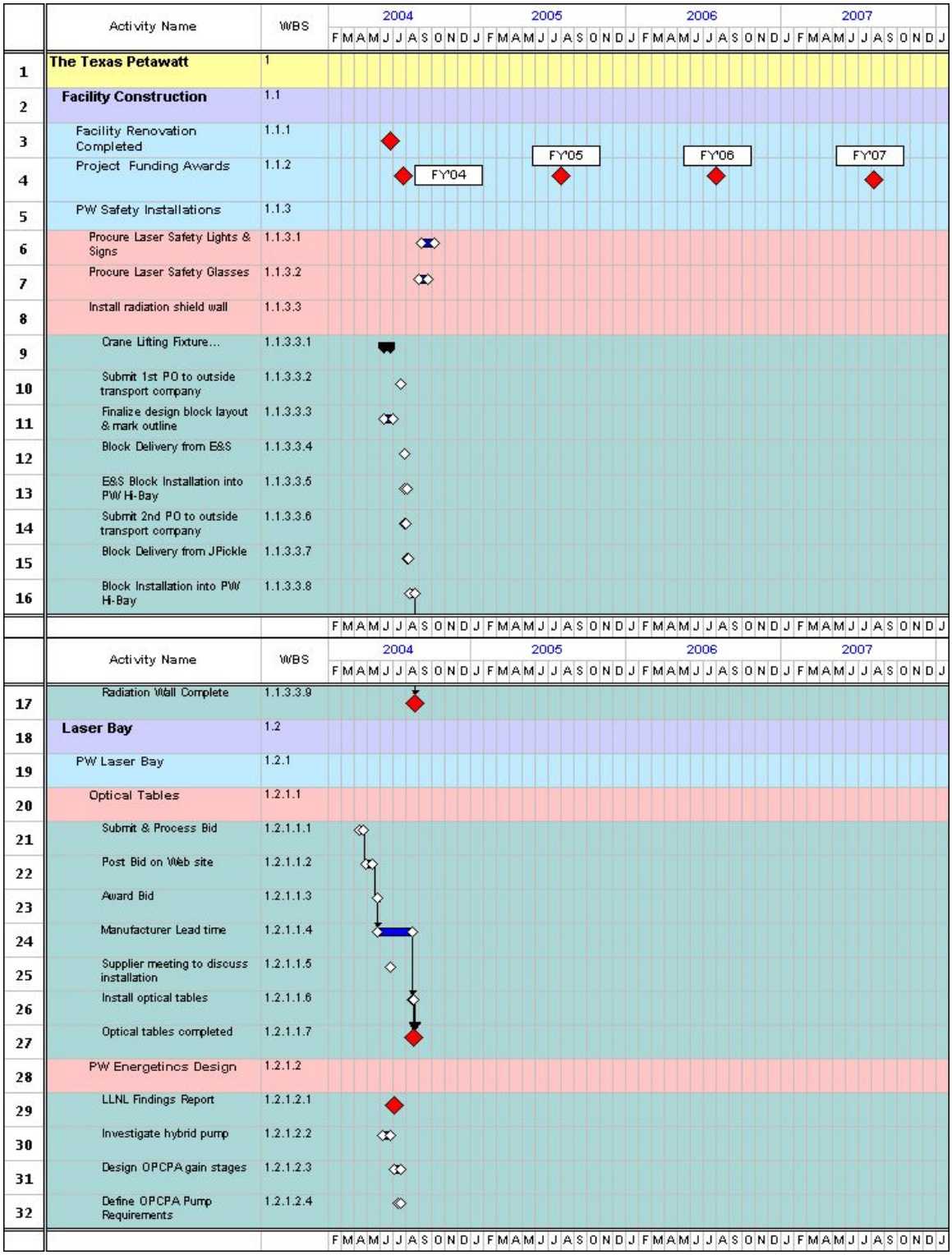

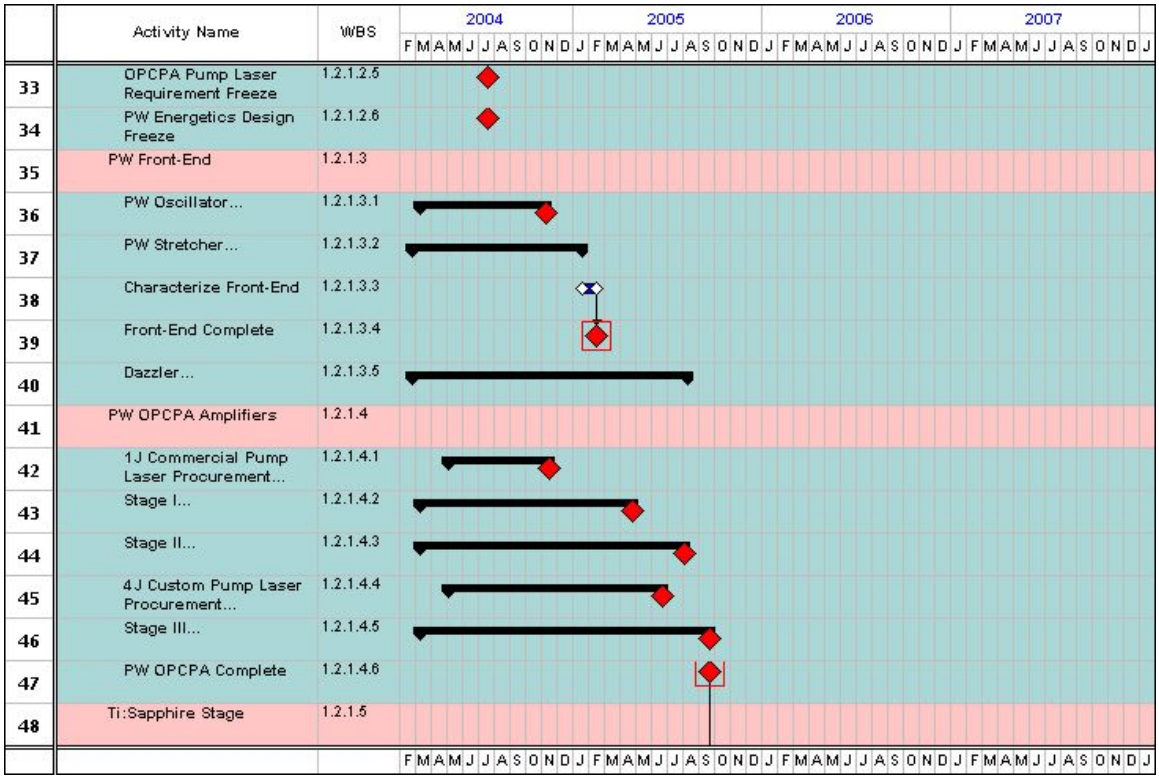
Activity Name
WBS
2004
2005
2006
2007
F M A M J J A S O N D J F M A M J J A S O N D J F M A M J J A S O N D J F M A M J J A S O N D J
33 OPCPA Pump Laser Requirement Freeze 1.2.1.2.5
34 PW Energetics Design Freeze 1.2.1.2.6
35 PW Front-End 1.2.1.3
36 PW Oscillator... 1.2.1.3.1
37 PW Stretcher... 1.2.1.3.2
38 Characterize Front-End 1.2.1.3.3
39 Front-End Complete 1.2.1.3.4
40 Dazzler... 1.2.1.3.5
41 PW OPCPA Amplifiers 1.2.1.4
42 1J Commercial Pump Laser Procurement... 1.2.1.4.1
43 Stage I... 1.2.1.4.2
44 Stage II... 1.2.1.4.3
45 4J Custom Pump Laser Procurement... 1.2.1.4.4
46 Stage III... 1.2.1.4.5
47 PW OPCPA Complete 1.2.1.4.6
48 Ti:Sapphire Stage 1.2.1.5

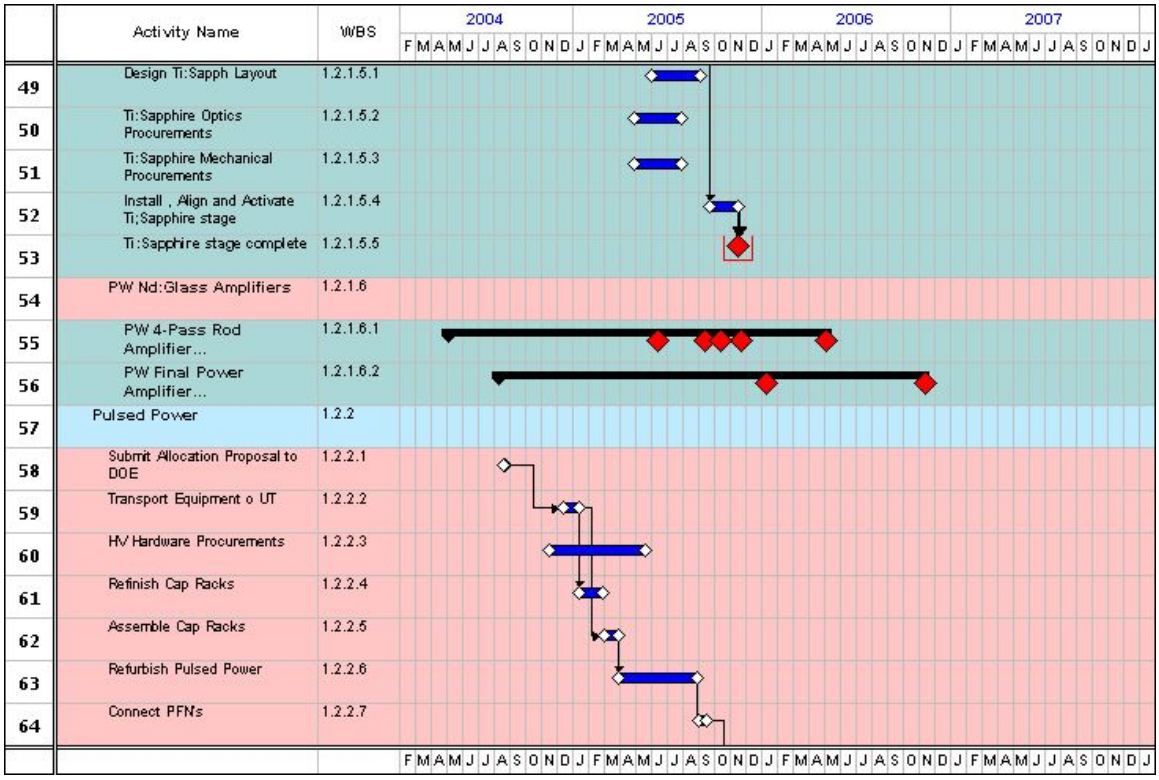
Activity Name
WBS
2004
2005
2006
2007
F M A M J J A S O N D J F M A M J J A S O N D J F M A M J J A S O N D J F M A M J J A S O N D J
49 Design Ti:Sapph Layout 1.2.1.5.1
50 Ti:Sapphire Optics Procurements 1.2.1.5.2
51 Ti:Sapphire Mechanical Procurements 1.2.1.5.3
52 Install , Align and Activate Ti;Sapphire stage 1.2.1.5.4
53 Ti:Sapphire stage complete 1.2.1.5.5
54 PW Nd:Glass Amplifiers 1.2.1.6
55 PW 4-Pass Rod Amplifier... 1.2.1.6.1
56 PW Final Power Amplifier... 1.2.1.6.2
57 Pulsed Power 1.2.2
58 Submit Allocation Proposal to DOE 1.2.2.1
59 Transport Equipment o UT 1.2.2.2
60 HV Hardware Procurements 1.2.2.3
61 Refinish Cap Racks 1.2.2.4
62 Assemble Cap Racks 1.2.2.5
63 Refurbish Pulsed Power 1.2.2.6
64 Connect PFNs 1.2.2.7

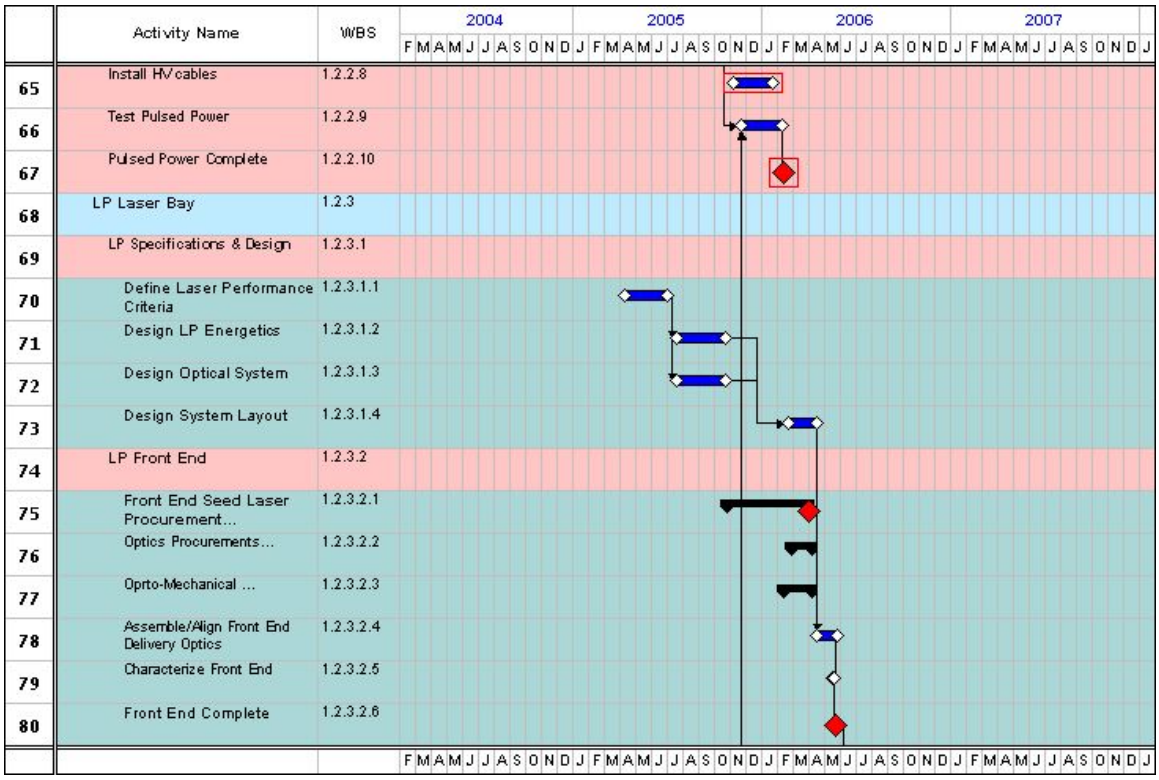
Activity Name
WBS
2004
2005
2006
2007
F M A M J J A S O N D J F M A M J J A S O N D J F M A M J J A S O N D J F M A M J J A S O N D J
65 Install HV cables 1.2.2.8
66 Test Pulsed Power 1.2.2.9
67 Pulsed Power Complete 1.2.2.10
68 LP Laser Bay 1.2.3
69 LP Specifications & Design 1.2.3.1
70 Define Laser Performance Criteria 1.2.3.1.1
71 Design LP Energetics 1.2.3.1.2
72 Design Optical System 1.2.3.1.3
73 Design System Layout 1.2.3.1.4
74 LP Front End 1.2.3.2
75 Front End Seed Laser Procurement... 1.2.3.2.1
76 Optics Procurements... 1.2.3.2.2
77 Oprto-Mechanical ... 1.2.3.2.3
78 Assemble/Align Front End Delivery Optics 1.2.3.2.4
79 Characterize Front End 1.2.3.2.5
80 Front End Complete 1.2.3.2.6

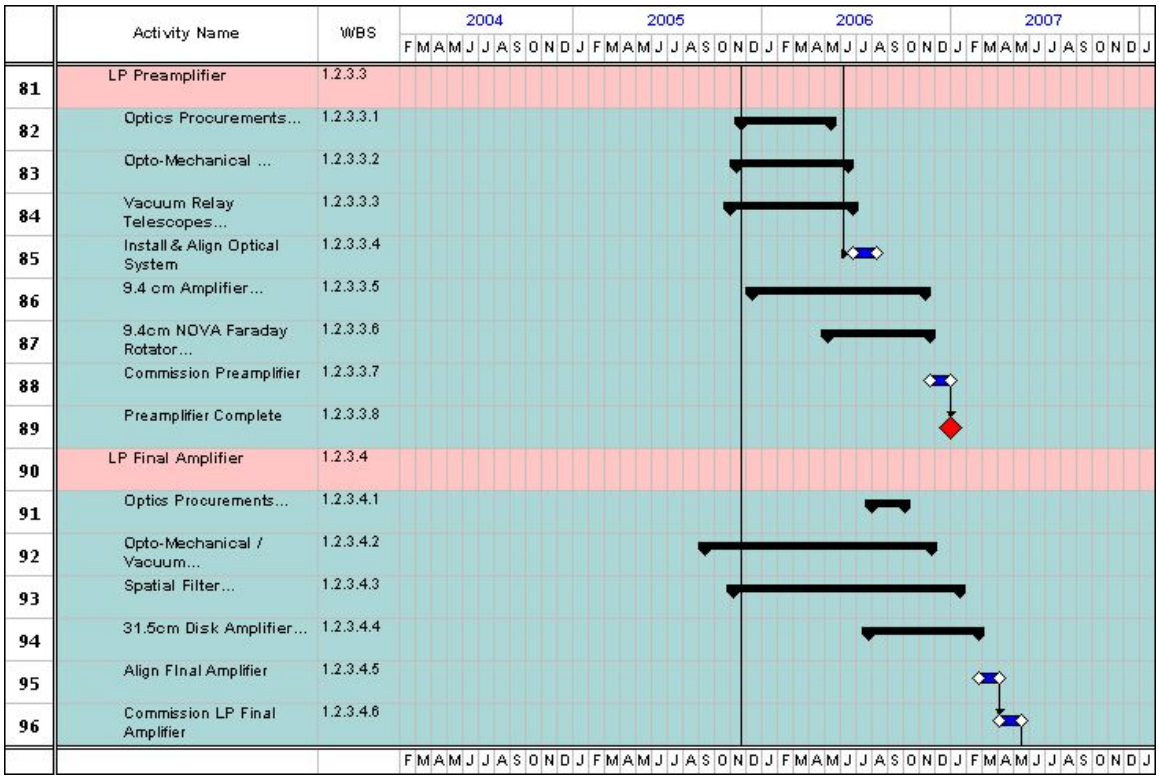
Activity Name
WBS
2004
2005
2006
2007
F M A M J J A S O N D J F M A M J J A S O N D J F M A M J J A S O N D J F M A M J J A S O N D J
81 LP Preamplifier 1.2.3.3
82 Optics Procurements... 1.2.3.3.1
83 Opto-Mechanical ... 1.2.3.3.2
84 Vacuum Relay Telescopes... 1.2.3.3.3
85 Install & Align Optical System 1.2.3.3.4
86 9.4 cm Amplifier... 1.2.3.3.5
87 9.4cm NOVA Faraday Rotator... 1.2.3.3.6
88 Commission Preamplifier 1.2.3.3.7
89 Preamplifier Complete 1.2.3.3.8
90 LP Final Amplifier 1.2.3.4
91 Optics Procurements... 1.2.3.4.1
92 Opto-Mechanical / Vacuum... 1.2.3.4.2
93 Spatial Filter... 1.2.3.4.3
94 31.5cm Disk Amplifier... 1.2.3.4.4
95 Align FInal Amplifier 1.2.3.4.5
96 Commission LP Final Amplifier 1.2.3.4.6

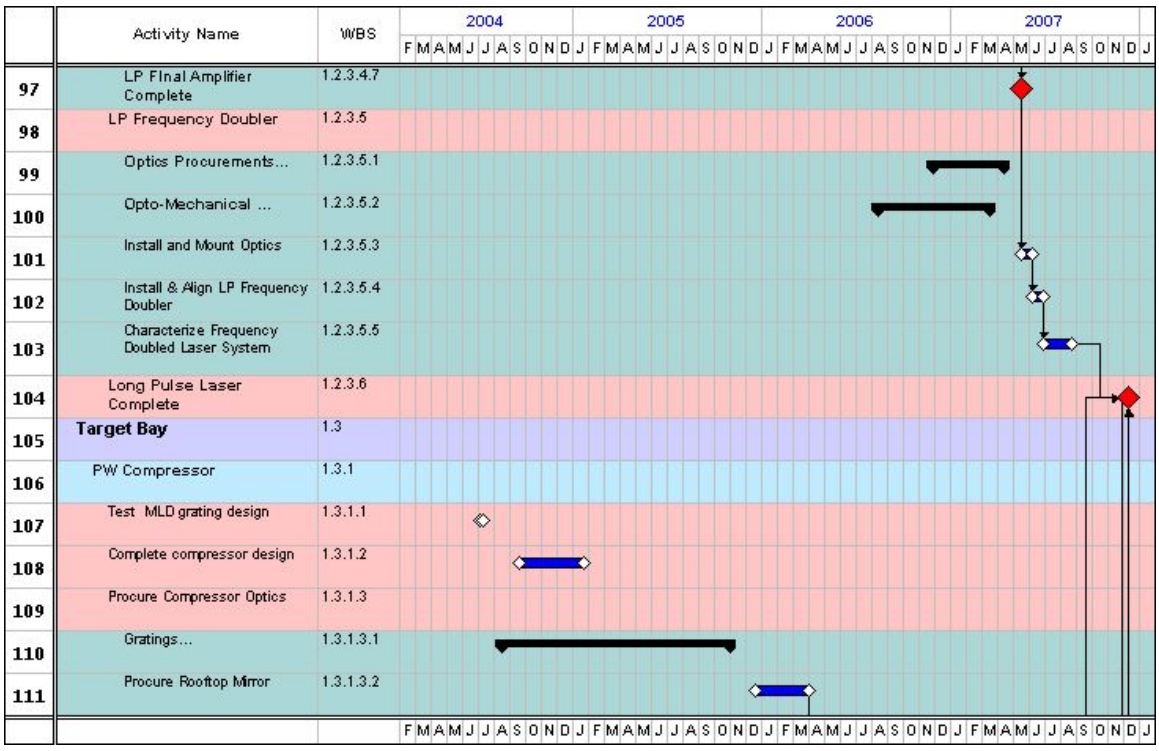
Activity Name
WBS
2004
2005
2006
2007
97 LP FInal Amplifier Complete 1.2.3.4.7
98 LP Frequency Doubler 1.2.3.5
99 Optics Procurements... 1.2.3.5.1
100 Opto-Mechanical ... 1.2.3.5.2
101 Install and Mount Optics 1.2.3.5.3
102 Install & Align LP Frequency Doubler 1.2.3.5.4
103 Characterize Frequency Doubled Laser System 1.2.3.5.5
104 Long Pulse Laser Complete 1.2.3.6
105 Target Bay 1.3
106 PW Compressor 1.3.1
107 Test MLD grating design 1.3.1.1
108 Complete compressor design 1.3.1.2
109 Procure Compressor Optics 1.3.1.3
110 Gratings... 1.3.1.3.1
111 Procure Rooftop Mirror 1.3.1.3.2

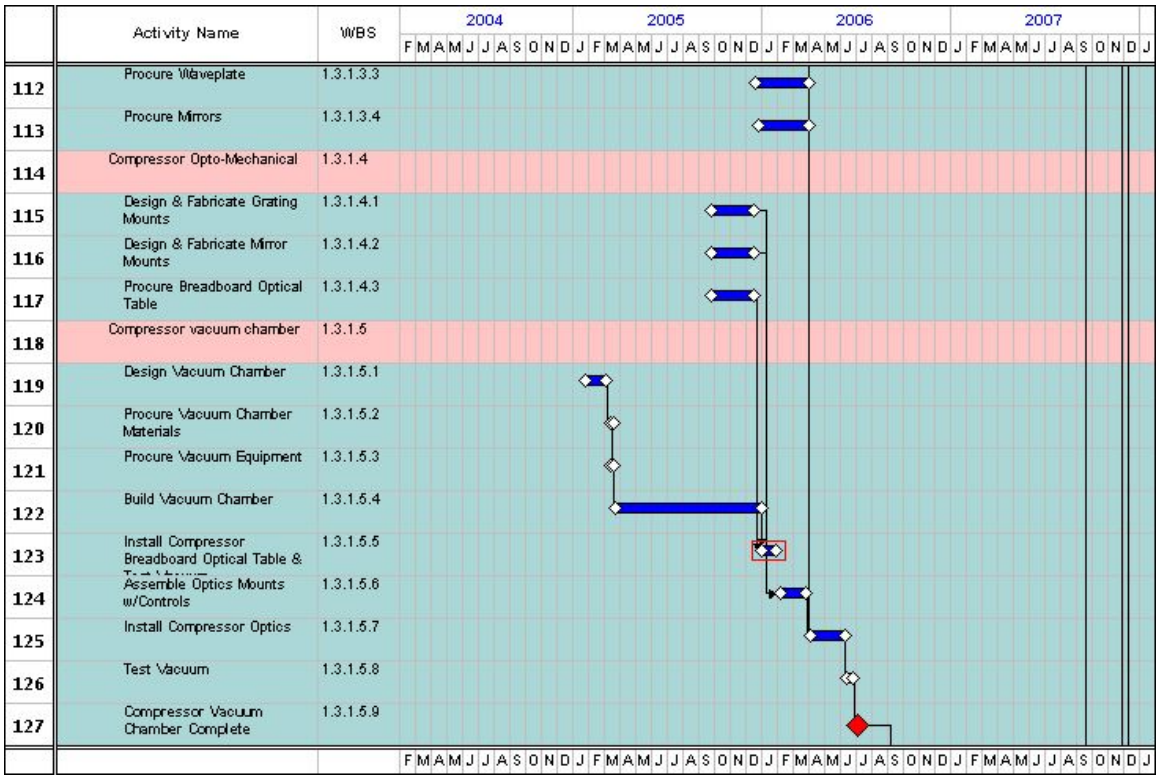
Activity Name
WBS
2004
2005
2006
2007
112 Procure Waveplate 1.3.1.3.3
113 Procure Mirrors 1.3.1.3.4
114 Compressor Opto-Mechanical 1.3.1.4
115 Design & Fabricate Grating Mounts 1.3.1.4.1
116 Design & Fabricate Mirror Mounts 1.3.1.4.2
117 Procure Breadboard Optical Table 1.3.1.4.3
118 Compressor vacuum chamber 1.3.1.5
119 Design Vacuum Chamber 1.3.1.5.1
120 Procure Vacuum Chamber Materials 1.3.1.5.2
121 Procure Vacuum Equipment 1.3.1.5.3
122 Build Vacuum Chamber 1.3.1.5.4
123 Install Compressor Breadboard Optical Table & 1.3.1.5.5
124 Assemble Optics Mounts w/Controls 1.3.1.5.6
125 Install Compressor Optics 1.3.1.5.7
126 Test Vacuum 1.3.1.5.8
127 Compressor Vacuum Chamber Complete 1.3.1.5.9

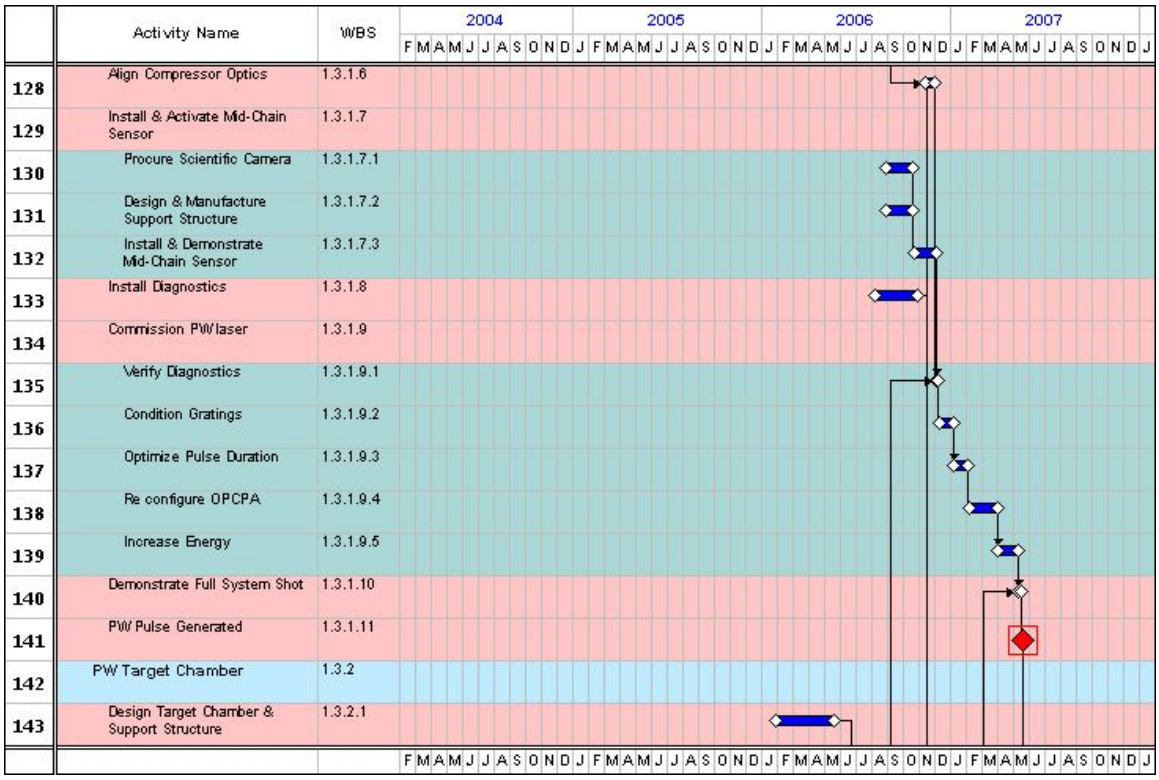
Activity Name
WBS
2004
2005
2006
2007
F M A M J J A S O N D J F M A M J J A S O N D J F M A M J J A S O N D J F M A M J J A S O N D J
128 Align Compressor Optics 1.3.1.6
129 Install & Activate Mid-Chain Sensor 1.3.1.7
130 Procure Scientific Camera 1.3.1.7.1
131 Design & Manufacture Support Structure 1.3.1.7.2
132 Install & Demonstrate Mid-Chain Sensor 1.3.1.7.3
133 Install Diagnostics 1.3.1.8
134 Commission PW laser 1.3.1.9
135 Verify Diagnostics 1.3.1.9.1
136 Condition Gratings 1.3.1.9.2
137 Optimize Pulse Duration 1.3.1.9.3
138 Re configure OPCPA 1.3.1.9.4
139 Increase Energy 1.3.1.9.5
140 Demonstrate Full System Shot 1.3.1.10
141 PW Pulse Generated 1.3.1.11
142 PW Target Chamber 1.3.2
143 Design Target Chamber & Support Structure 1.3.2.1

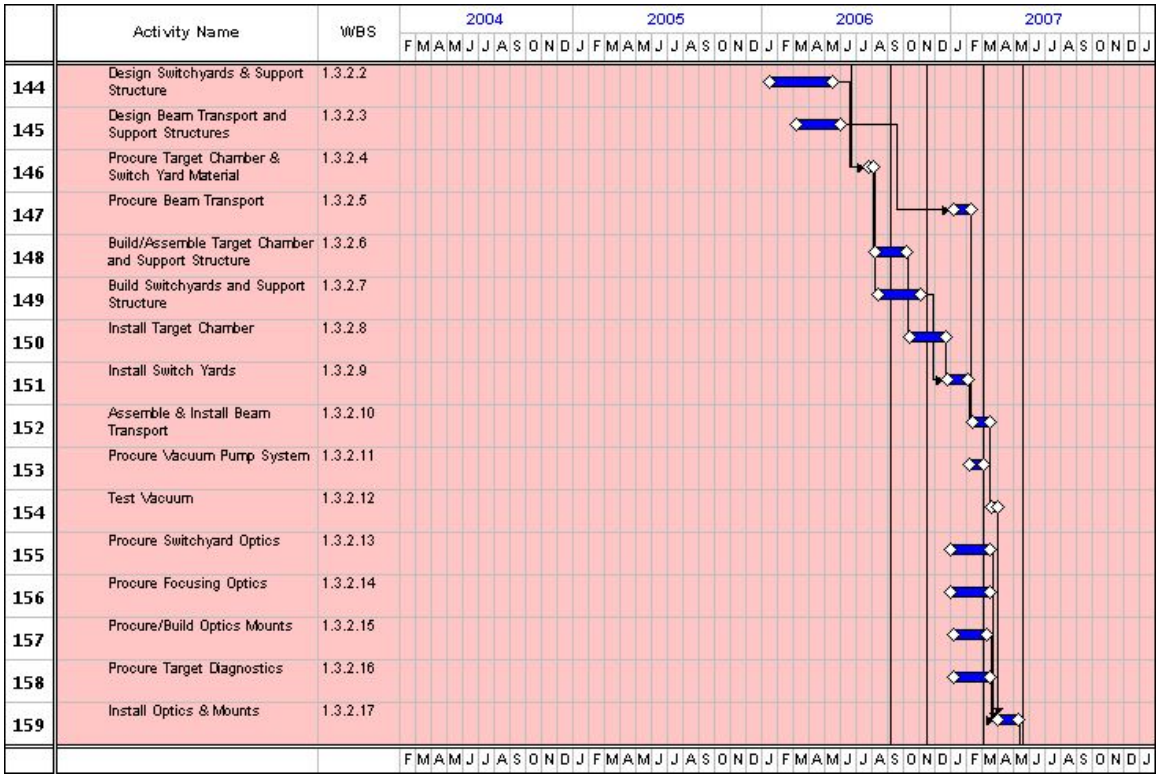
Activity Name
WBS
2004
2005
2006
2007
F M A M J J A S O N D J F M A M J J A S O N D J F M A M J J A S O N D J F M A M J J A S O N D J
144 Design Switchyards & Support Structure 1.3.2.2
145 Design Beam Transport and Support Structures 1.3.2.3
146 Procure Target Chamber & Switch Yard Material 1.3.2.4
147 Procure Beam Transport 1.3.2.5
148 Build/Assemble Target Chamber and Support Structure 1.3.2.6
149 Build Switchyards and Support Structure 1.3.2.7
150 Install Target Chamber 1.3.2.8
151 Install Switch Yards 1.3.2.9
152 Assemble & Install Beam Transport 1.3.2.10
153 Procure Vacuum Pump System 1.3.2.11
154 Test Vacuum 1.3.2.12
155 Procure Switchyard Optics 1.3.2.13
156 Procure Focusing Optics 1.3.2.14
157 Procure/Build Optics Mounts 1.3.2.15
158 Procure Target Diagnostics 1.3.2.16
159 Install Optics & Mounts 1.3.2.17

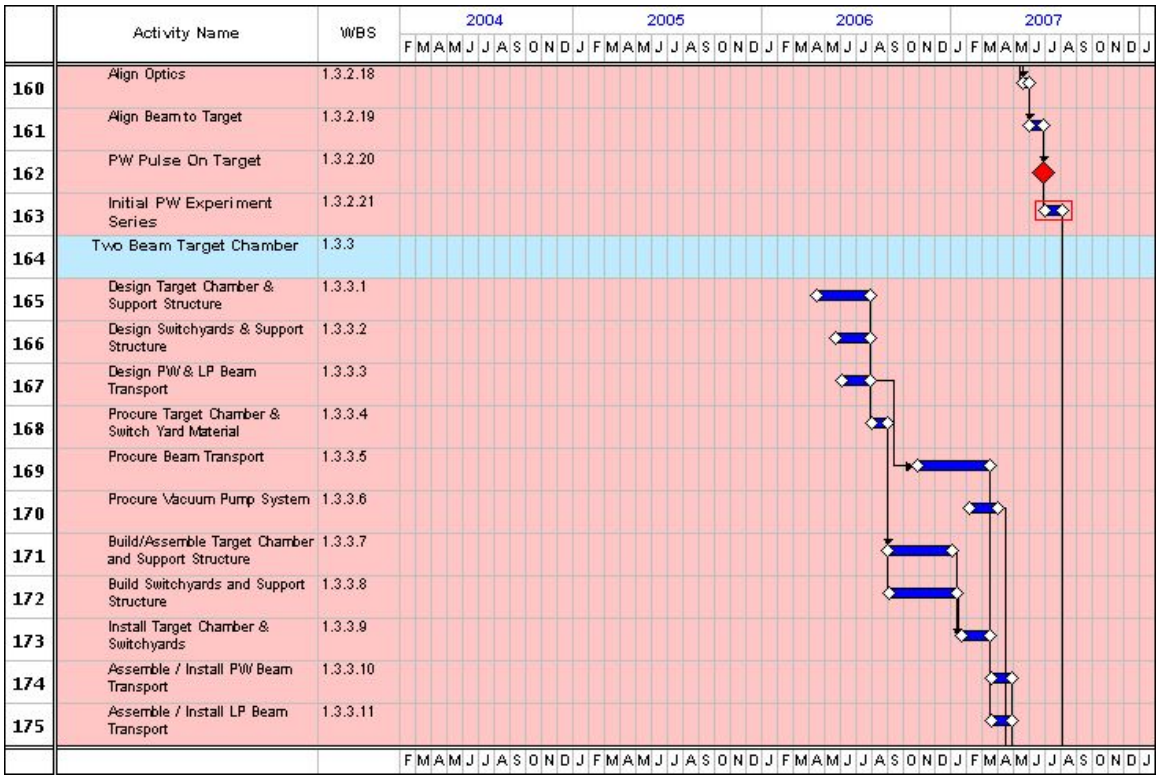

	Activity Name	WBS
160	Align Optics	1.3.2.18
161	Align Beam to Target	1.3.2.19
162	PW Pulse On Target	1.3.2.20
163	Initial PW Experiment Series	1.3.2.21
164	Two Beam Target Chamber	1.3.3
165	Design Target Chamber & Support Structure	1.3.3.1
166	Design Switchyards & Support Structure	1.3.3.2
167	Design PW & LP Beam Transport	1.3.3.3
168	Procure Target Chamber & Switch Yard Material	1.3.3.4
169	Procure Beam Transport	1.3.3.5
170	Procure Vacuum Pump System	1.3.3.6
171	Build/Assemble Target Chamber and Support Structure	1.3.3.7
172	Build Switchyards and Support Structure	1.3.3.8
173	Install Target Chamber & Switchyards	1.3.3.9
174	Assemble / Install PW Beam Transport	1.3.3.10
175	Assemble / Install LP Beam Transport	1.3.3.11

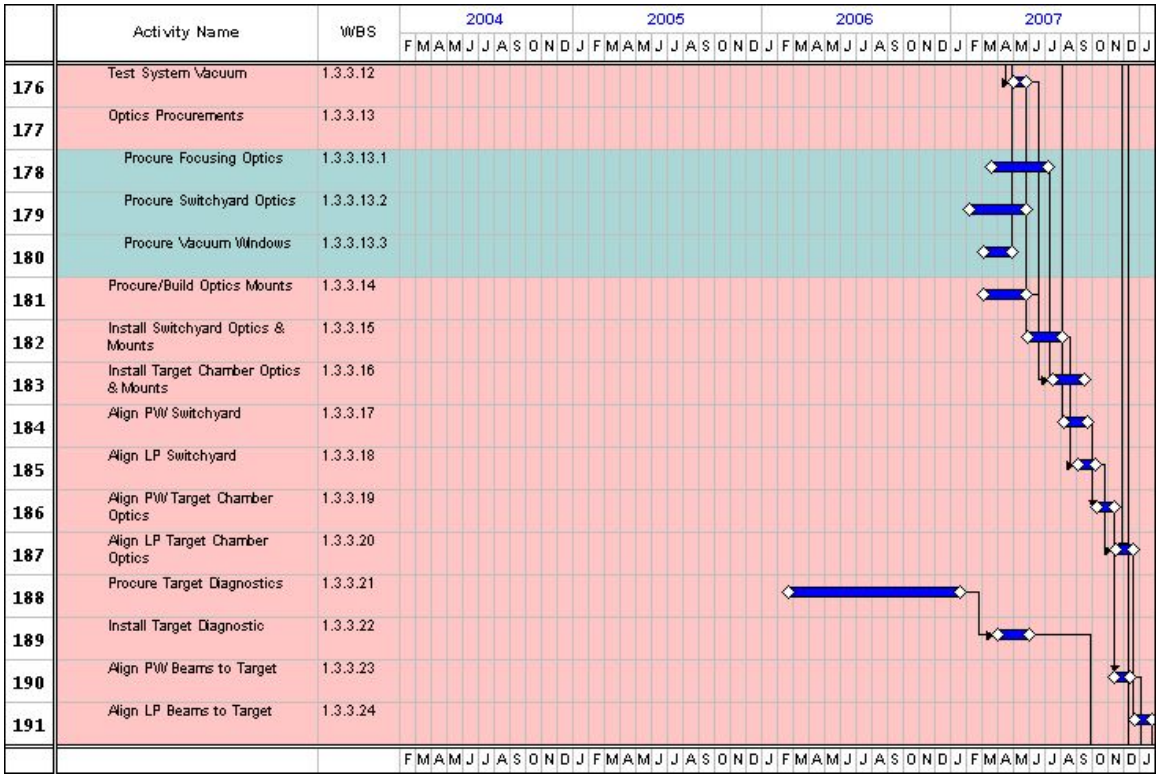

	Activity Name	WBS
176	Test System Vacuum	1.3.3.12
177	Optics Procurements	1.3.3.13
178	Procure Focusing Optics	1.3.3.13.1
179	Procure Switchyard Optics	1.3.3.13.2
180	Procure Vacuum Windows	1.3.3.13.3
181	Procure/Build Optics Mounts	1.3.3.14
182	Install Switchyard Optics & Mounts	1.3.3.15
183	Install Target Chamber Optics & Mounts	1.3.3.16
184	Align PW Switchyard	1.3.3.17
185	Align LP Switchyard	1.3.3.18
186	Align PW Target Chamber Optics	1.3.3.19
187	Align LP Target Chamber Optics	1.3.3.20
188	Procure Target Diagnostics	1.3.3.21
189	Install Target Diagnostic	1.3.3.22
190	Align PW Beams to Target	1.3.3.23
191	Align LP Beams to Target	1.3.3.24

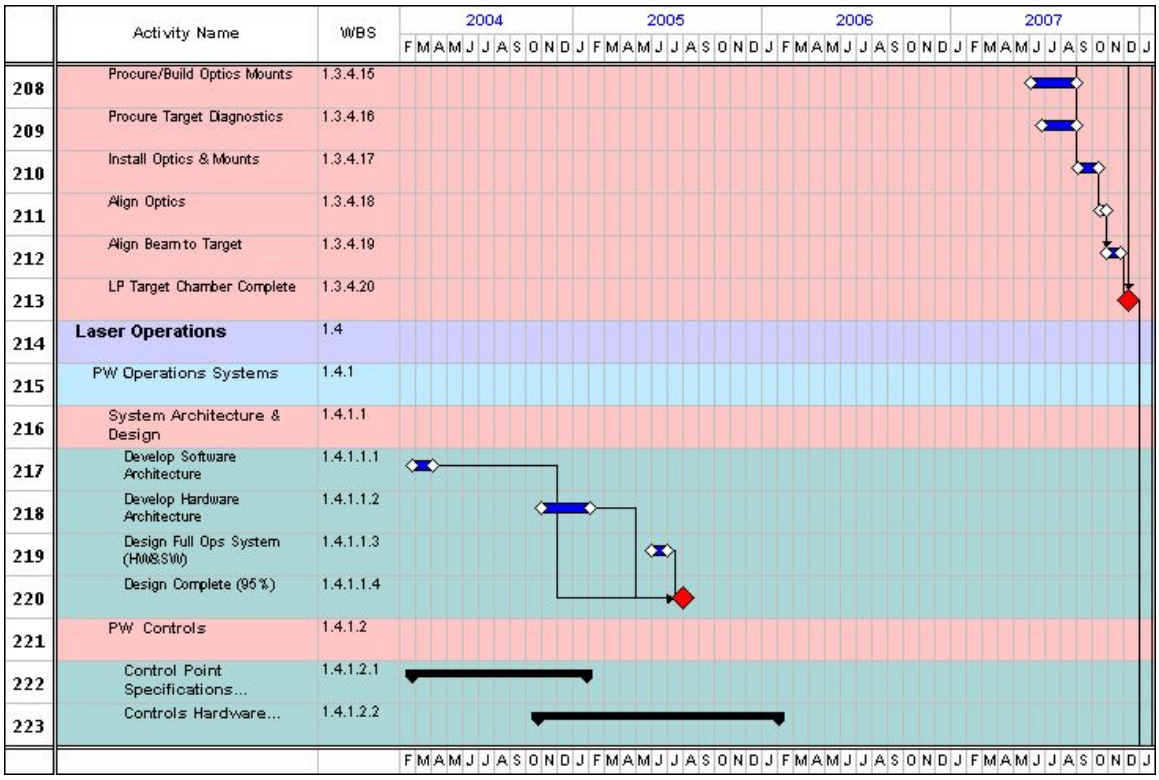
2004
2005
2006
2007
F M A M J J A S O N D J F M A M J J A S O N D J F M A M J J A S O N D J F M A M J J A S O N D J
208 Procure/Build Optics Mounts 1.3.4.15
209 Procure Target Diagnostics 1.3.4.16
210 Install Optics & Mounts 1.3.4.17
211 Align Optics 1.3.4.18
212 Align Beam to Target 1.3.4.19
213 LP Target Chamber Complete 1.3.4.20
214 Laser Operations 1.4
215 PW Operations Systems 1.4.1
216 System Architecture & Design 1.4.1.1
217 Develop Software Architecture 1.4.1.1.1
218 Develop Hardware Architecture 1.4.1.1.2
219 Design Full Ops System (HW&SW) 1.4.1.1.3
220 Design Complete (95%) 1.4.1.1.4
221 PW Controls 1.4.1.2
222 Control Point Specifications... 1.4.1.2.1
223 Controls Hardware... 1.4.1.2.2

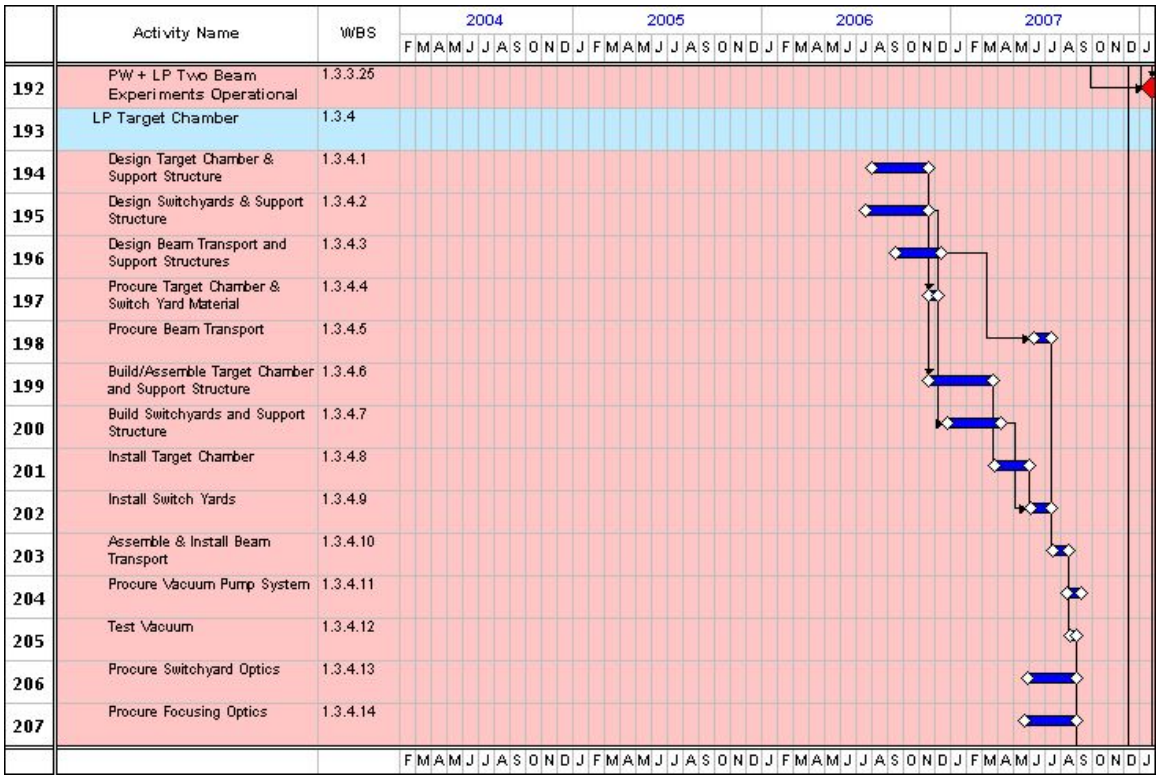
2004
2005
2006
2007
F M A M J J A S O N D J F M A M J J A S O N D J F M A M J J A S O N D J F M A M J J A S O N D J
192 PW + LP Two Beam Experiments Operational 1.3.3.25
193 LP Target Chamber 1.3.4
194 Design Target Chamber & Support Structure 1.3.4.1
195 Design Switchyards & Support Structure 1.3.4.2
196 Design Beam Transport and Support Structures 1.3.4.3
197 Procure Target Chamber & Switch Yard Material 1.3.4.4
198 Procure Beam Transport 1.3.4.5
199 Build/Assemble Target Chamber and Support Structure 1.3.4.6
200 Build Switchyards and Support Structure 1.3.4.7
201 Install Target Chamber 1.3.4.8
202 Install Switch Yards 1.3.4.9
203 Assemble & Install Beam Transport 1.3.4.10
204 Procure Vacuum Pump System 1.3.4.11
205 Test Vacuum 1.3.4.12
206 Procure Switchyard Optics 1.3.4.13
207 Procure Focusing Optics 1.3.4.14

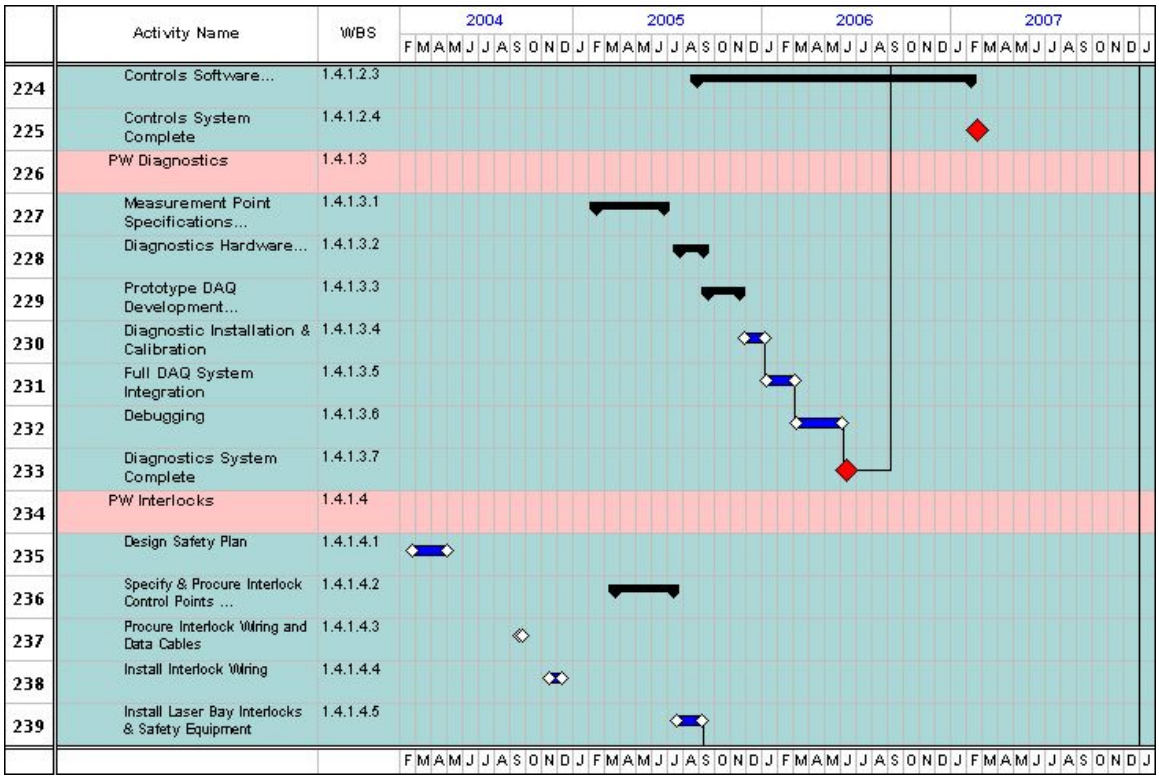
Activity Name
WBS
2004
2005
2006
2007
F M A M J J A S O N D J F M A M J J A S O N D J F M A M J J A S O N D J F M A M J J A S O N D J
224 Controls Software... 1.4.1.2.3
225 Controls System Complete 1.4.1.2.4
226 PW Diagnostics 1.4.1.3
227 Measurement Point Specifications... 1.4.1.3.1
228 Diagnostics Hardware... 1.4.1.3.2
229 Prototype DAQ Development... 1.4.1.3.3
230 Diagnostic Installation & Calibration 1.4.1.3.4
231 Full DAQ System Integration 1.4.1.3.5
232 Debugging 1.4.1.3.6
233 Diagnostics System Complete 1.4.1.3.7
234 PW Interlocks 1.4.1.4
235 Design Safety Plan 1.4.1.4.1
236 Specify & Procure Interlock Control Points ... 1.4.1.4.2
237 Procure Interlock Wiring and Data Cables 1.4.1.4.3
238 Install Interlock Wiring 1.4.1.4.4
239 Install Laser Bay Interlocks & Safety Equipment 1.4.1.4.5
F M A M J J A S O N D J F M A M J J A S O N D J F M A M J J A S O N D J F M A M J J A S O N D J

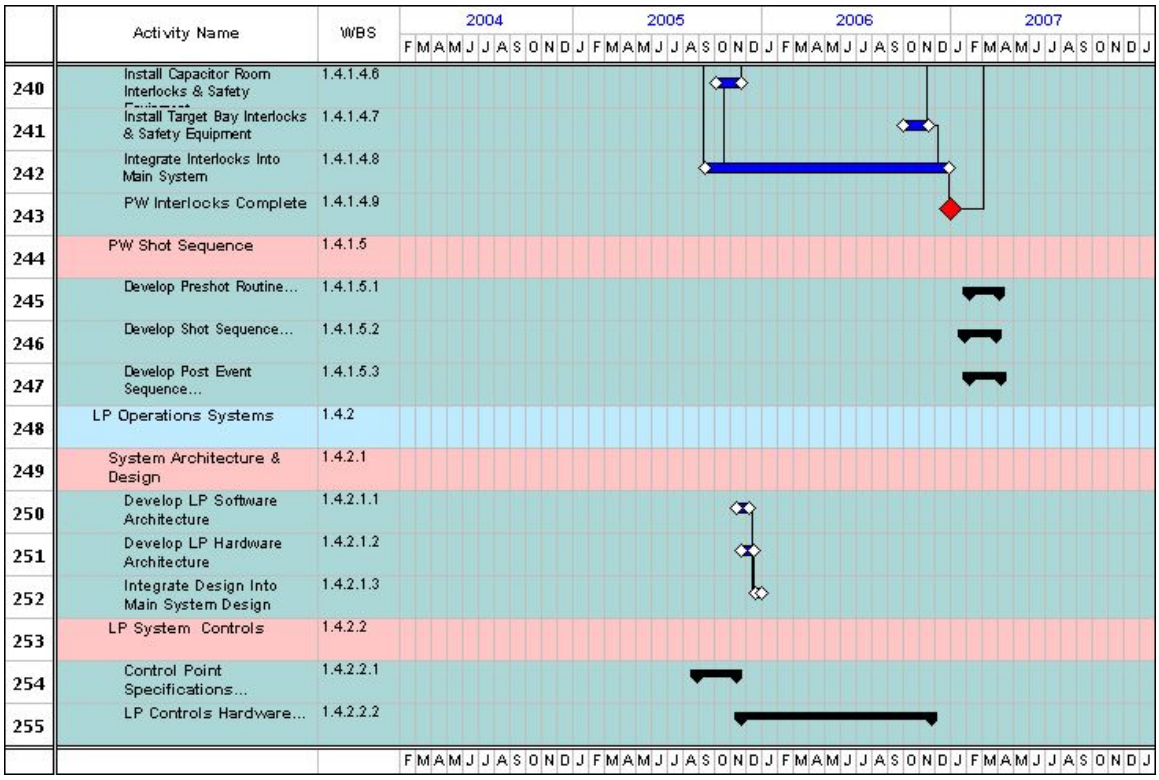
Activity Name
WBS
2004
2005
2006
2007
F M A M J J A S O N D J F M A M J J A S O N D J F M A M J J A S O N D J F M A M J J A S O N D J
240 Install Capacitor Room Interlocks & Safety
241 Install Target Bay Interlocks & Safety Equipment 1.4.1.4.7
242 Integrate Interlocks Into Main System 1.4.1.4.8
243 PW Interlocks Complete 1.4.1.4.9
244 PW Shot Sequence 1.4.1.5
245 Develop Preshot Routine... 1.4.1.5.1
246 Develop Shot Sequence... 1.4.1.5.2
247 Develop Post Event Sequence... 1.4.1.5.3
248 LP Operations Systems 1.4.2
249 System Architecture & Design 1.4.2.1
250 Develop LP Software Architecture 1.4.2.1.1
251 Develop LP Hardware Architecture 1.4.2.1.2
252 Integrate Design Into Main System Design 1.4.2.1.3
253 LP System Controls 1.4.2.2
254 Control Point Specifications... 1.4.2.2.1
255 LP Controls Hardware... 1.4.2.2.2
F M A M J J A S O N D J F M A M J J A S O N D J F M A M J J A S O N D J F M A M J J A S O N D J

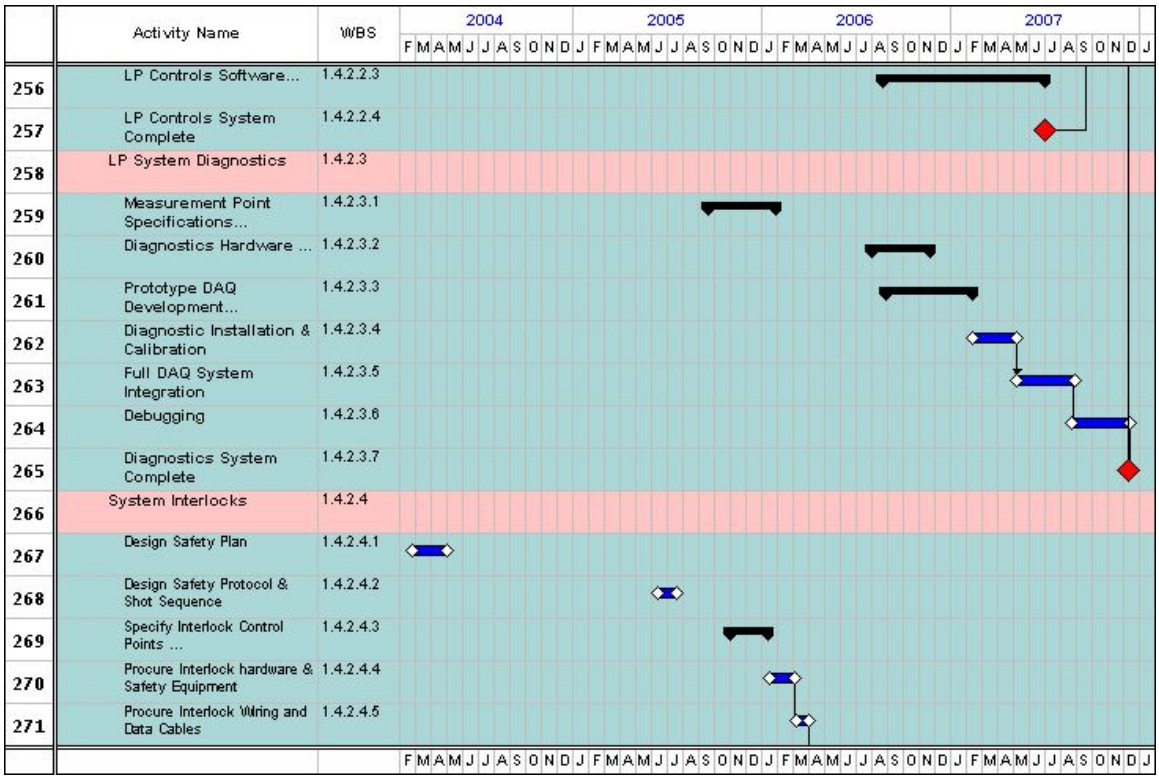
Activity Name
WBS
2004
2005
2006
2007
256 LP Controls Software... 1.4.2.2.3
257 LP Controls System Complete 1.4.2.2.4
258 LP System Diagnostics 1.4.2.3
259 Measurement Point Specifications... 1.4.2.3.1
260 Diagnostics Hardware ... 1.4.2.3.2
261 Prototype DAQ Development... 1.4.2.3.3
262 Diagnostic Installation & Calibration 1.4.2.3.4
263 Full DAQ System Integration 1.4.2.3.5
264 Debugging 1.4.2.3.6
265 Diagnostics System Complete 1.4.2.3.7
266 System Interlocks 1.4.2.4
267 Design Safety Plan 1.4.2.4.1
268 Design Safety Protocol & Shot Sequence 1.4.2.4.2
269 Specify Interlock Control Points ... 1.4.2.4.3
270 Procure Interlock hardware & Safety Equipment 1.4.2.4.4
271 Procure Interlock Wiring and Data Cables 1.4.2.4.5

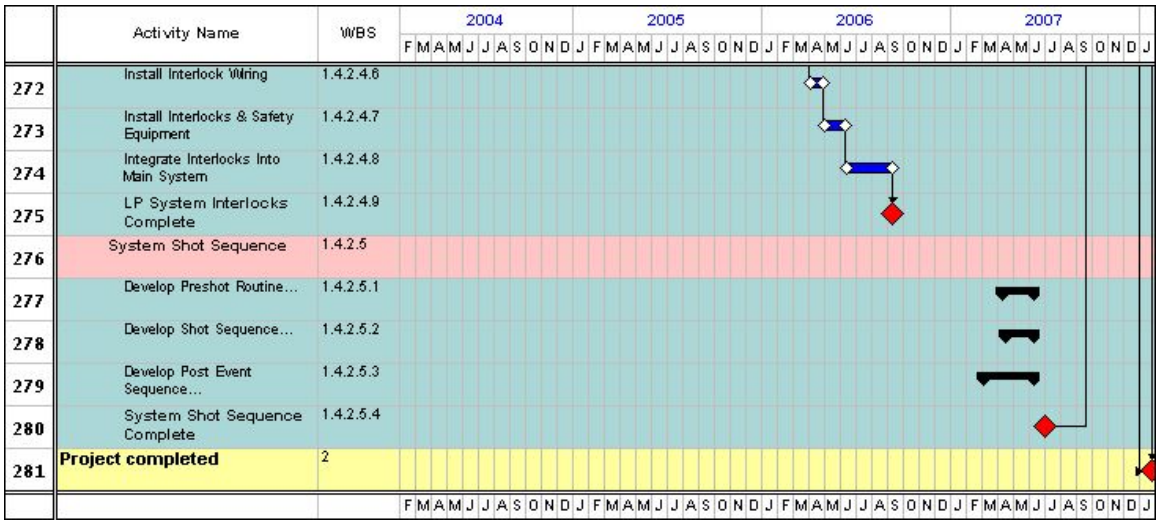
Activity Name
WBS
2004
2005
2006
2007
272 Install Interlock Wiring 1.4.2.4.6
273 Install Interlocks & Safety Equipment 1.4.2.4.7
274 Integrate Interlocks Into Main System 1.4.2.4.8
275 LP System Interlocks Complete 1.4.2.4.9
276 System Shot Sequence 1.4.2.5
277 Develop Preshot Routine... 1.4.2.5.1
278 Develop Shot Sequence... 1.4.2.5.2
279 Develop Post Event Sequence... 1.4.2.5.3
280 System Shot Sequence Complete 1.4.2.5.4
281 Project completed 2